DOCTOR OF PHILOSOPHY

Travelling waves in Lotka-Volterra competition models

Alzahrani, Ebraheem

Award date:
2011

DOCTOR OF PHILOSOPHY

Travelling waves in Lotka-Volterra competition models

Ebraheem Alzahrani

2011

University of Dundee

Travelling Waves in Lotka-Volterra Competition Models

By

Ebraheem Alzahrani

Doctor of Philosophy

Division of Mathematics

University of Dundee

Dundee

June 2011

Contents

Acknowledgements **xiv**

Abstract **xvii**

Introduction **1**

1 Background on Lotka-Volterra Competition Models **11**

1.1 Reaction-Diffusion Equation 11

1.1.1 Complex Movements 14

1.1.2 Kinetics (Reaction) 17

1.2 Lotka-Volterra Models 19

1.2.1 Nondimensionalisation 22

1.2.2 Kinetics 23

1.2.3 Travelling Wave Solutions 26

2 Bounds on the Wave Speed **32**

2.1 Sub- and Super-Solutions 32

2.2 Conclusion 42

3 Travelling Waves in Near-Degenerate Bistable Competition Models **43**

3.1 Introduction 43

3.2 Near Degenerate Case 45
3.2.1 Convergence in the limit $\epsilon \to 0$ 46
3.3 Computing the sign of the wave speed 47
3.4 Non-monotone nullclines 55
3.5 Conclusion 62

4 Reversing Invasion in Bistable Systems 63
4.1 Building a Picture of Motility vs Competition 64
4.1.1 Singular Perturbation 64
4.1.2 Some Specific Examples 69
4.1.3 The Mirror Problem 73
4.2 Relating the Original and Mirror Problems 79
4.2.1 Monotone Nullclines 79
4.2.2 Non-Monotone Nullclines 84
4.2.3 General remarks 94
4.3 Conclusions and Open Questions 94

5 Effects of Domain Size in 2-D Spatially Extended Lotka-Volterra Competition Models 97
5.1 2-D Spatially Extended Lotka-Volterra Models 97
5.2 Radially Symmetric Solutions 98
5.3 Planar and Non-Planar Interfaces 101
5.3.1 Domain Size and Curvature 103
5.3.2 Further Examples 107
5.4 Conclusion 110

6 Wave Behaviour in Tristable Competition Models 113
6.1 3-Species Competition Lotka-Volterra Model 113
6.1.1 Tristability 114

6.1.2 Initial Conditions 116
6.2 Type I initial conditions: bio-control 117
6.2.1 Annihilation of w 117
6.2.2 Persistence of w 121
6.3 Type II initial conditions: bio-buffers 127
6.3.1 Wave stalling 128
6.3.2 Species removal 128
6.3.3 Wave reversal 129
6.3.4 Annihilation and persistence of w regions 130
6.4 Conclusion 134

7 Conclusions and Future Work **136**

7.1 Conclusions 136
7.2 Future Work 137

List of Figures

1 Schematic representation of the nullclines f and g satisfying Assumption 0.0.1. 6

1.1 Schematic phase trajectories near the steady states for the dynamic behaviour of competing populations satisfying the model (1.30) for the various cases. (a) $\alpha_1 < 1$, $\beta_1 < 1$. Only the positive steady state S is stable and all trajectories tend to it. (b) $\alpha_1 > 1$, $\beta_1 > 1$. Here, $(1, 0)$ and $(0, 1)$ are stable steady states, each of which has a domain of attraction separated by separatrix which passes through $(\frac{1-\alpha}{1-\alpha\beta}, \frac{1-\beta}{1-\alpha\beta})$. (c) $\alpha_1 < 1$, $\beta_1 > 1$. Only one steady state exists, $(1, 0)$ with the whole positive quadrant its domain of attraction. (d) $\alpha_1 > 1$, $\beta_1 < 1$. The only stable steady state is $(0, 1)$ with the positive quadrant as its domain of attraction. 26

1.2 Left travelling wave solutions of system (1.30). Here $\alpha = 0.625$, $\beta = 0.8$, $D = 1$, $\delta = 1$ and $\gamma = 10^{-4}$ at $t = [0, 70]$. 28

1.3 Right travelling wave solutions of system (1.30). Here $\alpha = 3$, $\beta = 2$, $D = 1$, $\delta = 1$ and $\gamma = 10^{-4}$ at $t = [0, 320]$. 29

1.4 Left travelling wave solutions of system (1.30). Here $\alpha = 0.5$, $\beta = 2$, $D = 1$, $\delta = 1$ and $\gamma = 10^{-4}$ at $t = [0, 60]$. 30

2.1 The right solution $(\underline{u}, \overline{v})$, shown in (blue, red) and the solution (u, v) of system (2.2) shown in black. 36

2.2 The left solution $(\overline{u}, \underline{v})$, shown in (blue, red) and the solution (u, v) of system (2.2) shown in black. 39

3.1 Schematic representation of the $c_0 = 0$ solution to the reduced problem (3.2). 46

3.2 Schematic representation of the solutions paths $v = P_\epsilon(u)$ (solid line) and $v = P_0(u)$ (dashed line) in the cases (a) $h(S_+) < 0$; (b) $h(S_+) > 0$. The nullclines (dotted lines) are shown as straight lines for ease of visualisation and the path $v = \gamma(u)$ is shown in (a) (dot-dashed line). 49

3.3 Schematic representation of the nullcline $f = 0$ and $g = 0$ satisfying Assumption 0.0.1 with (4) replaced by (4*). The maximum of Γ occurs at v_1 with $u_1 = \Gamma(v_1) > \hat{u}$. 57

3.4 Schematic representation of the nullcline g satisfying Assumption 0.0.1 with condition (4*). The dashed area where we change the order of integrals of $\mathbf{I}$. 58

4.1 Travelling wave direction for the CLV problem (1) and (5). Locus of the $c_\epsilon = 0$ solutions is indicated by the dots. To the left (resp. right) of this curve, $c_\epsilon < 0$ (resp. $c_\epsilon > 0$) in plots (i)-(iv) and vice versa in plots (v)-(vi). In (i), (iii) and (v) $0 < \epsilon \leq 1$, (ii), (iv) and (vi) $1 \leq \epsilon \leq 1000$. Here, $\beta = 2$ in plots (i)-(iv), $\alpha = 2.25$ in plots (v)-(vi) and $\delta = 1$. 71

4.2 Travelling wave direction for the problem (4.11). Locus of the $c_\epsilon = 0$ solutions is indicated by the dots. To the left (resp. right) of this curve, $c_\epsilon < 0$ (resp. $c_\epsilon > 0$). (i) $0 < \epsilon \leq 1$, (ii) $1 \leq \epsilon \leq 1000$. Here, $\beta = 2$ and $\delta = 1$. 73

4.3 Schematic representation of the nullclines $f = 0$ and $g = 0$ satisfying Assumption 0.0.1 with condition (4f). 75

4.4 Schematic representation of the nullcline f satisfying Assumption 0.0.1 with condition (4f). The dashed area where we change the order of integrals of **I**. 77

4.5 Travelling wave direction for the mirror of CLV problem (4.13) and (5). Locus of the $c_D = 0$ solutions is indicated by the dots. To the left (resp. right) of this curve, $c_D < 0$ (resp. $c_D > 0$) in plots (i)-(iv) and vice versa in plots (v)-(vi). In (i), (iii) and (v) $0 < D \leq 1$, (ii), (iv) and (vi) $1 \leq D \leq 1000$. Here, $\beta = 2$ in plots (i)-(iv), $\alpha = 2.25$ in plots (v)-(vi) and $\delta = 1$. 81

4.6 Travelling wave direction for the mirror of problem (4.11). Locus of the $c_D = 0$ solutions is indicated by the dots. To the left (resp. right) of this curve, $c_D < 0$ (resp. $c_D > 0$). (i) $0 < D \leq 1$, (ii) $1 \leq D \leq 1000$. Here, $\beta = 2$ and $\delta = 1$. 82

4.7 The nullclines $f = 0$ and $g = 0$ for the kinetics in system (1) and (4.23). 84

4.8 Travelling wave direction for the problem (1), (4.23). Locus of the $c_\epsilon = 0$ solutions is indicated by the dots. To the left (resp. right) of this curve, $c_\epsilon < 0$ (resp. $c_\epsilon > 0$). (i) $0 < \epsilon \leq 1$, (ii) $1 \leq \epsilon \leq 1000$. Here, $\beta = 2$. 86

4.9 Travelling wave direction for the mirror of problem (4.13), (4.23). Locus of the $c_D = 0$ solutions is indicated by the dots. To the left (resp. right) of this curve, $c_D < 0$ (resp. $c_D > 0$). (i) $0 < D \leq 1$, (ii) $1 \leq D \leq 1000$. Here, $\beta = 2$. 87

4.10 The nullclines $f = 0$ and $g = 0$ for the kinetics in system (1) and (4.24). 88

4.11 Travelling wave direction for the problem (1), (4.24). Locus of the $c_\epsilon = 0$ solutions is indicated by the dots. To the left (resp. right) of this curve, $c_\epsilon < 0$ (resp. $c_\epsilon > 0$). (i) $0 < \epsilon \leq 1$, (ii) $1 \leq \epsilon \leq 1000$. Here, $\beta = 2$. 89

4.12 Travelling wave direction for the mirror of problem (4.13), (4.24). Locus of the $c_D = 0$ solutions is indicated by the dots. To the left (resp. right) of this curve, $c_D < 0$ (resp. $c_D > 0$). (i) $0 < D \leq 1$, (ii) $1 \leq D \leq 1000$. Here, $\beta = 2$. 90

4.13 The nullclines $f = 0$ and $g = 0$ for the kinetics in system (1) and (4.25). 91

4.14 Travelling wave direction for the problem (1), (4.25). Locus of the $c_\epsilon = 0$ solutions is indicated by the dots. To the left (resp. right) of this curve, $c_\epsilon < 0$ (resp. $c_\epsilon > 0$). (i) $0 < \epsilon \leq 1$, (ii) $1 \leq \epsilon \leq 1000$. Here, $\beta = 2$. 92

4.15 Travelling wave direction for the mirror of problem (4.13), (4.25). Locus of the $c_D = 0$ solutions is indicated by the dots. To the left (resp. right) of this curve, $c_D < 0$ (resp. $c_D > 0$). (i) $0 < D \leq 1$, (ii) $1 \leq D \leq 1000$. Here, $\beta = 2$. 93

5.1 (i) Right travelling wave solutions for the CLV system (1), (5), (ii) Right front solutions for the CLV system (5.3), (5), (iii) The blue line represents the position of the front of 1-D problem (1) and the red line the position of the front for radially symmetric solutions of (5.3). Here, $\alpha = 3$, $\beta = 2$, $\delta = 1$, $\epsilon = 1$ and $t = [0, 150]$ with rescaling factor $\gamma = 10^{-4}$. 100

5.2 Numerical solutions of system (5.3). Here, $\alpha = \beta = 2$, $\delta = 1$ and $\epsilon = 1$. u and v are represented by the blue and green lines, respectively. (i) Standing wave solutions exist for r large (*i.e.* system (5.3) is rescaled by the factor $\gamma = 10^{-6}$) and for $t = [0, 1000]$, (ii) No standing wave solutions exist for r small (*i.e.* system (5.3) is rescaled by the factor $\gamma = 10^{-2}$) and for $t = [0, 15]$. 101

5.3 Right travelling wave solution for the CLV problem (5.1), (5). u and v are represented by the red and blue colours, respectively. Here, $\alpha = 3$, $\beta = 2$, $\delta = 1$, $\epsilon = 1$ and $t = [0, 350]$ with rescaling factor $\gamma = 10^{-4}$. (a) $t = 0$, (b) $t = 35$, (c) $t = 175$ and (d) $t = 350$. 103

5.4 Right travelling wave solution for the CLV problem (5.1), (5). u and v are represented by the red and blue colours, respectively. Here, $\alpha = 3$, $\beta = 2$, $\delta = 1$, $\epsilon = 1$ and $t = [0, 350]$ with rescaling factor $\gamma = 10^{-4}$. (a) $t = 0$, (b) $t = 35$, (c) $t = 175$ and (d) $t = 350$. 104

5.5 Stable standing wave for the CLV problem (5.1), (5). u and v are represented by the red and blue colours, respectively. Here, $\alpha = \beta = 2$, $\delta = 1$, $\epsilon = 1$ and $t = [0, 50000]$ with rescaling factor $\gamma = 10^{-4}$. (a) $t = 0$, (b) $t = 200$, (c) $t = 300$ and (d) $t = 50000$. . . 105

5.6 Meta-stable wave solution for the CLV problem (5.1), (5). u and v are represented by the red and blue colours, respectively. Here, $\alpha = \beta = 2$, $\delta = 1$, $\epsilon = 1$ and $t = [0, 50000]$ with rescaling factor $\gamma = 10^{-5}$. (a) $t = 0$, (b) $t = 500$, (c) $t = 2500$ and (d) $t = 50000$. . 106

5.7 Meta-stable wave solution for the CLV problem (5.1), (5). u and v are represented by the red and blue colours, respectively. Here, $\alpha = \beta = 2$, $\delta = 1$, $\epsilon = 1$ and $t = [0, 50000]$ with rescaling factor $\gamma = 10^{-6}$. (a) $t = 0$ and (b) $t = 50000$. 106

5.8 Not fully smoothed interface solutions at final output for the CLV problem (5.2), (5). u and v are represented by the red and blue colours, respectively. Here, $\alpha = \beta = 2$, $\delta = 1$, $\epsilon = 1$ and $t = [0, 150]$ with rescaling factor $\gamma = 10^{-4}$. (a) $t = 0$, (b) $t = 7.5$, (c) $t = 15$ and (d) $t = 150$. 107

5.9 Nonsmoothed interface at final output solution for the CLV problem (5.2), (5). u and v are represented by the red and blue colours, respectively. Here, $\alpha = \beta = 2$, $\delta = 1$, $\epsilon = 1$ and $t = [0, 150]$ with rescaling factor $\gamma = 10^{-4}$. (a) $t = 0$, (b) $t = 12$, (c) $t = 45$ and (d) $t = 150$. 108

5.10 Travelling wave solutions moving inwards for the CLV problem (5.1), (5). u and v are represented by the red and blue colours, respectively. Here, $\alpha = \beta = 2$, $\delta = 1$, $\epsilon = 1$ and $t = [0, 1500]$ with rescaling factor $\gamma = 10^{-4}$. (a) $t = 0$, (b) $t = 75$, (c) $t = 750$ and (d) $t = 1500$. 109

5.11 Travelling wave solutions moving outwards for the CLV problem (5.1), (5). u and v are represented by the red and blue colours, respectively. Here, $\alpha = 1.5$, $\beta = 2$, $\delta = 1$, $\epsilon = 1$ and $t = [0, 200]$ with rescaling factor $\gamma = 10^{-4}$. (a) $t = 0$, (b) $t = 40$, (c) $t = 120$ and (d) $t = 200$. 109

5.12 Standing wave solutions for the CLV problem (5.1), (5). u and v are represented by the red and blue colours, respectively. Here, $\alpha = 1.9545$, $\beta = 2$, $\delta = 1$, $\epsilon = 1$ and $t = [0, 10000]$ with rescaling factor $\gamma = 10^{-4}$. (a) $t = 0$, (b) $t = 100$, (c) $t = 1000$ and (d) $t = 10000$. 110

5.13 Wave fronts solutions moving inwards for the CLV problem (5.1), (5). u and v are represented by the red and blue colours, respectively. Here, $\alpha = \beta = 2$, $\delta = 1$, $\epsilon = 1$ and $t = [0, 500]$ with rescaling factor $\gamma = 10^{-4}$. (a) $t = 0$, (b) $t = 5$, (c) $t = 150$ and (d) $t = 500$. 111

5.14 Wave fronts solutions moving outwards for the CLV problem (5.1), (5). u and v are represented by the red and blue colours, respectively. Here, $\alpha = 1.5$, $\beta = 2$, $\delta = 1$, $\epsilon = 1$ and $t = [0, 150]$ with rescaling factor $\gamma = 10^{-4}$. (a) $t = 0$, (b) $t = 15$, (c) $t = 90$ and (d) $t = 150$. 112

5.15 Standing wave solutions for the CLV problem (5.1), (5). u and v are represented by the red and blue colours, respectively. Here, $\alpha = 1.91204$, $\beta = 2$, $\delta = 1$, $\epsilon = 1$ and $t = [0, 7000]$ with rescaling factor $\gamma = 10^{-4}$. (a) $t = 0$, (b) $t = 70$, (c) $t = 700$ and (d) $t = 7000$. 112

6.1 The species are given by u (blue), v (green) and w (red). (a) Type I initial conditions for system (6.1) shows that w_0 represents as a bio-control for u_0 and v_0. (b) Type II initial conditions for system (6.1) where w_0 is plugged in between u_0 and v_0 as a bio-buffer. . . 116

6.2 Numerical solutions of system (6.1). For the following parameter set, $\alpha_1 = 2$, $\alpha_2 = 1.5$, $\beta_1 = 3$, $\beta_2 = 2$, $\gamma_1 = 3$ and $\gamma_2 = 2$ at $t = [0, 200]$, a left travelling wave solution is observed for species u and v while the third species w is annihilated. 118

6.3 Numerical solutions of system (6.1). For the following parameter set, $\alpha_1 = 3$, $\alpha_2 = 1.2$, $\beta_1 = 2.5$, $\beta_2 = 2.3$, $\gamma_1 = 1.5$ and $\gamma_2 = 2$ at $t = [0, 1200]$, a right travelling wave exists in the long-term involving u and v only and a left transient behaviour is observed. 121

6.4 Numerical solutions of system (6.1). Both the leading wave (v, w) and the rear wave (u, w) travel to the left with constant speed. Here, $\alpha_1 = 3$, $\alpha_2 = 1.5$, $\beta_1 = 2$, $\beta_2 = 2.5$, $\gamma_1 = 2.5$ and $\gamma_2 = 1.5$ at $t = [0, 150]$. 122

6.5 Numerical solutions of system (6.1). Left wave fronts, where the leading wave travels faster then the rear one forming an expanding region. The parameters are $\alpha_1 = 2$, $\alpha_2 = 2.8$, $\beta_1 = 2$, $\beta_2 = 3$, $\gamma_1 = 3$ and $\gamma_2 = 2.5$ at $t = [0, 400]$. 123

6.6 Numerical solutions of system (6.1). LTW of (v, w) and RTW of (u, w) are forming an expanding region in the long-term. Here, $\alpha_1 = 3$, $\alpha_2 = 3.5$, $\beta_1 = 3$, $\beta_2 = 2.3$, $\gamma_1 = 2.5$ and $\gamma_2 = 2$ at $t = [0, 250]$. 125

6.7 Numerical solutions of system (6.1). LTW involving (v, w) only and SW of (u, w), where $\alpha_1 = 3$, $\alpha_2 = 3$, $\beta_1 = 2$, $\beta_2 = 3.5$, $\gamma_1 = 3$ and $\gamma_2 = 3$ at $t = [0, 750]$. 126

6.8 Numerical solutions of system (6.1). SW in both waves (u, w) and (v, w) for the parameter set, $\alpha_1 = 2$, $\alpha_2 = 2.5$, $\beta_1 = 1.5$, $\beta_2 = 3$, $\gamma_1 = 2.5$ and $\gamma_2 = 3$ at $t = [0, 3000]$. 127

6.9 Numerical solutions of system (6.1). Both waves (u, w) and (v, w) are segregated for the parameter set, $\alpha_1 = 2$, $\alpha_2 = 3$, $\beta_1 = 3$, $\beta_2 = 2.5$, $\gamma_1 = 3$ and $\gamma_2 = 2.5$ at $t = [0, 3000]$. 129

6.10 Numerical solutions of system (6.1). The wave (u, w) travels to the right and (v, w) travels to the left. The parameter set are $\alpha_1 = 2$, $\alpha_2 = 3.5$, $\beta_1 = 2.5$, $\beta_2 = 3.5$ and $\gamma_1 = \gamma_2 = 3$ at $t = [0, 600]$. 130

6.11 Numerical solutions of system (6.1). Both the leading wave (u, w) and the rear wave (v, w) travel to the right. Here, the leading wave travels faster than the rear one. The parameter set are $\alpha_1 = 2$, $\alpha_2 = 2.5$, $\beta_1 = 3$, $\beta_2 = 2.3$, $\gamma_1 = 2$ and $\gamma_2 = 2.5$ at $t = [0, 400]$. . . 131

6.12 The curve represents the threshold of the minimum width (d_w) of w for fixed height (w_0) or otherwise the minimum height of w for fixed width of w. w persists in the right region of the curve and annihilates to the left. Here, d_w represents the minimum width of w while w_0 is the height of w. 132

6.13 The curve represents the threshold of the minimum distance (d) of w for fixed height (w_0) or otherwise the minimum height of w for fixed width of w. w persists in the right region of the curve and annihilates to the left. Here, d represents the minimum width of w while w_0 is the height of w. 133

Acknowledgements

Praise be to ALLAH, the Almighty, with whose gracious help it made it easy to accomplish successfully this project. Foremost I would like to express my deep thanks and appreciation to my supervisor, Dr Fordyce Davidson whose support, constant guidance and continuous encouragements made my thesis work possible. He has always been available to advise me. I wish to thank him for his understanding, patience, motivation, enthusiasm and his immense knowledge. I owe him lots of gratitude for having shown me this way of research. He could not even realize how much I have learned from him.

I wish also to thank the other members of staff of the Department of Mathematics, in particular Dr Niall Dodds for his help and support. I am also grateful to Mr Nick Dawes for providing me with mathematical software and solving any technical problems I encountered.

I am greatly indebted to my father, mother, brothers, sisters and the rest of my family for encouragement, prayers and support they have provided me during my studies. My sincere thanks are due to my wife, Futoon, who has managed patiently to look after our little stars, Rama, Rami and Aaram, so that I could concentrate on my studies. May ALLAH bless them all.

My great pleasure and appreciations go to my friends Mohannad Al-Tameemi, Faik Mayah, Ali Al-Taie, Ali Al-Hachami, Marc Sturrock and Vivi Andasari for their moral support and encouragement throughout my studies.

Finally, I would like to thank the Saudi Arabian Cultural Bureau and the Department of Mathematics at King Abdulaziz University for their financial support and otherwise.

Declaration

I declare that the following thesis is my own composition and that it has not been submitted before in application for a higher degree.

Ebraheem Alzahrani

Certification

This is to certify that Ebraheem Alzahrani has complied with all the requirements for the submission of this Doctor of Philosophy thesis to the University of Dundee.

Dr Fordyce Davidson

Dr Niall Dodds

Abstract

In this thesis, we study a class of multi-stable reaction-diffusion systems used to model competing species. Systems in this class possess uniform stable steady states representing semi-trivial solutions.

We start by considering a bistable, two-species interaction, where the interactions are of classic "Lotka-Volterra" type and we consider a particular problem with relevance to applications in population dynamics: essentially, we study under what conditions the interplay of relative motility (diffusion) and competitive strength can cause waves of invasion to be halted and reversed. By establishing rigorous results concerning related degenerate and near-degenerate systems, we build a picture of the dependence of the wave speed on system parameters. Our results lead us to conjecture that this class of competition model has three "zones of response" in which the wave direction is left-moving, reversible and right-moving, respectively and indeed that in all three zones, the wave speed is an increasing function of the relative motility.

Moreover, we study the effects of domain size on planar and non-planar interfaces and show that curvature plays an important role in determining competitive outcomes.

Finally, we study a 3-species Lotka-Volterra model, where the third species is treated as a bio-control agent or a bio-buffer and investigate under what conditions the third species can alter the existing competition interaction.

Introduction

To provide motivation for the structure of the thesis we begin with a brief overview of the main points and section layout.

We are interested in component-wise monotone travelling wave solutions of the system of equations

$$\begin{aligned} u_t &= u_{xx} + f(u,v), \\ v_t &= \epsilon^2 v_{xx} + g(u,v), \end{aligned} \tag{1}$$

for $(x,t) \in \mathbb{R} \times \mathbb{R}^+$ for which the asymptotic conditions

$$(u,v)(-\infty,t) = S_-, \quad (u,v)(\infty,t) = S_+, \quad t > 0 \tag{2}$$

are satisfied. The literature concerning the analysis and applications of systems of the form (1) is now vast and travelling wave solutions have been studied for many decades see *e.g.* [13, 29, 73, 74, 87, 102] and the references therein. One well-studied application has been to population dynamics where the components u, v are assumed to be interacting species. The term "species" is used in its loosest sense here and can be taken to represent different species of animals, microbes or plants, chemical species, cell types, *etc.* The species are assumed to move in a random manner (modelled via the diffusion term). The ratio of the diffusion coefficients, denoted by ϵ^2, is not necessarily small, but in the following chapters we sometimes are interested in the case where $\epsilon \to 0$. This represents the case where the motility of one species is relatively much greater than that

of the other. For example, in [33, 34] the competition is taken to be between normal and malignant cells, where the common resource can be considered to be oxygen. It is assumed that normal cells denoted here by v diffuse little, where as the malignant cells, denoted here by u, are taken to be highly motile.

The interaction of the species occurs through the functions f, g and can be synergistic, of predator-prey type or competitive. Here, we focus on the last of these, where competition between the species is for a common resource.

Much of the work in this thesis will concern travelling waves. As is standard, by first setting $z = x - ct$ for some constant c, a travelling wave solution of (1), (2) is defined to be a function $(u(z), v(z)) \in [C^2(\mathbb{R})]^2$ that satisfies

$$\begin{aligned} -cu' &= u'' + f(u,v), \\ -cv' &= \epsilon^2 v'' + g(u,v), \\ (u,v)(-\infty) = S_-, &\quad (u,v)(\infty) = S_+. \end{aligned} \tag{3}$$

If $c > 0$ then such a solution represents a wave front, joining S_- to S_+ moving to the right in the $x-$frame.

As indicated above, our principal interest resides in studying how motility and competition interact. As a starting point, it may be helpful therefore to recall some basic, well-known properties of simpler reaction-diffusion (R-D) systems, in order to give context to the present work. The simplest and now archetypal R-D equation exhibiting travelling wave behaviour has the following generic form

$$u_t = Du_{xx} + f(u), \quad (x,t) \in \mathbb{R} \times \mathbb{R}^+, \tag{4}$$

with appropriate asymptotic conditions relating to the zeros of the function, f. For definiteness, suppose that $f(u) = ru(1-u)$, then (4) is usually called Fisher's equation and it is well-known that this equation has a monotone travelling wave solution joining $u = 1$ at $x = -\infty$ to $u = 0$ at $x = \infty$ for all wave speeds $c \geq c_0$ where $c_0 = 2\sqrt{rD}$. Indeed, it can be shown that all initial data that decays

sufficiently fast as $x \to \infty$, tends asymptotically to a wave with the minimum speed c_0. Key points here are: (i) the wave moves the system from an unstable state to a stable one (as would be expected) and (ii) the (minimum) wave speed is a monotonically increasing function of the "motility parameter", D. Suppose now that $f(u) = ru(a-u)(u-1)$, $0 < a < 1$. Then (4) is often referred to as Nagumo's equation or the bistable Fisher equation because it has two stable, uniform steady states $u = 0, 1$ (the steady state $u = a$ is unstable). In this bistable case, it is well-known that a unique travelling wave exists with a speed c, the sign of which is determined by the sign of the integral of the reaction function over a certain interval (see e.g. p175 *et seq.* in [23]). For general bistable functions, f, a mini-max formula provides the value of the unique wave speed (see e.g. [103]). However, for the simple example given here, the wave speed can be written down explicitly as $c = \sqrt{rD/2}(1-2a)$. The two key points we wish to highlight here are (i) there is no *a prior* obvious directionality to the wave as both asymptotic states are stable and (ii) the wave speed is again directly proportional to $\sqrt{D}$.

For systems of the type (1), teasing out the relationship between diffusion and reaction is significantly more involved than it is for the scalar case. Despite much being known about existence and stability of waves (see [102] for the definitive discussion on travelling waves), there still appear to be no explicit formulae for wave speeds or magnitudes. From hereon, we focus on the bistable case and motivate our work with the following simple question.

Suppose the species u and v in (1) have roughly the same motility and so we can model this by setting $\epsilon = 1$. Moreover, suppose that the species are similar and so we can reasonably assume that $f = g$. As an illustration, consider the simple case where $f(u,v) = u(1-u-\alpha v)$; $g(u,v) = v(1-v-\beta u)$ with $\alpha = \beta$. (This implies that u and v are competitors of equal strength.) Note that here we can set $S_- = (0,1)$, $S_+ = (1,0)$ and for $\alpha = \beta > 1$ both these states are stable.

One might reasonably guess that in this case, there is a "stand-off" with neither population dominating and therefore a standing wave is formed, which denotes zones with $v \approx 1,\ u \approx 0$ and *vice versa*, separated by some mixing or coexistence layer. This can easily be confirmed by numerical integration. Suppose now we increase α. We would anticipate that v would be the stronger competitor and thus dominate, producing a wave travelling to the right. Apparently increasing α further still, would simply increase the wave speed. Contrary behaviour would be expected on increasing β (or decreasing α). Again, this is easy to confirm using MATLAB, say. However, what happens if we vary ϵ? It is now not so clear. One might argue that increasing ϵ means v is (relatively) more motile and thus can "spread faster" following the Fisher analogy. On the contrary, one could consider that spreading out too fast could lead to reduced competitive strength and therefore be disadvantageous.

To be precise regarding the interactions, we make the following assumptions on f and g (see [33] as will be stated shortly). Here and below, we will employ the following notation. The pair (u, v) will be used to represent a specific solution. However, for ease of notation, if $K : \mathbb{R}^2 \to \mathbb{R}$ is any sufficiently differentiable function, then K_u and K_v will denote the partial derivatives of K with respect to the first and second variables, respectively. Also, we use the notation $|\cdot|_i$ to represent the standard uniform norm associated with $C^i(\mathbb{R})$, $i = 0, 1, 2$.

Assumption 0.0.1. *The non-linearities $f, g \in C^2([0,1]^2, \mathbb{R})$ satisfy:*

(1) $f(0,v) = 0 = g(u,0)$.

(2) (1) *has exactly two stable, uniform equilibria* $S_- = (0,1)$ *and* $S_+ = (1,0)$ *and two unstable, uniform equilibria* $(0,0)$ *and* (u_s, v_s).

(3) $f_v(u,v) < 0$, $g_u(u,v) < 0$ *for* $(u,v) \in (0,1)^2$.

(4) The non-trivial solutions (u,v) *of* $g(u,v) = 0$ *are given by* $u = \Gamma(v)$ *for a monotonically decreasing function* Γ. *Setting* $\Gamma(1) = 0$ *and* $\Gamma(0) = \hat{u}$, *where* $0 < \hat{u} < 1$, Γ *has an inverse* $\hat{\gamma} \in C^1([0,\hat{u}],[0,1])$, *which can be extended trivially to a function* $\gamma \in C^0([0,1],[0,1])$ *where*

$$\gamma(u) = \begin{cases} \hat{\gamma} & u \in [0,\hat{u}], \\ 0 & u \in (\hat{u},1]. \end{cases}$$

Moreover, $\Gamma'(v) = 0$ implies Γ has a local maximum.

In Chapter 3, we discuss how condition (4) of Assumption 0.0.1 can be relaxed to include a class of non-monotone functions g. However, for ease of exposition we provide a detailed account of the monotone case first.

Stability, as required by condition (2), is equivalent to both the eigenvalues of the Jacobian $D(u,v)(f,g)$ having negative real parts when evaluated at the equilibrium point (instability is defined accordingly).

A sketch of typical nullclines satisfying Assumption 0.0.1 is given in Figure 1, where the points u_1 and v_1 are identified by

$$u_1 = \min\left\{1, \sup_{\tau\in(0,1)} \Gamma(\tau)\right\}, \quad v_1 := \gamma_m(u_1),$$

where γ_m is the unique maximal inverse of Γ, *i.e.* $\gamma_m(0) = 1$ and

$$\gamma_m(\sigma) := \max_{\tau\in(0,1)} \{\Gamma(\tau) = \sigma\}.$$

Note that γ_m is monotone decreasing on $(0,u_1)$. Also, the conditions on g allow for the local maximum of Γ to be located above $u = 1$. However, in this case

$u_1 = 1$ by definition. Notice also, that if $\Gamma(v)$ is monotone decreasing, then $u_1 = \hat{u}$ and $v_1 = 0$.

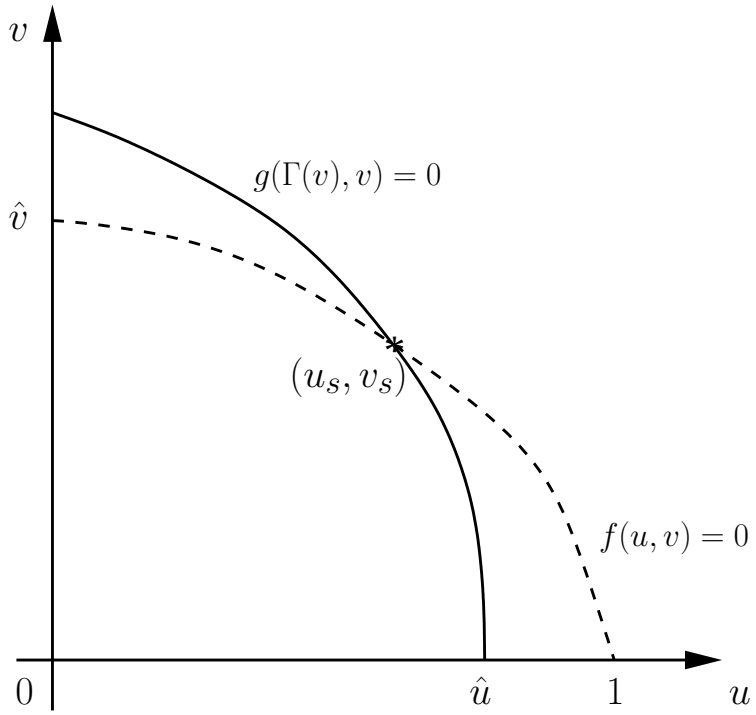

Figure 1: Schematic representation of the nullclines f and g satisfying Assumption 0.0.1.

For future reference, we call the following definition of f and g, the "Classic Lotka-Volterra" terms and denote these by CLV:

$$f(u,v) = u(1-u-\alpha v), \quad g(u,v) = \delta v(1-v-\beta u), \tag{5}$$

where α, β and δ are positive constants. It is straightforward to show that the conditions of Assumption 0.0.1 are satisfied by the CLV terms, provided the inter-specific competition rates satisfy $\alpha, \beta > 1$. Note also that in this case the nullclines shown in Figure 1 are simply straight lines and the points of intersection $\hat{u}$ and $\hat{v}$ are equal to $1/\beta$ and $1/\alpha$, respectively.

Using the change of variables $w = 1 - u$, (3) becomes

$$\begin{aligned} -cw' &= w'' - f(1-w,v) := w'' + F(w,v), \\ -cv' &= \epsilon^2 v'' + g(1-w,v) := \epsilon^2 v'' + G(w,v), \\ (w,v)(-\infty) &= (1,1), \quad (w,v)(\infty) = (0,0). \end{aligned} \tag{6}$$

It follows from the assumptions on the kinetics, that the monotonicity conditions $F_v \geq 0$, $G_w \geq 0$ hold and therefore, we may directly apply Theorem 1.1 on p155 in [102] to ensure the existence of a monotone solution to (6). Thus a (component-wise) monotone solution of (3) exists corresponding to a unique (up to translation) travelling wave for (1) and (2).

The thesis is ordered as follows. In Chapter 1, some mathematical background concerning to the Lotka-Volterra competition models is given, before presenting a number of fundamental results. We briefly give an overview on

- Derivation of reaction-diffusion equations.
- Modelling movement via advection, chemotaxis, haptotaxis and backwards diffusion.
- Kinetics, that represent competition, prey-predator and symbiosis interactions.
- Importance of nondimensionalisation.
- The linear stability to Lotka-Volterra competition models is studied with some ecological considerations relying on the competition strengths.
- Background on travelling wave solutions to Lotka-Volterra competition models.

In Chapter 2, we investigate the structure of bounds for the wave speed c presented in [34]. By constructing appropriate sub- and super-solutions to (3)

similar to those introduced in [34] and using essentially identical arguments, it can be shown that

$$-K \leq c \leq L\epsilon, \tag{7}$$

where K and L are positive constants independent of ϵ. One immediate consequence of this result is that in the limit $\epsilon \to 0$ only left travelling waves exist. We investigate the sharpness of these bounds in the special case of CLV kinetics. We show that

- The bounds of the wave speed given in [34] are optimal for the given left and right solutions (sub-solutions and super-solutions).

We develop in Chapter 3 an understanding of the relationship between the solutions of the system (3) and those of a reduced or degenerate problem

$$\begin{aligned} -cu' &= u'' + f(u,v), \\ -cv' &= g(u,v), \\ (u,v)(-\infty) = S_-, &\quad (u,v)(\infty) = S_+. \end{aligned} \tag{8}$$

The reduced problem (8) provides certain analytical advantages over the full problem. However, given its singular nature, it is not surprising that the solutions to (8), denoted here by (u_0, v_0, c_0), have quite different regularity properties to those of (3) (see [33, 34]). Therefore, it is not obvious *a priori* how the solutions of (3) behave in the limit as $\epsilon \to 0$ or how any such limit is related to (u_0, v_0, c_0). A connection between these problems was established in Chapter 3. In this chapter

- We construct a general potential energy for the general problem (3) and relate it to the definition of the energy function for (8).

- We use the general energy function to determine the sign of the wave speed c for any $\epsilon > 0$.

- We relax condition (4) in Assumption 0.0.1 to include a class of non-monotone functions g.

In Chapter 4, we will consider a particular problem with relevance to many applications in population dynamics. Essentially, we study how the interplay of relative motility and competitive strength can cause waves of invasion to be halted and reversed. In Chapter 4, we attempt to build an understanding of how direction of travelling waves is mediated by the relative motility, ϵ^2, and the relative competitive strengths of the species u and v. In Chapter 4, we build on the connection between the degenerate and near-degenerate problems developed in Chapter 3. We attempt to build on this connection and develop an understanding of the global picture, *i.e.* how the interplay between motility and competition determines the direction of wave fronts. We will show that

- The direction of travelling wave solutions to (1) is mediated by the relative energies of the end states $S_{\pm}$.

- Within a given range of competition strengths, increasing ϵ can cause waves to slow, halt and reverse. Outside this range, increasing ϵ has no effect on the direction of the wave.

- In a limiting case, (approximately) standing waves (very low speed travelling waves) exist for all values of $\epsilon \geq 0$.

- The wave speed remains bounded as $\epsilon \to \infty$ and the limiting value can be determined via a *mirror* problem.

In Chapter 5, we present extensions of our work from Chapters 3-4 to two spatial dimensions. Furthermore, we discuss the effect of domain size on wave behaviour resulting from planar and non-planar interfaces. We will show in the chapter

- We study radially symmetric fronts and compare them to 1-D travelling waves.

- We show that curvature of the interface plays a crucial role in determining competitive outcomes.

Suppose now that a third species is introduced to system (1). Given that we have established how u and v compete, can the third species alter this interaction, *e.g.* can it stop or even reverse a wave of invasion? In Chapter 6, we address this question.

- We discuss two types of initial conditions, where the third species w is introduced as a bio-control agent or a bio-buffer.

- Considering w as is a bio-control agent, we observe 13 cases of wave behaviour which are essentially divided into two sets: w is annihilated or persistent.

- Considering w as is a bio-buffer, we get the same wave behaviours as the first type but we focus here on some interesting cases. For example, if we know that v is a strong competitor than u, can we reverse the wave (u, v) or stop it?

- We consider how much of the species w needs to be introduced, for w to persist in the long-term dynamics of the system, *i.e.* for w to not be annihilated by either u or v, or both.

Finally, in Chapter 7 we conclude by summarising a number of important points, and then suggest some possible topics for future work.

Chapter 1

Background on Lotka-Volterra Competition Models

1.1 Reaction-Diffusion Equation

The reaction-diffusion equation is a mathematical model that has been used to describe how the concentration of one or more substances disperses through space under the influence of two processes: local reactions in which the substances interact with each other, and diffusion which causes the substances to spread out in space.

Guided by [22, 72], in order to derive the reaction-diffusion equation, we first consider the *Fickian diffusion* which says that the flux, J, of material, which can be cells, amount of chemical, number of animals and so on, is proportional to the gradient of the concentration of the material. That is, in one dimension

$$J \propto -\frac{\partial u}{\partial x} \quad \Rightarrow \quad J = -D\frac{\partial u}{\partial x}, \tag{1.1}$$

where $u(x,t)$ is the concentration of the species and D is its diffusivity. The minus sign simply indicates that diffusion transports matter from a high to a low concentration.

We now write a general conservation equation, which says that the rate of change of the amount of material in a region is equal to the rate of flow across the boundary plus any that is created within the boundary. If the region is $x_0 < x < x_1$ and no material is created, then we have

$$\frac{\partial}{\partial t}\int_{x_0}^{x_1} u(x,t)dx = J(x_0,t) - J(x_1,t). \tag{1.2}$$

If we take $x_1 = x_0 + \Delta x$, take the limit as $\Delta x \to 0$ and use (1.1) we get the *classical diffusion equation* in one dimension, namely,

$$\frac{\partial u}{\partial t} = -\frac{\partial J}{\partial x} = \frac{\partial \left(D\frac{\partial u}{\partial x}\right)}{\partial x}, \tag{1.3}$$

which, if D is constant, becomes

$$\frac{\partial u}{\partial t} = D\frac{\partial^2 u}{\partial x^2}. \tag{1.4}$$

Mathematically, this is identical to the *heat equation.*

We now consider diffusion in three space dimensions. Let S be an arbitrary surface enclosing a volume V. The general conservation equation says that the rate of change of the amount of material in V is equal to the rate of flow of material across S into V plus the material created in V. Thus

$$\frac{\partial}{\partial t}\int_V u(\mathbf{x},t)dV = -\int_S \mathbf{J}\cdot\mathbf{dS} + \int_V f dV, \tag{1.5}$$

where J is the flux of material and f, which represents the source of material, may be a function of u, $\mathbf{x}$ and t. Applying the divergence theorem to the surface integral and assuming $u(\mathbf{x},t)$ is continuous, (1.5) becomes

$$\int_V \left[\frac{\partial u}{\partial t} + \nabla\cdot\mathbf{J} - f(u,\mathbf{x},t)\right] dV = 0. \tag{1.6}$$

Since the volume V is arbitrary the integrand must be zero and so the conservation equation for u is given by

$$\frac{\partial u}{\partial t} = -\nabla\cdot\mathbf{J} + f(u,\mathbf{x},t). \tag{1.7}$$

This equation holds for a general flux transport $\mathbf{J}$. If, for example, we choose the transport process to be classical diffusion, then

$$\mathbf{J} = -D\nabla u \tag{1.8}$$

and (1.7) becomes

$$\frac{\partial u}{\partial t} = \nabla \cdot (D\nabla u) + f(u, \mathbf{x}, t), \tag{1.9}$$

where D may be a function of $\mathbf{x}$ and u. Situations where D is space-dependent are arising in more and more modelling situations of biomedical importance, from diffusion of genetically engineered organisms in heterogeneous environments to the effect of white and grey matter in the growth and spread of brain tumours, for additional details see [89, 90, 91]. The source term f in an ecological context, for example, could represent the birth and/or death process and u the population density.

If we further generalise (1.9) to the situation in which there are, for example, several interacting species or chemicals we then have a vector $u_i(\mathbf{x}, t), i = 1, ..., m$ of densities or concentrations each diffusing with its own diffusion coefficient D_i and interacting according to the vector source term f. Then (1.9) becomes

$$\frac{\partial \mathbf{u}}{\partial t} = \nabla \cdot (D\nabla \mathbf{u}) + \mathbf{f}(\mathbf{u}), \tag{1.10}$$

where now D is a matrix of the diffusivities which, if there is no cross diffusion among the species, is simply a diagonal matrix. In (1.10), $\nabla \mathbf{u}$ is a tensor so $\nabla \cdot D\nabla \mathbf{u}$ is a vector, see [67, 72].

Cross-diffusion can arise in genuinely practical models, for examples see [58, 74, 83]. Moreover, cross-diffusion systems can pose interesting mathematical problems particularly regarding their well-posedness.

Equation (1.10) is referred to as a reaction-diffusion system. Such a mechanism was proposed as a model for the chemical basis of morphogenesis by Turing

[99] in one of the most important papers in theoretical biology of the last century. Such systems have been widely studied since about 1970. We shall mainly be concerned with reaction diffusion systems where D is a diagonal and constant and $\mathbf{f}$ is a function only of $\mathbf{u}$.

1.1.1 Complex Movements

Besides the process of diffusion, there are many physical factors that affect the movement of organisms, cells or chemical. These factors include

- **Advection**: The movement of particles or molecules within fluids (*i.e.* liquids or gases). These particles take on the fluid's velocity and participate in a net collective motion. If $\boldsymbol{\nu}$ is the velocity of the fluid, then the flux of particles is given by

$$\mathbf{J}_{\text{adv}} = \boldsymbol{\nu} u. \tag{1.11}$$

  The advection equation with a source term is

$$\frac{\partial u}{\partial t} = -\nabla \cdot J_{\text{adv}} + f = -\nabla \cdot (\boldsymbol{\nu} u) + f. \tag{1.12}$$

  If we have both advection and diffusion (1.8), $J = J_{\text{adv}} + J_{\text{diff}}$ and the advection-diffusion equation with a source term is

$$\frac{\partial u}{\partial t} = -\nabla \cdot (\boldsymbol{\nu} u) + \nabla \cdot (D \nabla u) + f. \tag{1.13}$$

  For further references see [11, 13, 22, 85]. In biological systems, advection typically transports molecules over distances for which diffusion is too slow. For example, blood transports oxygen bound to hemoglobin in red blood cells over large distances in the larger blood vessels of the body by advection. In the smallest blood vessels, blood flow is very slow and oxygen is transported to local tissue by advection, see [96].

- **Chemotaxis**: A biological phenomenon describing the change of motion in population densities or a single species in response (taxis) to an external chemical stimulus spread in the environment where they reside. Suppose that the presence of a gradient in an attractant, $c(x,t)$, gives rise to a movement of the cells up the gradient. The flux of cells will increase with the number of cells, $u(x,t)$, present. Thus, we may reasonably take as the chemotactic flux

$$\mathbf{J} = u\chi(c)\nabla c, \tag{1.14}$$

where $\chi(c)$ is a function of the attractant concentration. In the general conservation equation (1.7) for $c(x,t)$, namely,

$$\frac{\partial u}{\partial t} = -\nabla \cdot \mathbf{J} + f(u), \tag{1.15}$$

where $f(u)$ represents the growth term for the cells, the flux

$$\mathbf{J} = \mathbf{J}_{\text{diff}} + \mathbf{J}_{\text{chem}},$$

where the diffusion is from $\mathbf{J} = -D\nabla u$ with the chemotaxis flux from (1.14). Therefore, a basic reaction-diffusion-chemotaxis equation is

$$\frac{\partial u}{\partial t} = -\nabla \cdot (u\chi(c)\nabla c) + \nabla \cdot (D\nabla u) + f(u), \tag{1.16}$$

where D is the diffusion coefficient of cells, see [11, 17, 72, 93].

Chemotaxis plays an important role in a wide range of practical phenomena such as in wound healing [95], cancer growth [90] and immune system cells moving in response to bacterial inflammation. For example, when a bacterial infection invades the body it may be attacked by immune system cells, which locate the source of infection by means of chemotaxis. Convincing evidence suggests that, in particular, leukocyte cells in the blood move towards a region of bacterial inflammation, to counter it, by moving up a chemical gradient caused by the infection, see [72] and the references

therein. Until recently, relatively little work had been done where cell populations are not constant; one exception was the travelling wave model of [54] where the bacteria reproduce and die as well as migrate.

- **Haptotaxis**: The tendency of cells to translocate unidirectionally up a steep gradient of increasing adhesiveness of the substratum, see [12, 65, 73, 93]. One example in cancer modelling shows that a gradient is created by proteases, a group of enzymes emitted by the tumour cells which then degrade the connective tissue, for further details see [78]. Assume that adhesive site density $\rho(x,t)$ is proportional to the substratum density, then the haptotactic flux may be modelled by

$$\mathbf{J}_h = \alpha u \nabla \rho, \tag{1.17}$$

where α is the positive haptotactic coefficient. Thus, the cell conservation equation is

$$\frac{\partial u}{\partial t} = \underbrace{D\nabla^2 u}_{\text{diffusion}} \underbrace{-\alpha \nabla \cdot (u \nabla \rho)}_{\text{haptotaxis}} + f(u), \tag{1.18}$$

where $u(x,t)$ represents the density of cells while $\rho(x,t)$ is the density of the substratum, where D and α are assumed to be constants for simplicity. Haptotaxis can be somewhat more complex than is implied here since chemical processes can be involved.

- **Aggregation (Backwards Diffusion)**: A direct mutual attraction between particles (atoms, molecules, cells or organisms). It is usually explained in terms of forces, external and/or internal, acting upon individuals. A remarkable aspect of this global organization is that individuals move altogether in a coordinated (though random) fashion even though interaction among them via relevant senses (sight, smell, hearing, *etc.*) are typically limited to much shorter distances than the size of the group, for further

references see [19, 22, 70]. Precisely, the backwards diffusion equation can be obtained from the classical diffusion equation (1.4) by redefining time $t \to -t$ so that time will run backwards. Thus, the backwards diffusion equation is

$$\frac{\partial u}{\partial t} = -D\frac{\partial^2 u}{\partial x^2}. \tag{1.19}$$

In [98], it is stated that attraction among individuals leads to movement which is biased towards areas of high population density. However, aggregations can arise only if mutual attraction is strong enough to dominate the dispersive effect due to random motion. A specific equation is widely used is the reaction-diffusion-aggregation equation

$$u_t = (D(u)u_x)_x + f(u), \quad t \geq 0, \ \ x \in \mathbb{R}, \tag{1.20}$$

where f is a monostable (*i.e.*, Fisher-type) nonlinear reaction term and $D(u)$ is a changing-sign nonlinear term, modelling repulsive-attractive population dynamic. Recently, some models of reaction-diffusion-aggregation processes have been proposed, describing the tendency of a population to cluster, to avoid the risk of extinction (see [25, 98]).

1.1.2 Kinetics (Reaction)

We now focus on the reaction terms and thus consider spatially uniform solutions of (1.10). The deterministic model of population growth is given by

$$\frac{du}{dt} = ru,$$

where $r = b - d$ is the difference between the birth and death rates. If $r > 0$, then the population grows exponentially (so-called Malthusian growth (linear growth) [66]). Populations when left alone, however, do not grow exponentially forever. Eventually their growth will be checked by the over-consumption of resources. If

it is assumed that the environment has an intrinsic carrying capacity K, then populations larger than this size experience heightened death rates.

To model population growth with an environmental carrying capacity K, a nonlinear equation of the form

$$\frac{du}{dt} = ruf(u), \tag{1.21}$$

is required, where $f(u)$ provides a model for environmental regulations. This function should satisfy $f(0) = 1$ (the population grows exponentially with growth rate r when u is small), $f(K) = 0$ (the population stops growing at the carrying capacity) and $f(u) < 0$ when $u > K$ (the population decays when it is larger than the carrying capacity). The simplest function $f(u)$ satisfying these conditions is linear and given by $f(u) = 1 - \frac{u}{K}$. The resulting model is the well-known logistic equation (see [101]),

$$\frac{du}{dt} = ru(1 - \frac{u}{K}),$$

an important model for many processes besides bounded population growth. Another function $f(u)$ is known as the growth with Allee effect [3],

$$f(u) = ru(u - a)(1 - \frac{u}{K}) \text{ with } a \in (0, K).$$

for further references see [10, 11, 14].

For systems modelling ecological phenomena, typical reaction terms are those that represent competition, predator-prey and symbiosis interactions. These include more general models such as predator-prey models with a functional response. If u and v are population densities, a generic two-species system would have the form

$$\begin{aligned} \frac{du}{dt} &= F(u, v) = uf(u, v), \\ \frac{dv}{dt} &= G(u, v) = vg(u, v). \end{aligned} \tag{1.22}$$

A fairly typical predator prey model has the form

$$\begin{aligned} \frac{du}{dt} &= h(u) - af(u,v), \\ \frac{dv}{dt} &= -bv + cf(u,v), \end{aligned} \tag{1.23}$$

where $f(u,v) = vg(u,v)$ with $g(u,v)$ being the functional response, see [47], *e.g.* $g(u,v) = ku$ (see [26]). Other common forms are

$$\begin{aligned} g(u,v) &= \frac{au}{1+bu} && \text{(Holling type II, see [46, 77])}, \\ g(u,v) &= \frac{au^2}{1+bu^2} && \text{(Holling type III, see [6, 44])}, \\ g(u,v) &= \frac{au}{1+bu+cv} && \text{(Beddington - DeAngelis, see [15, 45])}. \end{aligned} \tag{1.24}$$

These sorts of formulation can be extended to encompass more species or more trophic levels (green plants, herbivore and carnivore), or modified to describe symbiosis or other sorts of population interactions. Often, an important aspect of the analysis of models such as (1.21)-(1.23) is to find their equilibria and determine the stability of those equilibria, because (stable) equilibria represent the most likely state of the system. The equilibrium solution of the ODE (1.21) means $\frac{du}{dt} = 0$, so the uniform equilibrium solutions of PDE are the solutions of the equation $\mathbf{f}(\mathbf{u}) = 0$. Therefore, in the case of systems, the stability analysis often involves studying the eigenvalues of matrices obtained by linearizing about the equilibria, see [10, 11, 47].

1.2 Lotka-Volterra Models

The Lotka-Volterra models are a class of models that are used to interpret the interactions amongst species in which two or more species interact. The first such model was initially proposed independently by Alfred Lotka [63] in 1925 and Vito Volterra [104, 105] in 1926. In this thesis, we will study the "spatially extended"

Lotka-Volterra models, which can be written generally in the following form:

$$\begin{aligned} \frac{\partial U}{\partial T} &= D_1 \nabla^2 U + F(U,V), \\ \frac{\partial V}{\partial T} &= D_2 \nabla^2 V + G(U,V), \end{aligned} \tag{1.25}$$

where $U(X,T)$ and $V(X,T)$ denote the population densities at position X and time T. Lotka-Volterra models can categorize the dynamics of biological systems into three groups:

1. **Predator-Prey Model** [10, 11, 22, 47, 57, 72, 73]: Here the growth rate of one population is decreased and the other increased by the interaction of the two. This can be mathematically expressed as

$$\frac{\partial F}{\partial V} < 0, \quad \frac{\partial G}{\partial U} > 0.$$

2. **Competition Model** [10, 11, 26, 22, 47, 57, 69, 72, 73, 79, 107]: Here the growth rate of each population is decreased by the interaction of the two. This can be mathematically expressed as

$$\frac{\partial F}{\partial V} < 0, \quad \frac{\partial G}{\partial U} < 0.$$

3. **Symbiosis** [9, 21, 71, 72, 80]: Here two species live in close association for long periods. This can be mathematically expressed as

$$\frac{\partial F}{\partial V} > 0, \quad \frac{\partial G}{\partial U} > 0.$$

   Symbiosis can be further divided into three parts:

   - *Mutualism* [9, 13, 20, 72, 80, 81]: A biological interaction in which the existence of each species is of benefit to each other. (Sometimes Mutualism and Symbiosis are used synonymously, but this is strictly incorrect because Symbiosis is a broad category and Mutualism is only one type of it, for further reading see [9, 80].)

- *Commensalism* [8, 68, 81, 86]: Symbiotic relationships in which one organism consumes the unused food of another.
- *Parasitism* [22, 28, 36, 94]: A parasite is an organism that lives on or in the body of another organism (the host).

In this thesis, we will focus on competition models. In particular, we will consider the equations of the generic form

$$\begin{aligned} \frac{\partial U}{\partial T} &= D_1 \nabla^2 U + U.f(U,V), \\ \frac{\partial V}{\partial T} &= D_2 \nabla^2 V + V.g(U,V), \end{aligned} \tag{1.26}$$

with

$$\frac{\partial f}{\partial V} < 0, \quad \frac{\partial g}{\partial U} < 0.$$

As an example, much of the following work will focus on systems of the form

$$\begin{aligned} \frac{\partial U}{\partial T} &= D_1 \nabla^2 U + a_1 U(1 - b_1 U - c_1 V), \\ \frac{\partial V}{\partial T} &= D_2 \nabla^2 V + a_2 V(1 - b_2 V - c_2 U), \end{aligned} \tag{1.27}$$

where, for $i = 1, 2$, a_i are net birth rates, $\frac{1}{b_i}$ are carrying capacities, c_i are competition coefficients and D_i are diffusion coefficients, which are all assumed non-negative. The interaction terms give a simple representation of logistic growth with competition.

As we will discuss this case later in the thesis, we note that similarly, the competition between three species we consider to be expressed as

$$\begin{aligned} \frac{\partial U}{\partial T} &= D_1 \nabla^2 U + a_1 U \left(1 - b_1 U - c_1 V - d_1 W\right), \\ \frac{\partial V}{\partial T} &= D_2 \nabla^2 V + a_2 V \left(1 - b_2 V - c_2 U - d_2 W\right), \\ \frac{\partial W}{\partial T} &= D_3 \nabla^2 W + a_3 W \left(1 - b_3 W - c_3 U - d_3 V\right). \end{aligned} \tag{1.28}$$

1.2.1 Nondimensionalisation

Before analysing the model (1.27) it is helpful to express it in nondimensional terms. As stated in, *e.g.* [72], nondimensionalisation has several advantages. For example, the units used in the analysis are then unimportant and the parameters small and large have a definite relative meaning. It also can reduce the number of relevant parameters to fewer, dimensionless groupings, which determine the dynamics. For a nice article with several practical examples, see [84], which discusses the advantages of nondimensionalisation and scaling in general.

We now consider in one spatial dimension, we introduce nondimensional quantities by writing

$$\begin{aligned} &u = b_1 U, \quad v = b_2 V, \quad t = a_1 T, \quad x = \sqrt{\gamma \tfrac{a_1}{D_1}} X, \\ &\alpha = \tfrac{c_1}{b_2}, \quad \beta = \tfrac{c_2}{b_1}, \quad \delta = \tfrac{a_2}{a_1}, \qquad D = \tfrac{D_2}{D_1}. \end{aligned} \tag{1.29}$$

Note that this nondimensionalisation in fact works for all space dimensions. Now, substituting the new variables from (1.29) into the (1.27), we obtain

$$\begin{aligned} \frac{\partial\left(\frac{1}{b_1}u\right)}{\partial\left(\frac{1}{a_1}t\right)} &= D_1 \frac{\partial^2\left(\frac{1}{b_1}u\right)}{\partial\left(\sqrt{\frac{D_1}{\gamma a_1}}x\right)^2} + a_1\left(\frac{1}{b_1}u\right) - a_1 b_1\left(\frac{1}{b_1}u\right)^2 - a_1 c_1\left(\frac{1}{b_1}u\right)\left(\frac{1}{b_2}v\right), \\ \frac{\partial\left(\frac{1}{b_2}v\right)}{\partial\left(\frac{1}{a_1}t\right)} &= D_2 \frac{\partial^2\left(\frac{1}{b_2}v\right)}{\partial\left(\sqrt{\frac{D_1}{\gamma a_1}}x\right)^2} + a_2\left(\frac{1}{b_2}v\right) - a_2 b_2\left(\frac{1}{b_2}v\right)^2 - a_2 c_2\left(\frac{1}{b_1}u\right)\left(\frac{1}{b_2}v\right), \end{aligned}$$

that is on cancelling terms,

$$\begin{aligned} \frac{\partial u}{\partial t} &= \gamma \frac{\partial^2 u}{\partial x^2} + u(1 - u - \alpha v), \\ \frac{\partial v}{\partial t} &= \gamma D \frac{\partial^2 v}{\partial x^2} + \delta v(1 - v - \beta u), \end{aligned} \qquad (x,t) \in \mathbb{R} \times \mathbb{R}^+, \tag{1.30}$$

with D, γ, α, β and δ defined as above. Note that (1.30) is stated as holding for $x \in \mathbb{R}$. In numerical computations it is necessary to use a bounded domain. Hence, to avoid imposing boundary condition unnecessarily influencing the results, a scaling parameter γ is introduced, changing γ changes the effective size of

the domain. Hence, for γ chosen sufficiently small, solution behaviour in the interior of the domain can be viewed as accurately representing the solution of (1.30). These scaling arguments also hold for 2-dimensional spatial domain considered later.

1.2.2 Kinetics

First, we study the associate kinetic problem,

$$\begin{aligned} \frac{du}{dt} &= f(u,v), \\ \frac{dv}{dt} &= g(u,v), \end{aligned} \tag{1.31}$$

where $f(u,v) = u(1-u-\alpha v)$, $g(u,v) = \delta v(1-v-\beta u)$, $\alpha \geq 0$, $\beta \geq 0$ and $\delta > 0$. The steady states, (u_*, v_*), are solutions of $f(u,v) = g(u,v) = 0$ which, from (1.30), are

$$\begin{aligned} &(u_*, v_*) = (0,0); \quad (u_*, v_*) = (1,0); \quad (u_*, v_*) = (0,1); \\ &(u_*, v_*) = (\frac{1-\alpha}{1-\alpha\beta}, \frac{1-\beta}{1-\alpha\beta}). \end{aligned} \tag{1.32}$$

The last of these is only of biological relevance if both α and β are greater than one or both less than one.

Following standard theory (see *e.g.* [10, 72, 100, 107]), the linear asymptotic stability of the steady states (1.32) is determined by the eigenvalues of the Jacobian matrix, which for (1.31) is

$$J(u_*, v_*) = \begin{pmatrix} \frac{\partial f}{\partial u} & \frac{\partial f}{\partial v} \\ \frac{\partial g}{\partial u} & \frac{\partial g}{\partial v} \end{pmatrix} = \begin{pmatrix} 1-2u-\alpha v & -\alpha u \\ -\beta\delta v & \delta - 2\delta v - \beta\delta u \end{pmatrix}_{(u_*, v_*)}. \tag{1.33}$$

Thus, it is straightforward to confirm that $(0,0)$ is an unstable node, since the Jacobian matrix and corresponding eigenvalues are

$$J(0,0) = \begin{pmatrix} 1 & 0 \\ 0 & \delta \end{pmatrix}. \qquad |J(0,0) - \lambda I| = \begin{vmatrix} 1-\lambda & 0 \\ 0 & \delta - \lambda \end{vmatrix} = 0,$$

$$\Rightarrow \lambda_1 = 1, \lambda_2 = \delta.$$

The result follows as $\lambda_{1,2}$ are both positive.

For $(1,0)$, (1.33) gives $J(1,0) = \begin{pmatrix} -1 & -\alpha \\ 0 & \delta(1-\beta) \end{pmatrix}$. Hence,

$$|J(1,0) - \lambda I| = \begin{vmatrix} -1-\lambda & -\alpha \\ 0 & \delta(1-\beta)-\lambda \end{vmatrix} = 0,$$

$$\Rightarrow \lambda_1 = -1, \lambda_2 = \delta(1-\beta).$$

Therefore, $(1,0)$ is a $\begin{cases} \text{stable node} & \text{if} \quad \beta > 1, \\ \text{saddle point} & \text{if} \quad \beta < 1. \end{cases}$

Similarly, for $(0,1)$, from (1.33) we have

$$J(0,1) = \begin{pmatrix} 1-\alpha & 0 \\ -\beta\delta & -\delta \end{pmatrix}; \qquad |J(0,1) - \lambda I| = \begin{vmatrix} (1-\alpha)-\lambda & 0 \\ -\beta\delta & \delta-\lambda \end{vmatrix} = 0,$$

$$\Rightarrow \lambda_1 = 1-\alpha,\ \lambda_2 = -\delta,$$

and thus, $(0,1)$ is a $\begin{cases} \text{stable node} & \text{if} \quad \alpha > 1, \\ \text{saddle point} & \text{if} \quad \alpha < 1, \end{cases}$

Finally, for $(\frac{1-\alpha}{1-\alpha\beta}, \frac{1-\beta}{1-\alpha\beta})$, with α and β chosen so that this point lies in the positive quadrant, we have

$$J(\tfrac{1-\alpha}{1-\alpha\beta}, \tfrac{1-\beta}{1-\alpha\beta}) = \tfrac{1}{1-\alpha\beta} \begin{pmatrix} \alpha-1 & \alpha(\alpha-1) \\ \beta\delta(\beta-1) & \delta(\beta-1) \end{pmatrix},$$

which has eigenvalues

$$\lambda_{1,2} = \tfrac{1}{2(1-\alpha\beta)} \left[(\alpha-1) + \delta(\beta-1) \pm \sqrt{[(\alpha-1)+\delta(\beta-1)]^2 - 4\delta(1-\alpha\beta)(\alpha-1)(\beta-1)} \right].$$

Thus, the sign of λ, or $\mathbf{Re}(\lambda)$ if complex and hence the stability of the steady state

depends on the size of α, β and δ. There are several cases we have to consider, all of which have ecological applications which we come to below.

Ecological considerations:

In terms of the ecology, we understand the four cases as follows:

Case (i): $\alpha < 1$, $\beta < 1$

If the interspecific competition is not too strong the two populations can coexist stably, but at lower populations than their respective carrying capacities, see Figure 1.1(a).

Case (ii): $\alpha > 1$, $\beta > 1$

Interspecific competition is aggressive and ultimately one population wins, while the other is driven to extinction. The winner depends upon which has the starting advantage, see Figure 1.1(b).

Cases (iii) and (iv): $\alpha < 1$, $\beta > 1$ or $\alpha > 1$, $\beta < 1$

Interspecific competition of one species dominates the other and since the stable node in each case globally attracts $\mathbb{R}^2 > 0$, the species with the strongest competition always drives the other to extinction as shown Figure 1.1(c)-(d). These cases illustrate the *competitive exclusion principle* whereby two species competing for the same limited resource cannot in general coexist.

We note again that the steady states (u_*, v_*) of (1.31) provide spatially uniform steady states $(u(x), v(x)) \equiv (u_*, v_*)$ of (1.30).

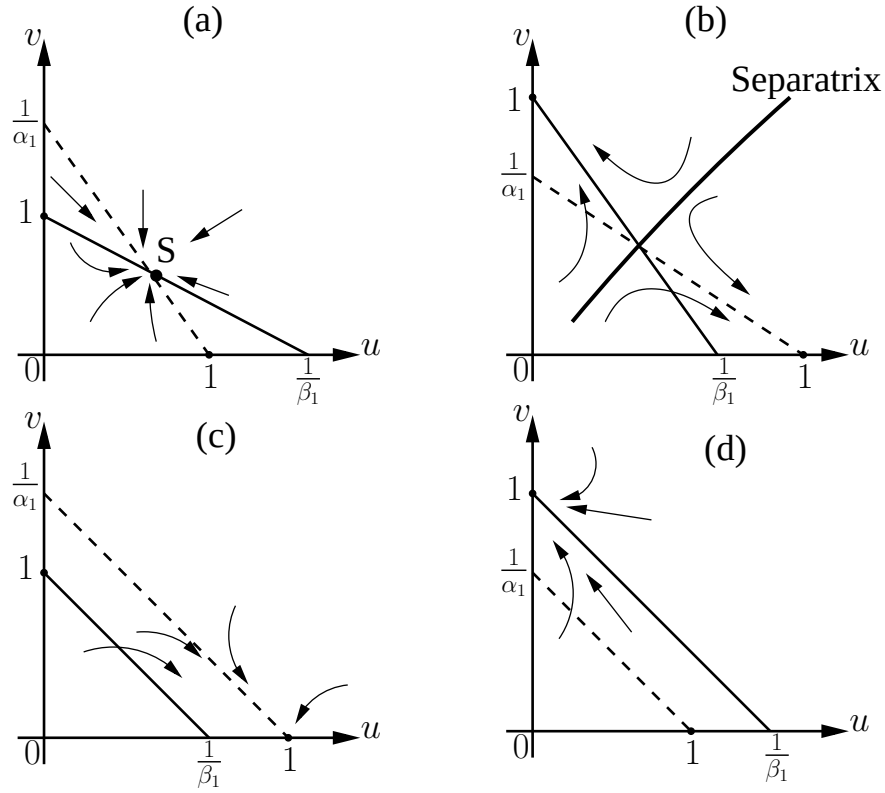

Figure 1.1: Schematic phase trajectories near the steady states for the dynamic behaviour of competing populations satisfying the model (1.30) for the various cases. (a) $\alpha_1 < 1$, $\beta_1 < 1$. Only the positive steady state S is stable and all trajectories tend to it. (b) $\alpha_1 > 1$, $\beta_1 > 1$. Here, $(1, 0)$ and $(0, 1)$ are stable steady states, each of which has a domain of attraction separated by separatrix which passes through $(\frac{1-\alpha}{1-\alpha\beta}, \frac{1-\beta}{1-\alpha\beta})$. (c) $\alpha_1 < 1$, $\beta_1 > 1$. Only one steady state exists, $(1, 0)$ with the whole positive quadrant its domain of attraction. (d) $\alpha_1 > 1$, $\beta_1 < 1$. The only stable steady state is $(0, 1)$ with the positive quadrant as its domain of attraction.

1.2.3 Travelling Wave Solutions

Background

Travelling wave solutions to reaction-diffusion equations have received considerable attention and there is now a vast literature on the mathematical properties and applications of such solutions. Applications include biophysics, ecology,

chemistry, population dynamics, medicine and so on. For examples and reviews see [7, 13, 29, 32, 72, 73, 82, 102].

Recall that travelling wave solutions to (1.30) take the form

$$u(x,t) = u(z),\ v(x,t) = v(z), \quad \text{where} \quad z = x - ct,\ c > 0, \tag{1.34}$$

where c is the wave speed. $u(z)$ and $v(z)$ represent wave solutions of constant shape that travel with the same velocity c. Hence, substituting (1.34) into (1.30), we obtain

$$\begin{aligned} \frac{d^2u}{dz^2} + c\frac{du}{dz} + u(1-u-\alpha v) = 0, \\ D\frac{d^2v}{dz^2} + c\frac{dv}{dz} + \delta v(1-v-\beta u) = 0, \end{aligned} \tag{1.35}$$

In the next section, we will discuss the cases where by varying α and β in equations (1.30) can affect the wave behaviour.

Competitive Effects

To set the scene for later chapters, we begin with an outline study of the effects of varying α and β in (1.30).

- (i) $\alpha < 1$, $\beta < 1$: In the absence of diffusion, it is obvious from the local stability discussed above that system (1.30) has four steady states, which are $(0,0)$ an unstable node, $(0,1)$ and $(1,0)$ saddle points and $(\frac{1-\alpha}{1-\alpha\beta}, \frac{1-\beta}{1-\alpha\beta})$ a stable node. System (1.30) has been discussed extensively and the existence of travelling wave solution to (1.30) that connect two steady states has been proved. In [43], it was proved that a travelling wave solution exists connecting $(0,1)$ with $(\frac{1-\alpha}{1-\alpha\beta}, \frac{1-\beta}{1-\alpha\beta})$ as shown in Figure 1.2 using the method of upper and lower solutions and sliding method to prove the uniqueness of the solution.

  Tang and Fife [92] proved the existence of travelling wave solutions moving from $(0,0)$ to the positive coexistence equilibrium $(\frac{1-\alpha}{1-\alpha\beta}, \frac{1-\beta}{1-\alpha\beta})$ applying

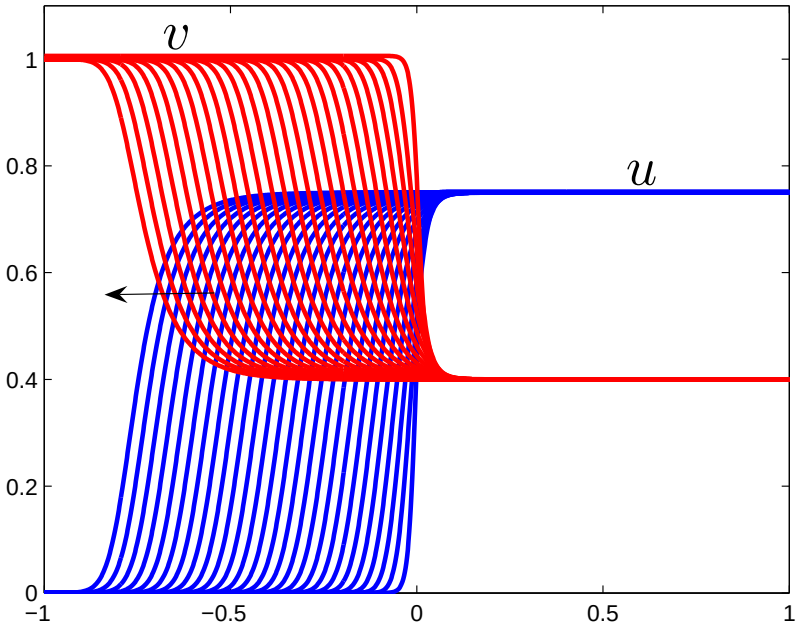

Figure 1.2: Left travelling wave solutions of system (1.30). Here $\alpha = 0.625$, $\beta = 0.8$, $D = 1$, $\delta = 1$ and $\gamma = 10^{-4}$ at $t = [0, 70]$.

the stable-unstable manifold theorem. This was extended to an arbitrary number of interacting populations by Ahmad and Lazer [1] and to more general kinetics by Van Vuuren [106]. By improving the results given in [1] and [92], Ahmad *et al.* [2] showed the existence of travelling front solutions for n species. While in [60], the existence of a travelling wave solution connecting the latter equilibrium points was observed and proved using the Laplace transform.

Not only these possibilities that display travelling wave solutions connecting the steady states where discussed above but there are some other possibilities showing the existence of travelling wave solution. For example, travelling wave solutions from $(0, 0)$ to $(0, 1)$, from $(0, 0)$ to $(1, 0)$, from $(0, 1)$ to $(1, 0)$ or reversely and from $(1, 0)$ to $(\frac{1-\alpha}{1-\alpha\beta}, \frac{1-\beta}{1-\alpha\beta})$ can be obtained.

- (ii) $\alpha > 1$ **and** $\beta > 1$: It is straightforward that (1.30) has exactly two stable, uniform equilibria $(0, 1)$ and $(1, 0)$ and two unstable, uniform equilibria $(0, 0)$ and $(\frac{1-\alpha}{1-\alpha\beta}, \frac{1-\beta}{1-\alpha\beta})$. Conley and Gardner [16], Volpert *et al.* [102] and Kan-On [49] proved the existence of travelling fronts connecting $(0, 1)$ and $(1, 0)$ for (1.30) using different approaches. Figure 1.3 shows right travelling wave solution connecting the rest points $(0, 1)$ and $(1, 0)$.

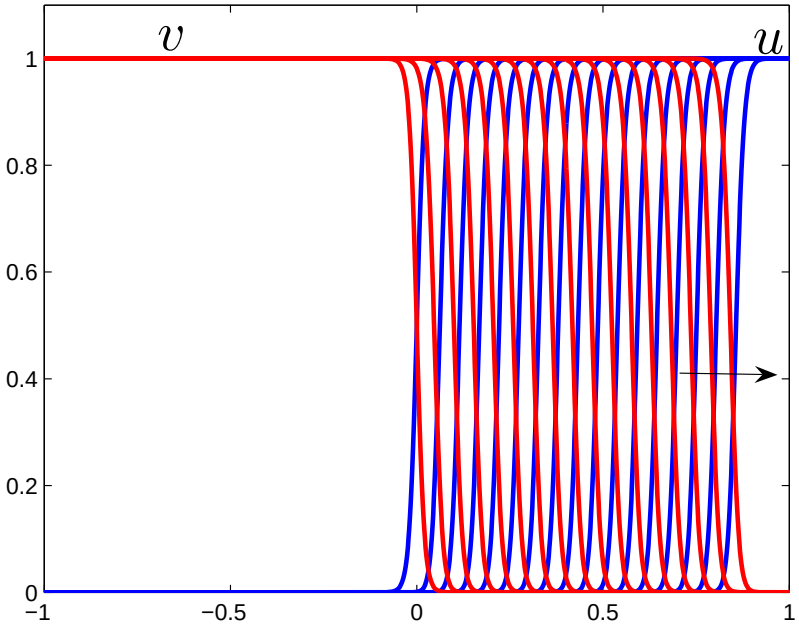

Figure 1.3: Right travelling wave solutions of system (1.30). Here $\alpha = 3$, $\beta = 2$, $D = 1$, $\delta = 1$ and $\gamma = 10^{-4}$ at $t = [0, 320]$.

Furthermore, Hosono and Mimura [42] used the method of singular perturbation to prove the existence of travelling waves for system (1.30) provided $D \ll 1$. While Kanel [50] proved the existence of travelling waves of (1.30) from $(\frac{1-\alpha}{1-\alpha\beta}, \frac{1-\beta}{1-\alpha\beta})$ to $(1, 0)$ with $D \neq 1$ relying essentially on the results of KPP [56]. There are also other possible ways of finding travelling wave solutions to (1.30), specifically connecting $(0, 0)$ to $(1, 0)$, $(0, 0)$ to $(0, 1)$, $(0, 0)$ to $(\frac{1-\alpha}{1-\alpha\beta}, \frac{1-\beta}{1-\alpha\beta})$ or $(\frac{1-\alpha}{1-\alpha\beta}, \frac{1-\beta}{1-\alpha\beta})$ to $(0, 1)$.

- (iii) $\alpha < 1$ **and** $\beta > 1$ or $\alpha > 1$ **and** $\beta < 1$: Under either of these conditions, system (1.30) has three uniform steady states: $(0, 0)$ an unstable node, $(1, 0)$ a stable node (a saddle point for $\alpha > 1$, $\beta < 1$) and $(0, 1)$ a saddle point (a stable node for $\alpha > 1$, $\beta < 1$). The existence of travelling wave solutions connecting $(1, 0)$ and $(0, 1)$ were first discussed by Gardner [27] for slightly different nonlinearities from those in (1.30). Later, Hosono [39, 41] used the singular perturbation method to prove the existence of travelling wave solutions for the latter equilibrium points, see Figure 1.4.

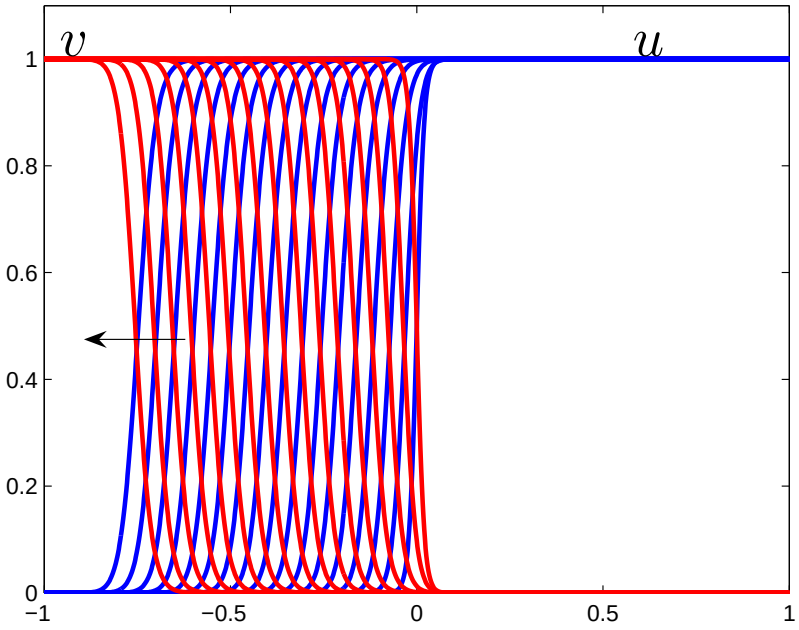

Figure 1.4: Left travelling wave solutions of system (1.30). Here $\alpha = 0.5$, $\beta = 2$, $D = 1$, $\delta = 1$ and $\gamma = 10^{-4}$ at $t = [0, 60]$.

Furthermore, the travelling wave solution connecting the two semi-extinction states were also studied by Hosono [40] supposing $D = 0$ in the second equation of (1.30) using the shooting method. Recently, Leung *et al.* [59] used the method of upper and lower solutions to prove the existence of the travelling wave solution from $(0, 1)$ to $(1, 0)$. They also used the maximum

principle and sliding domain method to derive the uniqueness, strict monotonicity as well as the local stability of the travelling wave solutions when the asymptotic behaviours of the travelling wave solutions are known.

In these cases, there are two possibilities to obtain travelling wave solutions; one from $(0, 0)$ to $(0, 1)$ and from $(0, 0)$ to $(1, 0)$.

Chapter 2

Bounds on the Wave Speed

2.1 Sub- and Super-Solutions

The method of sub-solutions and super-solutions and its associated monotone iteration is a powerful tool in establishing existence results for differential equations. This method can be applied to systems of coupled equations and to equations with nonlinear boundary conditions. The basic idea of this method is to use a sub-solution or super-solution as the initial iteration in a suitable iterative process, so that the resulting sequence of iterations is monotone and converges in some suitable function space to a solution of the problem. The underlying monotone iterative scheme can also be used for the computation of numerical solutions when these equations are replaced by corresponding finite difference equations, see [76]. Note that in some literature sub-solutions and super-solutions are sometimes referred to as lower and upper solutions or sub-functions and super-functions, respectively, see again [76].

Another use of sub-solutions and super-solutions is to obtain bounds for the wave speed of travelling waves. It is this subject that we concentrate on in this chapter.

In [34], Heinze *et al.* stated the following theorem and proved it by considering upper and lower solutions (or left and right solutions as we called them below) of a particular form, as we will discuss below.

Theorem 2.1.1. [34]. *For each fixed $\epsilon > 0$, let $(u_\epsilon, v_\epsilon, c_\epsilon)$ be the unique monotone solution of* (3). *Then*

$$-2\sqrt{L} \leq c_\epsilon \leq 2\sqrt{K}\epsilon, \tag{2.1}$$

where

$$K := \sup_{0<v<1} \frac{g(0,v)}{v} \quad \textit{and} \quad L := \sup_{0<u<1} \frac{f(u,0)}{u}.$$

Note that the upper bound implies that as $\epsilon \to 0$ the only type of travelling waves that can exist are left travelling waves.

Heinze *et al.* [34] choose a specific structure for left and right solutions (which will be discussed below) to obtain these bounds. This structure was introduced with no motivation and also it is not clear whether the wave speed bounds obtained are sharp for the given form. In this chapter we investigate these bounds further for the special case of the CLV kinetics (5).

We are interested in systems that satisfy Assumption 0.0.1. By setting $z = x - ct$ for some constant c, the travelling wave solution of (1), (2) is defined to be a function $(u(z), v(z)) \in [C^2(\mathbb{R})]^2$ that satisfies (3). Alternatively, if we make the substitution $z = x - ct$, but do not assume that the solution is a travelling wave, *i.e.* if we assume (u, v) is of the form $(u(z,t), v(z,t))$, then (1) becomes

$$\begin{aligned} u_t - cu_z - u_{zz} &= f(u,v), \\ v_t - cv_z - \epsilon^2 v_{zz} &= g(u,v). \end{aligned} \tag{2.2}$$

Any solutions $u(z,t)$, $v(z,t)$ of (2.2) provides a solution $u(x,t)$, $v(x,t)$ of (1). Moreover, travelling waves are steady states of this system ($u_t = v_t = 0$). Below, we will apply sub-solution and super-solution techniques (from [76]) to system (2.2).

In order to employ the comparison solutions mentioned above, the following definitions and results given in [76] are required.

Definition 2.1.2. *A function* $Q(u,v) := (f(u,v), g(u,v))$ *is called* quasimonotone nonincreasing *in* $\mathbb{R}^+ \times \mathbb{R}^+$ *if both* $f(u,v)$ *and* $g(u,v)$ *are* quasimonotone nonincreasing *for* $(u,v) \in \mathbb{R}^+ \times \mathbb{R}^+$, *i.e.*

$$\partial f/\partial v \leq 0, \quad \partial g/\partial u \leq 0 \qquad for \qquad (u,v) \in \mathbb{R}^+ \times \mathbb{R}^+.$$

Definition 2.1.3. *If* $Q(u,v) := (f(u,v), g(u,v))$ *is quasimonotone nonincreasing in* $\mathbb{R}^+ \times \mathbb{R}^+$, *then a pair of functions* $\hat{w} = (\hat{u}, \hat{v})$ *and* $\tilde{w} = (\tilde{u}, \tilde{v})$ *are called ordered sub-solution and super-solution of* (2.2) *if they satisfy the relation* $\tilde{w} > \hat{w}$ *and if*

$$\begin{aligned} \tilde{u}_t - \tilde{c}\tilde{u}_z - \tilde{u}_{zz} - f(\tilde{u}, \hat{v}) \geq 0 \geq \hat{u}_t - \hat{c}\hat{u}_z - \hat{u}_{zz} - f(\hat{u}, \tilde{v}), \\ \tilde{v}_t - \tilde{c}\tilde{v}_z - \epsilon^2\tilde{v}_{zz} - g(\hat{u}, \tilde{v}) \geq 0 \geq \hat{v}_t - \hat{c}\hat{v}_z - \epsilon^2\hat{v}_{zz} - g(\tilde{u}, \hat{v}). \end{aligned} \tag{2.3}$$

Note that in this section it is actually combinations of sub-solution and super-solution that are useful in obtaining our results. We therefore make the following definition.

Definition 2.1.4. *We say that* $(\underline{u}, \overline{v})$ *is a* right solution *of* (2.2) *iff* $\underline{u}$ *is a sub-solution and* $\overline{v}$ *is a super-solution. Similarly, we define a* left solution *to be a pair* $(\overline{u}, \underline{v})$ *where* $\overline{u}$ *is a super-solution and* $\underline{v}$ *is a sub-solution. Hence, a direct consequence from the Definition 8.1.2 in* [76] *we have that* $(\underline{u}, \overline{v})$ *is a right solution of* (2.2) *iff it satisfies*

$$\begin{aligned} \hat{u}_t - c_r\hat{u}_z - \hat{u}_{zz} - f(\hat{u}, \tilde{v}) \leq 0, \\ \tilde{v}_t - c_r\tilde{v}_z - \epsilon^2\tilde{v}_{zz} - g(\hat{u}, \tilde{v}) \geq 0, \end{aligned} \tag{2.4}$$

and $(\overline{u}, \underline{v})$ *is a left solution of* (2.2) *iff it satisfies*

$$\begin{aligned} \tilde{u}_t - c_l\tilde{u}_z - \tilde{u}_{zz} - f(\tilde{u}, \hat{v}) \geq 0, \\ \hat{v}_t - c_l\hat{v}_z - \epsilon^2\hat{v}_{zz} - g(\tilde{u}, \hat{v}) \leq 0. \end{aligned} \tag{2.5}$$

In [76], following Theorem 8.3.2 on page 397, we know that if we have a sub-solution and super-solution, then a solution must lie between that sub-solution and super-solution.

In the CLV case, then in the bound (2.1), we have

$$K := \sup_{0<v<1} \delta(1-v) = \delta \quad \text{and} \quad L := \sup_{0<u<1} (1-u) = 1.$$

In this chapter, we will show that these values are optimal for the form of left and right solutions introduced in [34].

In order to do this we reformulate the left and right solutions.

i) ***Right solution***:

Following [34] we define the right solution:

$$\begin{aligned}
\overline{c} &= c_r, \\
\underline{u} &= u_m \max\left\{1 - e^{Fz}, 0\right\}, \\
\overline{v} &= \begin{cases} \min\{v_m e^{Tz}, 1\}, & z \le \frac{M}{\epsilon}, \\ \frac{1}{2}\overline{v}\left(\frac{M}{\epsilon}\right)\left(1 + e^{S(z-\frac{M}{\epsilon})}\right), & z > \frac{M}{\epsilon}, \end{cases}
\end{aligned}$$

where $z \in \mathbb{R}$, $F < 0$, $T < 0$, $S < 0$, $M > 0$ and $c_r \ge 0$ are constants to be defined later and $\epsilon \ge 0$, (see Figure 2.1). We seek values of F, T, S and M, that give the smallest value of c_r, *i.e.* the sharpest right bound on the wave speed.

First, note that $\underline{u}_t = \overline{v}_t = 0$. Hence we must choose u_m and v_m so that $f(\underline{u}, \overline{v}) \ge 0$.

First consider the equation for u. For $z < 0$, $\underline{u} \equiv 0$. Therefore,

$$c_r\, \underline{u}_z + \underline{u}_{zz} + f(\underline{u}, \overline{v}) = 0 = \underline{u}_t.$$

In the case $z > 0$,

$$\underline{u} = u_m \left(1 - e^{Fz}\right).$$

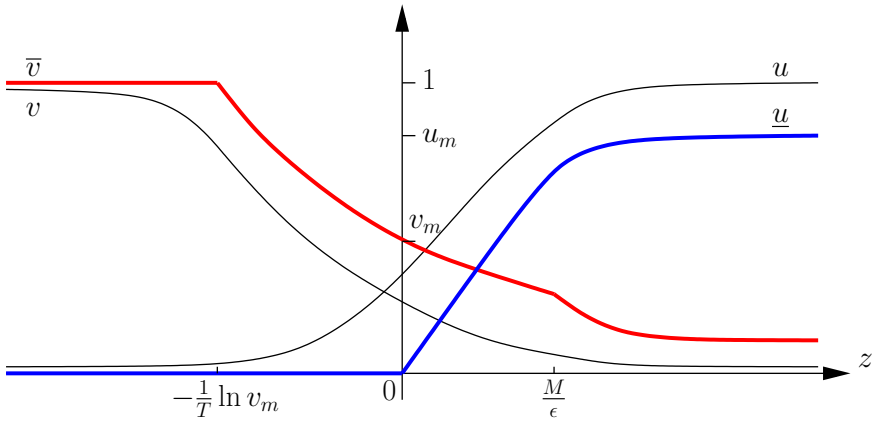

Figure 2.1: The right solution $(\underline{u}, \overline{v})$, shown in (blue, red) and the solution (u, v) of system (2.2) shown in black.

By

$$f(\underline{u}, \overline{v}) = u_m \left(1 - u_m - \frac{\alpha}{2} v_m e^{\frac{TM}{\epsilon}}\right),$$

it follows that $f(\underline{u}, \overline{v}) \geq 0$ because $v_m \in \left(0, \frac{1}{\alpha}(1 - u_m)\right)$. Therefore,

$$\begin{aligned} c_r\, \underline{u}_z + \underline{u}_{zz} + f(\underline{u}, \overline{v}) &\geq c_r\, \underline{u}_z + \underline{u}_{zz} \\ &= c_r \left[-u_m F e^{Fz}\right] + \left[-u_m F^2 e^{Fz}\right] \\ &= -u_m F e^{Fz} \left[c_r + F\right] \\ &\geq 0 = \underline{u}_t, \end{aligned}$$

iff

$$c_r \leq -F. \tag{2.6}$$

Thus, we ensured that the first relation in (2.4) is satisfied.

We can obtain $f(\underline{u}, \overline{v}) \geq 0$ by taking $u_m \in \left(\frac{1}{\beta}, 1\right)$ and $v_m \in \left(0, \frac{1}{\alpha}(1 - u_m)\right)$. Next we check that upon setting $\overline{v} = \frac{1}{2} v_m \left(1 + e^{\frac{TM}{\epsilon}}\right)$ for large positive z, that

$$\lim_{z \to \infty} \overline{v}(z) \in \left(0, \frac{1}{\alpha}\left(1 - u_m\right)\right).$$

Fix F and choose $M > 0$ sufficiently large, such that

$$\underline{u}\left(\frac{M}{\epsilon}\right) = u_m \left(1 - e^{\frac{FM}{\epsilon}}\right) \geq \frac{1}{\beta}. \tag{2.7}$$

Hence, for an appropriately chosen u_m and an arbitrarily chosen F, we require M to be chosen such that

$$M \leq \frac{\epsilon}{F} \ln\left(\frac{\beta u_m - 1}{\beta u_m}\right). \tag{2.8}$$

We now consider the v-equation which ensures the second relation in (2.4) holds. For $z < -\frac{1}{T}\ln v_m$, $\underline{u} \equiv 0$ and $\overline{v} \equiv 1$. Therefore,

$$c_r\,\overline{v}_z + \epsilon^2 \overline{v}_{zz} + g(\underline{u}, \overline{v}) = 0 = \overline{v}_t.$$

For $z > \frac{M}{\epsilon}$

$$\overline{v} = \frac{1}{2}\overline{v}\left(\frac{M}{\epsilon}\right)\left(1 + e^{S\left(z - \frac{M}{\epsilon}\right)}\right) < v_m.$$

Since from equation (2.7), $\underline{u}(z) \geq \underline{u}\left(\frac{M}{\epsilon}\right) \geq \frac{1}{\beta}$ for $z \geq \frac{M}{\epsilon}$. By

$$g(\underline{u}, \overline{v}) = \frac{\delta}{2} v_m e^{\frac{TM}{\epsilon}}\left(1 - \frac{1}{2} v_m e^{\frac{TM}{\epsilon}} - \beta u_m\right),$$

it follows that $g(\underline{u}, \overline{v}) \leq 0$ for any $\overline{v} \geq 0$ because $u_m \in \left(\frac{1}{\beta}, 1\right)$. Therefore,

$$\begin{aligned} c_r\,\overline{v}_z + \epsilon^2 \overline{v}_{zz} + g(\underline{u}, \overline{v}) &\leq c_r\,\overline{v}_z + \epsilon^2 \overline{v}_{zz} \\ &= c_r\left[\frac{1}{2}\overline{v}\left(\frac{M}{\epsilon}\right) S e^{S\left(z - \frac{M}{\epsilon}\right)}\right] + \epsilon^2\left[\frac{1}{2}\overline{v}\left(\frac{M}{\epsilon}\right) S^2 e^{S\left(z - \frac{M}{\epsilon}\right)}\right] \\ &= \frac{1}{2}\overline{v}\left(\frac{M}{\epsilon}\right) S e^{S\left(z - \frac{M}{\epsilon}\right)}\left[c_r + \epsilon^2 S\right] \\ &\leq 0 = \overline{v}_t, \end{aligned}$$

iff

$$c_r \leq -\epsilon^2 S. \tag{2.9}$$

In the case $z < \frac{M}{\varepsilon}$ and $\overline{v} < 1$, *i.e.* $-\frac{1}{T}\ln v_m < z < \frac{M}{\epsilon}$, we have that

$$\overline{v} = v_m e^{Tz}.$$

Note also that for all $0 \leq u, v \leq 1$, $g(u,v) \leq \delta v$. So, in this case,

$$\begin{aligned} c_r\,\overline{v}_z + \epsilon^2 \overline{v}_{zz} + g(\underline{u}, \overline{v}) &\leq c_r\,\overline{v}_z + \epsilon^2 \overline{v}_{zz} + \delta \overline{v} \\ &= c_r[v_m T e^{Tz}] + \epsilon^2[v_m T^2 e^{Tz}] + \delta[v_m e^{Tz}] \\ &= v_m e^{Tz}[\epsilon^2 T^2 + c_r T + \delta] \\ &\leq 0 = \overline{v}_t, \end{aligned}$$

iff $\epsilon^2 T^2 + c_r T + \delta \leq 0$. By solving this quadratic equation, we get $T_- \leq T \leq T_+$ where

$$T_\pm = \frac{1}{2\epsilon^2}\left[-c_r \pm \sqrt{c_r^2 - 4\epsilon^2\delta}\right].$$

We need $T_\pm$ real so the smallest c_r can be is $2\epsilon\sqrt{\delta}$ at which point $T_+ = T_- = -\frac{c_r}{2\epsilon^2} = -\frac{\sqrt{\delta}}{\epsilon}$.

Also, as from (2.6) and (2.9) we require $c_r \leq \min\{-F, -\epsilon^2 S\}$, we may set $-F = -\epsilon^2 S = c_r$, *i.e.* $F = -2\epsilon\sqrt{\delta}$ and $S = -\frac{2\sqrt{\delta}}{\epsilon}$. Finally, M is given by (2.8) and hence we find that the choice of u_m and v_m and thus M does not affect the wave speed. Hence, we have shown that the right solution

$$\begin{aligned} c_r &= 2\epsilon\sqrt{\delta}, \\ \underline{u} &= u_m \max\left\{1 - e^{-2\epsilon\sqrt{\delta}z}, 0\right\}, \\ \overline{v} &= \begin{cases} \min\left\{v_m e^{-\frac{\sqrt{\delta}}{\epsilon}z}, 1\right\}, & z \leq \frac{M}{\epsilon}, \\ \frac{1}{2}\overline{v}\left(\frac{M}{\epsilon}\right)\left(1 + e^{-2\frac{\sqrt{\delta}}{\epsilon}(z - \frac{M}{\epsilon})}\right), & z > \frac{M}{\epsilon}, \end{cases} \end{aligned}$$

is in some sense optimal: c_r is an upper bound for the wave speed of travelling waves of (1) and $2\epsilon\sqrt{\delta}$ is the lowest upper bound in this case. Note that for any $\epsilon > 0$ the profile $(\underline{u}, \overline{v})$ remains in both components at a positive distance from $S_+ = (1,0)$ for all $z > 0$. Furthermore, $(\underline{u}, \overline{v})(z) = (0,1)$ for all $z < 0$. Thus, any initial data (u_0, v_0) of problem (2.2) with $(u_0, v_0)(z) \to (1,0)$ as $z \to \infty$ can be shifted to be comparable with $(\underline{u}, \overline{v})$. This implies that no travelling wave solution of (3) can travel at speeds faster than the comparison solution, *i.e.* $c_\epsilon \leq c_r = 2\epsilon\sqrt{\delta}$.

ii) ***Left solution***.

Following [34] we define the left solution:

$$\begin{aligned} \underline{c} &= c_l, \\ \overline{u} &= \begin{cases} \min\left\{u_m e^{Rz}, 1\right\}, & z \geq -M, \\ \frac{1}{2}\overline{u}(-M)\left(1 + e^{P(z+M)}\right), & z < -M, \end{cases} \\ \underline{v} &= v_m \max\{1 - e^{Qz}, 0\}, \end{aligned} \tag{2.10}$$

as shown in Figure 2.2, where $R > 0$, $P > 0$, $Q > 0$, $M > 0$ and $c_l \leq 0$ are constants to be determined. We seek values of R, P, Q and M, that give the smallest value of c_l, *i.e.* the sharpest left bound on the wave speed.

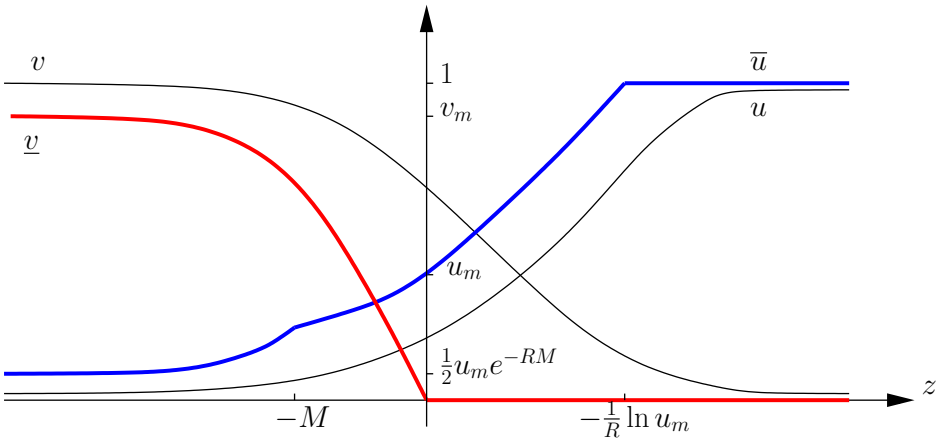

Figure 2.2: The left solution $(\overline{u}, \underline{v})$, shown in (blue, red) and the solution (u, v) of system (2.2) shown in black.

First, note that $\overline{u}_t = \underline{v}_t = 0$. Hence we must choose u_m and v_m so that $g(\overline{u}, \underline{v}) \geq 0$.

We have $g(\overline{u}, \underline{v}) = \delta v_m \left(1 - v_m - \frac{\beta}{2} u_m e^{-RM}\right)$, it follows that $g(\overline{u}, \underline{v}) \geq 0$ by taking $v_m \in \left(\frac{1}{\alpha}, 1\right)$ and $u_m \in \left(0, \frac{1}{\beta}(1 - v_m)\right)$. Next we check that upon setting $\overline{u} = \frac{1}{2} u_m \left(e^{-RM}\right)$ for large negative z, that

$$\lim_{z \to -\infty} \overline{u}(z) \in \left[0, \frac{1}{\beta}(1 - v_m)\right].$$

Fix Q and choose $M > 0$ sufficiently large, such that

$$\underline{v}(-M) = v_m \left(1 - e^{-QM}\right) \geq \frac{1}{\alpha}. \tag{2.11}$$

Hence, for an appropriately chosen v_m and an arbitrarily chosen Q, we require M to be chosen such that

$$M \geq \frac{1}{Q} \ln \left(\frac{\alpha v_m}{\alpha v_m - 1} \right). \tag{2.12}$$

Equations (2.10) describe a left solution if we can find the constants R, P, Q and M satisfy system (2.10) and $M > 0$ such that $(\overline{u}, \underline{v}, c_l)$.

Next we ensure that the first relation in (2.5) is satisfied. First consider the u-equation. For $z > -\frac{1}{R} \ln u_m$, $\overline{u} \equiv 1$ and $\underline{v} \equiv 0$. Therefore,

$$c_l \, \overline{u}_z + \overline{u}_{zz} + f(\overline{u}, \underline{v}) = 0 = \overline{u}_t.$$

If $z < -M$ and M is sufficiently large, we have

$$\overline{u} = \frac{1}{2} \overline{u}(-M) \left(1 + e^{P(z+M)}\right) < u_m. \tag{2.13}$$

Since $f(\overline{u}, \underline{v}) = \overline{u}(1 - \overline{u} - \alpha \underline{v})$ and $\underline{v}(z) \geq \underline{v}(-M) \geq \frac{1}{\alpha}$ from equation (2.11) for $z \leq -M$, so $f(\overline{u}, \underline{v}) = \frac{1}{2} u_m e^{-RM} \left(1 - \frac{1}{2} u_m e^{-RM} - \alpha v_m\right) \leq 0$ because $v_m \in \left(\frac{1}{\alpha}, 1\right)$. We deduce that

$$\begin{aligned} c_l \, \overline{u}_z + \overline{u}_{zz} + f(\overline{u}, \underline{v}) &\leq c_l \, \overline{u}_z + \overline{u}_{zz} \\ &= c_l \left[\frac{1}{2} \overline{u}(-M) P e^{P(z+M)} \right] + \left[\frac{1}{2} \overline{u}(-M) P^2 e^{P(z+M)} \right] \\ &= \frac{1}{2} \overline{u}(-M) P e^{P(z+M)} \left[c_l + P \right] \\ &\leq 0 = \overline{u}_t, \end{aligned}$$

iff

$$c_l \leq -P. \tag{2.14}$$

For $z > -M$ and $\overline{u} < 1$, it follows that

$$\overline{u} = \min \left\{ u_m e^{Rz}, 1 \right\} = u_m e^{Rz}.$$

Also, for all $0 \leq u, v \leq 1$, $f(u,v) \leq u$. Hence in this case,

$$\begin{aligned} c_l\,\overline{u}_z + \overline{u}_{zz} + f(\overline{u},\underline{v}) &\leq c_l\,\overline{u}_z + \overline{u}_{zz} + \overline{u} \\ &= c_l\left[u_m R e^{Rz}\right] + \left[u_m R^2 e^{Rz}\right] + \left[u_m e^{Rz}\right] \\ &= u_m e^{Rz}\left[R^2 + c_l R + 1\right] \\ &\leq 0 = \overline{u}_t, \end{aligned}$$

iff $R^2 + c_l R + 1 \leq 0$. Solving this quadratic inequality, yields $R_- \leq R \leq R_+$ where

$$R_\pm = \frac{1}{2}\left[-c_l \pm \sqrt{c_l^2 - 4}\right].$$

As we are seeking $c_l \leq 0$, this requires $c_l \leq -2$. The sharpest left solution is therefore $c_l = -2$, and in this case $R = 1$.

Now consider the v-equation to ensure that the second relation (2.5) is satisfied. For $z > 0$, $\underline{v} \equiv 0$ so

$$c_l\,\underline{v}_z + \epsilon^2 \underline{v}_{zz} + \delta\underline{v}(1 - \overline{v} - \beta\overline{u}) = 0 = \underline{v}_t.$$

For $z < 0$, we have

$$\underline{v} = v_m(1 - e^{Qz}).$$

By the choice of u_m and v_m, $g(\overline{u},\underline{v}) = \delta v_m\left(1 - v_m - \frac{\beta}{2}u_m e^{-RM}\right) \geq 0$, because $u_m \in \left(0, \frac{1}{\beta}(1 - v_m)\right)$ Hence, we get

$$\begin{aligned} c_l\,\underline{v}_z + \epsilon^2\underline{v}_{zz} + g(\overline{u},\underline{v}) &\geq c_l\,\underline{v}_z + \epsilon^2\underline{v}_{zz} \\ &= c_l\left[-v_m Q e^{Qz}\right] + \epsilon^2\left[-v_m Q^2 e^{Qz}\right] \\ &= -v_m Q e^{Qz}\left[c_l + \epsilon^2 Q\right] \\ &\geq 0 = \overline{v}_t, \end{aligned}$$

iff

$$c_l \leq -\epsilon^2 Q. \tag{2.15}$$

From (2.14) and (2.15), we now establish an upper bound for c_l, we therefore require

$$c_l \leq \min\{-P, -\epsilon^2 Q\}$$

Therefore, the sharpest left solution for the wave speed that can be obtained with this form of left solution is $c_l = -2$. Hence, we have shown that the left solution

$$\begin{aligned} c_l &= -2, \\ \overline{u} &= \begin{cases} \min\{u_m e^z, 1\}, & z \geq -M, \\ \frac{1}{2}\overline{u}(-M)\left(1 + e^{2(z+M)}\right), & z < -M, \end{cases} \\ \underline{v} &= \max\{v_m\left(1 - e^{\frac{2}{\epsilon^2}z}\right), 0\}, \end{aligned}$$

is in some sense optimal, where M is given by (2.12).

Hence, c_l is a lower bound for the wave speed of travelling waves of (1) and -2 is the largest lower bound in this case. Since $\overline{u}$ and $\underline{v}$ are uniformly bounded away from 0 and 1, respectively, and $(\overline{u}, \underline{v})(z) = (1, 0)$ for $z > 0$ we can always shift initial data (u_0, v_0) of problem (2.2) with $(u_0, v_0)(z) \to (1, 0)$ for $z \to -\infty$ to be comparable with the left solution. We conclude $c_\epsilon \geq c_l = -2$.

2.2 Conclusion

In this chapter, we demonstrated that, for the CLV case at least, the bounds of the wave speed given in [34] are optimal for the given left and right solution pair. We have tried to find other right and left solutions in order to improve the bounds on the wave speed that is stated in Theorem 2.1.1. However, we could not find an alternative that would allow for the kind of explicit calculations done above. Notwithstanding this, the fact that the wave speed must be ≤ 0 in the limit as $\epsilon \to 0$ and that $c_\epsilon \leq C.\epsilon$ for some positive constant C for $\epsilon > 0$, will be very useful in the results to come.

Chapter 3

Travelling Waves in Near-Degenerate Bistable Competition Models

3.1 Introduction

Results from this chapter form part of the publication [5]. The aim of this chapter is to develop an understanding of the relationship between the solutions of the system

$$\begin{aligned} -cu' &= u'' + f(u,v), \\ -cv' &= \epsilon^2 v'' + g(u,v), \\ (u,v)(-\infty) = S_-, &\quad (u,v)(\infty) = S_+. \end{aligned} \tag{3.1}$$

and those of the reduced or degenerate problem

$$\begin{aligned} -cu' &= u'' + f(u,v), \\ -cv' &= g(u,v), \\ (u,v)(-\infty) = S_-, &\quad (u,v)(\infty) = S_+. \end{aligned} \tag{3.2}$$

Given its singular nature, it is not surprising that the solutions to (3.2), denoted here by (u_0, v_0, c_0), may have quite different regularity properties to those of (3.1) (see [33, 34]). Therefore, it is not obvious *a priori* how the solutions of (3.1) behave in the limit as $\epsilon \to 0$ or how any such limit is related to (u_0, v_0, c_0). In the following, we establish this connection.

Singular limit problems in systems of reaction-diffusion equations is a subject which has received considerable interest, particularly using methods of singular perturbation theory (see *e.g.* [39, 42] and the references therein). However, these papers have in general focused on the construction of solutions via asymptotic expansions while in [5] the regularity of the solutions in the limit is discussed. Regularity of solutions of such limiting problems has again attracted considerable previous interest and most relevant to the work presented here are the methods for dealing with partially degenerate equations as developed by [51, 52, 53] (see also [30, 97]). The systems of equations studied in these latter papers are much larger than that considered here and contain kinetics of a different type.

For scalar bistable reaction-diffusion equations, it is well-known that the sign of the wave speed is determined by the sign of the integral of the reaction function over a certain interval. This integral forms part of an energy function for the scalar equation (see *e.g.* p175 *et seq.* in [23]). For systems of bistable equations, the situation is far more complex and to date, no general energy function has been derived. However, in [33, 34] a potential for the reduced system (3.2) was introduced as follows.

Suppose (u, v) is a solution of (3.2), then define the function $h(u, v)$ by

$$[h(u_0, v_0)](z) = -\int_0^{u_0(z)} f(\sigma, v_0(z))d\sigma - \int_{v_0(z)}^1 \int_0^{\Gamma(\tau)} f_v(\sigma, \tau)d\sigma d\tau, \quad z \in \mathbb{R}, \tag{3.3}$$

where, as detailed above, Γ is given by $g(\Gamma(\tau), \tau) = 0$, for $0 < \tau < 1$. After a little manipulation, it can be shown that $[h(1, 0)](z) \equiv h(S_+)$ where, if Γ is monotone,

$$h(S_+) = -\left(\int_0^{\hat{u}} f(\sigma, \hat{\gamma}(\sigma))d\sigma + \int_{\hat{u}}^1 f(\sigma, 0)d\sigma\right) = -\int_0^1 f(\sigma, \gamma(\sigma))d\sigma \tag{3.4}$$

and more easily that $[h(0,1)](z) \equiv h(S_-) = 0$. It is shown in [34] that the sign of $h(S_+) - h(S_-) = h(S_+)$ determines the direction of the wave and the regularity of the solution. A key point here is that for any given kinetics f and g, the potential $h(S_+)$ can be directly computed without knowledge of the solutions. To assist the reader, we include the key results concerning such solutions, that will be referenced below. The proofs can be found in [33] and [34].

Theorem 3.1.1. *Suppose f and g satisfy Assumption* 0.0.1*.*

(i) If $h(S_+) < 0$, then there exists a monotone solution (u_0, v_0, c_0) to (3.2) *with $c_0 < 0$ and $(u_0, v_0) \in C^2(\mathbb{R}) \times C^1(\mathbb{R})$. If $c_0 > 0$, then no monotone solution to* (3.2) *exists.*

(ii) If $h(S_+) \geq 0$, then there exists a monotone solution (u_0, v_0, c_0) to (3.2) *with $c_0 = 0$. In this case, v_0 has a unique singularity at z^*, say, and $u_0(z) = \Gamma(v_0)(z)$ for $z \leq z^*$ and $v_0 \equiv 0$ otherwise. Hence, whilst $u_0 \in C^1(\mathbb{R})$, v_0 is only continuous if $h(S_+) = 0$ and only bounded if $h(S_+) > 0$. However, away from this point, (u_0, v_0) is in $[C^2(\mathbb{R}\backslash z^*)]^2$. If $c_0 \neq 0$, then no monotone solution to* (3.2) *exists.*

In both cases, these solutions correspond to monotone travelling waves for (1)*,* (2) *with $\epsilon = 0$, that are unique up to translation.*

A schematic representation of the $c_0 = 0$ solution is given in Figure 3.1. The singularity is at the point $(u^*, v^*) =: (u_0(z^*), v_0(z^*))$. As detailed in [34], finding such a solution is equivalent to finding the (unique) positive solution of the function equation $A(u^*) = 0$ (will be detailed later).

3.2 Near Degenerate Case

Unfortunately, it is straightforward to show that (3.3) does not form a suitable potential for the more general problem (3.1). In this chapter, we construct an

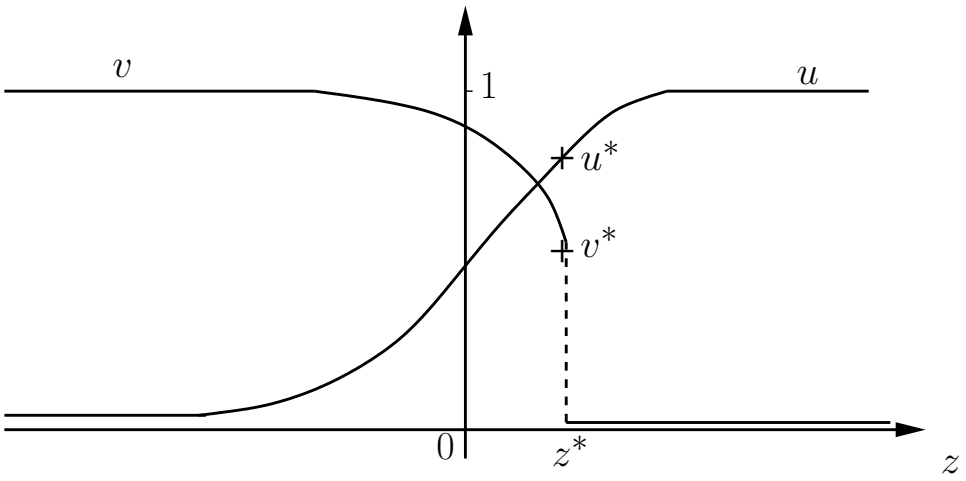

Figure 3.1: Schematic representation of the $c_0 = 0$ solution to the reduced problem (3.2).

alternative and relate it to the definition (3.3). Thus, at least for ϵ sufficiently small, we show that the direction of travelling wave solutions for the general competitive bistable system (1) can be determined directly from the kinetics of the problem.

3.2.1 Convergence in the limit $\epsilon \to 0$

Much of the work done in [5] concerns the following convergence result, which relates the regularity of solutions of (3.1) to the regularity of solutions to the degenerate problem.

Theorem 3.2.1. *Suppose that* $(u_\epsilon, v_\epsilon, c_\epsilon)$ *is a classical component-wise monotone solution of* (3.1) i.e. $u_\epsilon, v_\epsilon \in C^2(\mathbb{R})$, $u'_\epsilon(z) > 0 > v'_\epsilon(z)$ *for* $z \in \mathbb{R}$. *Let* (u_0, v_0, c_0) *denote the monotone solution of* (3.2) *as detailed above. Then, we have the following convergence results.*

(i) If $\lim_{\epsilon \to 0} c_\epsilon \neq 0$, *then after suitable translation,* $(u_\epsilon, v_\epsilon) \to (u_0, v_0)$ *uniformly on any closed interval of* $\mathbb{R}$.

(ii) If $\lim_{\epsilon\to 0} c_\epsilon = 0$*, then after suitable translation,* $(u_\epsilon, v_\epsilon) \to (u_0, v_0)$ *where the convergence is uniform on any closed interval in* $\mathbb{R} \setminus z^*$*.*

The proof can be found in [5]. Here we use this result to discuss the relationship between the wave speeds of the degenerate and non-degenerate problems.

Recall that for a sequence $\{f_n\}$ of functions, $f_n : \mathbb{R} \to \mathbb{R}$. Then f_n tends pointwise to f on $D \subset \mathbb{R}$ if for each fixed $x \in D$, $\lim_{n\to\infty} f_n(x) = f(x)$. f_n tends uniformly to f on D if $\lim_{n\to\infty} ||f_n - f|| = 0$ where $||f|| = \sup_{x\in D} |f(x)|$.

The important property of uniform convergence that we use in the following is that if $f_n \xrightarrow{uniformly} f$, then $\lim_{n\to\infty} \int_a^b f_n(x)dx = \int_a^b f(x)dx$.

In Section 3.3, we construct a free energy function for the general problem (3.1) and show how it can be used to determine the sign of c for any $\epsilon > 0$. Finally, using the convergence results developed in Section 3.3 in [5], the relationship between this new, general free energy function and the function given in (3.3) for the reduced problem is established. In Section 3.4, condition (4) of Assumption 0.0.1 is relaxed to include a class of non-monotone functions g.

3.3 Computing the sign of the wave speed

As detailed in the Introduction, when $\epsilon > 0$, (3.3) does not form a free energy function for (3.1). We now construct a suitable alternative and use it to determine the direction of the travelling wave solutions in the general case.

We begin by assuming the existence of a suitable energy function for (3.1) in order to demonstrate how it relates to the wave direction.

Lemma 3.3.1. *Fix* $\epsilon > 0$*. Let* (u, v, c) *be the corresponding monotone solution of* (3.1)*. Let*

$$F_\epsilon(u, v) := -\frac{1}{2}(u')^2 - \frac{1}{2}(\epsilon v')^2 + H_\epsilon(u, v), \tag{3.5}$$

where

$$\nabla H_\epsilon(u,v) = (-f(u,v), -g(u,v))^T. \tag{3.6}$$

Then,

$$\text{sign}\left(\frac{d}{dz}F_\epsilon\right) = \text{sign}\left(H_\epsilon(S_+) - H_\epsilon(S_-)\right) = \text{sign}(c).$$

Proof. The proof is straightforward. By differentiating F_ϵ wrt z and using (3.1), it follows that

$$\begin{aligned} F_\epsilon'(u,v) &= -u'u'' - \epsilon^2 v'v'' + (H_\epsilon)_u u' + (H_\epsilon)_v v' \\ &= -u'\left(u'' + f(u,v)\right) - v'\left(\epsilon^2 v'' + g(u,v)\right) \\ &= c((u')^2 + (v')^2). \end{aligned}$$

Therefore,

$$\begin{aligned} c\int_{\mathbb{R}} ((u')^2 + (v')^2)dz &= \int_{\mathbb{R}} F_\epsilon'(u,v)dz \\ &= F_\epsilon(u(z), v(z)) \Big|_{-\infty}^{\infty} = H_\epsilon(S_+) - H_\epsilon(S_-) \end{aligned}$$

and the results follow directly. □

The next result determines a class of functions that satisfy the required conditions on H_ϵ. For each fixed ϵ, define $P_\epsilon : [0,1] \to [0,1]$ be the one-to-one function defined by $P_\epsilon(1) = 0$, $P_\epsilon(0) = 1$, $P_\epsilon(u(z)) = v(z)$, $z \in \mathbb{R}$, where $(u(z), v(z), c)$ is the monotone solution of (3.1). (That is $v = P_\epsilon(u)$ is the unique monotone solution trajectory in the (u,v)-plane, parameterized by z and joining $(0,1)$ with $(1,0)$, which represents the travelling wave solution with speed c.) For ease of exposition let $(P_\epsilon)^{-1} \equiv Q_\epsilon$. Note that the convergence results given in Theorem 3.2.1 ensure that for ϵ sufficiently small, the solution path $v = P_\epsilon(u)$ is close to the solution path $v = P_0(u)$ for the degenerate problem (3.2). To assist the subsequent discussions, a schematic representation of this relationship and to the path $v = \gamma(u)$ is given in Figure 3.2. In the case $h(S_+) = 0$, all three paths coincide.

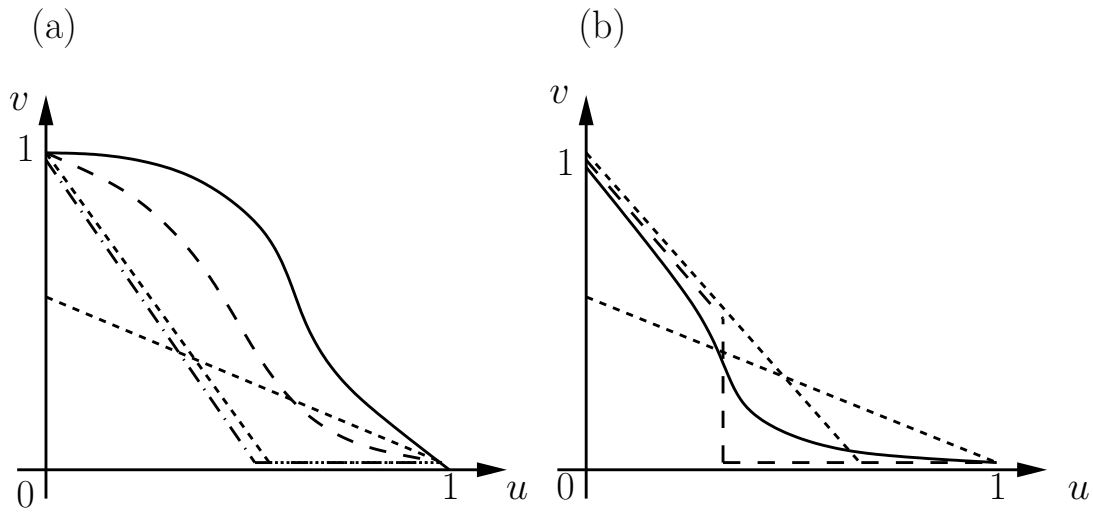

Figure 3.2: Schematic representation of the solutions paths $v = P_\epsilon(u)$ (solid line) and $v = P_0(u)$ (dashed line) in the cases (a) $h(S_+) < 0$; (b) $h(S_+) > 0$. The nullclines (dotted lines) are shown as straight lines for ease of visualisation and the path $v = \gamma(u)$ is shown in (a) (dot-dashed line).

Let $(\phi, \psi) \in [C^2(\mathbb{R})]^2$, $(\phi, \psi) : \mathbb{R} \to [0,1]^2$ and for each fixed ϵ, define $H_\epsilon(\phi, \psi)$ by

$$\begin{aligned}[H_\epsilon(\phi,\psi)](z) &= -\int_0^{\phi(z)} f(\sigma, \psi(z))d\sigma - \int_1^{\psi(z)} g(\phi(z), \tau)d\tau \\ &\quad - \int_{\psi(z)}^1 \int_0^{Q_\epsilon(\tau)} f_v(\sigma,\tau)d\sigma d\tau + \int_0^{\phi(z)} \int_1^{P_\epsilon(\sigma)} g_u(\sigma,\tau)d\tau d\sigma.\end{aligned} \tag{3.7}$$

Lemma 3.3.2. *The function H_ϵ defined in* (3.7) *satisfies the condition* (3.6) *required in Lemma 3.3.1. Moreover,*

$$[H_\epsilon(S_+)](z) \equiv H_\epsilon(S_+) = -\int_0^1 f(\sigma, P_\epsilon(\sigma))d\sigma + \int_0^1 g(Q_\epsilon(\tau), \tau)d\tau \tag{3.8}$$

and $H_\epsilon(S_-) = 0$ for all $\epsilon > 0$.

Proof. It follows directly from (3.7), that

$$\frac{\partial}{\partial\phi}\left(H_\epsilon(\phi,\psi)\right) = -f(\phi,\psi) - \int_1^{\psi} g_u(\phi,\tau)d\tau + \int_1^{P_\epsilon(\phi)} g_u(\phi,\tau)d\tau.$$

If $(\phi,\psi) = (u,v)$, the monotone solution of (3.1), then the first component of (3.6) follows from the identity $v = P_\epsilon(u)$. Also,

$$\frac{\partial}{\partial\psi}\left(H_\epsilon(\phi,\psi)\right) = -\int_0^{\phi} f_v(\sigma,\psi)d\sigma - g(\phi,\psi) + \int_0^{Q_\epsilon(\psi)} f_v(\sigma,\psi)d\sigma.$$

Again, if $(\phi,\psi) = (u,v)$, the monotone solution of (3.1), then the second component of (3.6) follows from the identity $u = Q_\epsilon(v)$. Next,

$$\begin{aligned}[H_\epsilon(S_+)](z) \equiv H_\epsilon(1,0) &= -\int_0^1 f(\sigma,0)d\sigma - \int_1^0 g(1,\tau)d\tau \\ &\quad -\int_0^1\int_0^{Q_\epsilon(\tau)} f_v(\sigma,\tau)d\sigma d\tau + \int_0^1\int_1^{P_\epsilon(\sigma)} g_u(\sigma,\tau)d\tau d\sigma.\end{aligned}$$

By changing the order of integration and recalling that $(P_\epsilon)^{-1} = Q_\epsilon$, it follows that

$$\begin{aligned}H_\epsilon(1,0) &= -\int_0^1 f(\sigma,0)d\sigma - \int_1^0 g(1,\tau)d\tau \\ &\quad -\int_0^1 \Big(\ f(\sigma,P_\epsilon(\sigma)) - f(\sigma,0)\ \Big)d\sigma + \int_1^0 \Big(\ g(1,\tau) - g(Q_\epsilon(\tau),\tau)\ \Big)d\tau \\ &= -\int_0^1 f(\sigma,P_\epsilon(\sigma))d\sigma + \int_0^1 g(Q_\epsilon(\tau),\tau)d\tau\end{aligned}$$

as required.

Finally, $H_\epsilon(S_-) = 0$ follows directly from the definition of H_ϵ. This scaling is obtained without loss of generality. □

Lemma 3.3.3.

$$\operatorname{sign}\left(-\int_0^1 f(\sigma,P_\epsilon(\sigma))d\sigma\right) = \operatorname{sign}\left(\int_0^1 g(Q_\epsilon(\tau),\tau)d\tau\right) = \operatorname{sign}(c).$$

Proof. Multiplying the first and second equations in (3.1) by u' and v', respectively and integrating over $\mathbb{R}$ yields

$$-c\int_{\mathbb{R}}(u')^2dz = \int_{\mathbb{R}} u''u'dz + \int_{\mathbb{R}} f(u,v)u'dz = \int_0^1 f(\sigma,P_\epsilon(\sigma))d\sigma$$

and

$$-c\int_{\mathbb{R}}(v')^2dz = \int_{\mathbb{R}} \epsilon^2 v''v'dz + \int_{\mathbb{R}} g(u,v)v'dz = \int_1^0 g(Q_\epsilon(\tau),\tau)d\tau.$$

The result follows immediately. □

These results can be summarised as follows:

Theorem 3.3.4. *For each fixed $\epsilon > 0$, let $(u_\epsilon, v_\epsilon, c_\epsilon)$ be the corresponding monotone solution of* (3.1)*. Let $H_\epsilon(\phi, \psi)$ be defined as in* (3.7)*. Then,*

$$H_\epsilon(S_+) > 0 \iff c_\epsilon > 0, \quad H_\epsilon(S_+) < 0 \iff c_\epsilon < 0, \quad H_\epsilon(S_+) = 0 \iff c_\epsilon = 0.$$

Remark 3.3.5. *The Maxwell Curve. It is clear that $H_\epsilon(S_+) = H_\epsilon(S_+, \mathbf{\Lambda})$ where $\mathbf{\Lambda}$ is the vector of the system parameters. With the functional forms fixed, $H_\epsilon(S_+, \mathbf{\Lambda}) = 0$ defines a relationship between ϵ and $\mathbf{\Lambda}$. Under certain genericity conditions, this defines a curve in $\epsilon - \mathbf{\Lambda}$ plane. We call this the Maxwell Curve for* (1)*, following the definition of the Maxwell Curve for 4th order problems see* e.g. *[62] and the references therein.*

The definition of the potential H_ϵ gives a formal way of determining the wave speed, although it is an implicit function of the solution itself. It would seem then that to compute the wave speed for any given problem, would therefore require (at least an approximate) evaluation of the solution. However, using the definition of the potential given in [34], the definition introduced here in (3.7) and the limiting arguments given in [5], we now show that the sign of the wave speed can be computed directly, at least for the case ϵ sufficiently small but non-zero, using only information directly related to the functions f and g. This result is particularly powerful in the case where $c_0 = 0$, *i.e.* the wave speed of the degenerate problem is zero. In this case, the sign of the wave speed for the ϵ-small case is entirely unclear. Indeed, in the section 3.4, where non-monotone functions g are considered, we show that in this case, the ϵ-small wave speed can be either positive or negative.

Theorem 3.3.6. *Let $H_\epsilon(S_+)$ be given as in* (3.8)*. Then, there exists a number $H_0(S_+)$ such that $\lim_{\epsilon \to 0} H_\epsilon(S_+) = H_0(S_+)$ but $H_0(S_+) \neq h(S_+)$ in general. However,*
(i) $h(S_+) < 0 \implies H_0(S_+) < 0$,

(ii) $h(S_+) = 0 \implies H_0(S_+) = 0,$

(iii) $h(S_+) > 0 \implies H_0(S_+) > 0.$

Proof. (i) If $h(S_+) < 0$, then Theorem 3.1.1 *(i)* ensures $c_0 < 0$ and thus that $g(u_0, v_0) < 0$ (apart from the end points where $g(S_\pm) = 0$). By Theorem 3.2.1 it follows that $f(., P_\epsilon(.)) \to f(., P_0(.))$ and $g(Q_\epsilon(.), .) \to g(Q_0(.), .)$ uniformly $[0,1] \times [0,1]$ as $\epsilon \to 0$, where $v = P_0(u)$ (alt. $u = Q_0(v)$) is the trajectory in the $(u, v)-$plane representing the solution (u_0, v_0) to (3.2). Hence, we may pass directly to the limit in (3.8) to yield

$$\begin{aligned}\lim_{\epsilon\to 0} H_\epsilon(S_+) &= \lim_{\epsilon\to 0}\left(-\int_0^1 f(\sigma, P_\epsilon(\sigma))d\sigma + \int_0^1 g(Q_\epsilon(\tau), \tau)d\tau\right)\\ &= -\int_0^1 f(\sigma, P_0(\sigma))d\sigma + \int_0^1 g(Q_0(\tau), \tau)d\tau =: H_0(S_+).\end{aligned}$$

From Lemma 3.3.3 and as $g(Q_0(\tau), \tau) < 0$, $\tau \in (0,1)$, it follows that $H_0(S_+) < 0$.

(ii) If $h(S_+) = 0$, then by Theorem 3.1.1 *(ii)* the solution v_0 is continuous at z^* as defined above but not differentiable. Moreover, in this case $c_0 = 0$ and the solution path is defined by $g(Q_0(\tau), \tau) = 0$ for $\tau \in [0,1]$. Hence, arguing as above, we may pass directly to the limit in (3.8) and $H_0(S_+) = 0$.

(iii) Finally, if $h(S_+) > 0$, then from Theorem 3.1.1 *(ii)* , v_0 has a unique discontinuity at $z = z^*$. Hence, from (3.8), and for any $\delta > 0$,

$$\begin{aligned}\lim_{\epsilon\to 0} H_\epsilon(S_+) &= \lim_{\epsilon\to 0}\left(-\int_0^1 f(\sigma, P_\epsilon(\sigma))d\sigma + \int_0^1 g(Q_\epsilon(\tau), \tau)d\tau\right)\\ &= -\lim_{\epsilon\to 0}\left(\int_0^{u^*-\delta} + \int_{u^*-\delta}^{u^*+\delta} + \int_{u^*+\delta}^1 f(\sigma, P_\epsilon(\sigma))d\sigma\right)\\ &\quad + \lim_{\epsilon\to 0}\left(\int_0^{\delta} + \int_{\delta}^{v^*-\delta} + \int_{v^*-\delta}^{v^*+\delta} + \int_{v^*+\delta}^1 g(Q_\epsilon(\tau), \tau)d\tau\right),\end{aligned} \tag{3.9}$$

where $(u^*, v^*) = (u_0(z^*), v_0(z^*))$. The uniformity of the limit away from $z = z^*$

ensures that

$$\begin{aligned} - & \lim_{\epsilon\to 0}\left(\int_0^{u^*-\delta} + \int_{u^*+\delta}^1 f(\sigma, P_\epsilon(\sigma))d\sigma\right) + \lim_{\epsilon\to 0}\left(\int_{v^*+\delta}^1 g(Q_\epsilon(\tau),\tau)d\tau\right) \\ = & -\left(\int_0^{u^*-\delta} + \int_{u^*+\delta}^1 \lim_{\epsilon\to 0} f(\sigma, P_\epsilon(\sigma))d\sigma\right) + \left(\int_{v^*+\delta}^1 \lim_{\epsilon\to 0} g(Q_\epsilon(\tau),\tau)d\tau\right) \\ = & -\left(\int_0^{u^*-\delta} + \int_{u^*+\delta}^1 f(\sigma, P_0(\sigma))d\sigma\right) + \left(\int_{v^*+\delta}^1 g(Q_0(\tau),\tau)d\tau\right). \end{aligned} \tag{3.10}$$

This holds for any $\delta > 0$ and all integrals are well-defined. Hence on taking the limit as $\delta \to 0$, (3.10) equates to

$$-\int_0^1 f(\sigma, P_0(\sigma))d\sigma + \int_{v^*}^1 g(Q_0(\tau),\tau)d\tau. \tag{3.11}$$

However, from the proof of Theorem 2.1 in [33], it follows directly that,

$$-\int_0^1 f(\sigma, P_0(\sigma))d\sigma = 0.$$

Moreover, on $[v^*, 1]$, $Q_0(v) = \hat{\gamma}(v)$ and hence $g(Q_0(\tau),\tau) = 0$. Hence, (3.11) equates to zero.

Also,

$$\left|\left(\int_{u^*-\delta}^{u^*+\delta} f(\sigma, P_\epsilon(\sigma))d\sigma\right)\right| \leq 2\delta \max_{(\sigma,\tau)\in[0,1]^2} |f(\sigma,\tau)| \tag{3.12}$$

and

$$\left|\left(\int_0^{\delta} + \int_{v^*-\delta}^{v^*+\delta} g(Q_\epsilon(\tau),\tau)d\tau\right)\right| \leq 3\delta \max_{(\sigma,\tau)\in[0,1]^2} |g(\sigma,\tau)|. \tag{3.13}$$

These bounds are independent of ϵ and consequently the limits (as $\epsilon \to 0$) of these integrals tend to zero on taking the limit as $\delta \to 0$. Hence, for any $\delta > 0$, we have from (3.9) that

$$\lim_{\epsilon\to 0} H_\epsilon(S_+) = \lim_{\epsilon\to 0} \int_\delta^{v^*-\delta} g(Q_\epsilon(\tau),\tau)d\tau.$$

But for any $\delta > 0$, $Q_\epsilon(.) \to u^*$ uniformly in $[\delta, v^* - \delta]$ and hence $g(Q_\epsilon(.),.)$ converges uniformly on $[\delta, v^* - \delta]$ to $g(u^*,.)$. Hence, on taking the limit as $\delta \to 0$, yields

$$\lim_{\epsilon\to 0} H_\epsilon(S_+) = \int_0^{v^*} g(u^*,\tau)d\tau =: H_0(S_+).$$

However,

$$\int_0^{v^*} g(u^*, \tau) d\tau > 0$$

because the path $u = u^*$, $v \in [0, v^*]$ lies below the g nullcline in the $(u, v)-$plane and hence $g > 0$ by Assumption 0.0.1. Thus, $H_0(S_+) > 0$ in this case.

Finally, recall that the curves in the $(u, v)-$plane described by $v = P_0(u)$ and $v = \gamma(u)$ are not the same in general (see Figure 3.2(b)). Hence, $H_0(S_+) \neq h(S_+)$ apart from when they are both zero. This completes the proof.

□

Remark 3.3.7. *From Theorem 3.1.1 it follows that $h(S_+) > 0$ implies that $c_0 = 0$. Also, Theorem 3.3.6 states that $h(S_+) > 0 \implies H_0(S_+) > 0$ and from Theorem 3.3.4 (and Lemma 3.3.3) we would therefore expect $c_0 > 0$. This apparent contradiction can be resolved by reconsidering the proof of Lemma 3.3.3, which is only true for each fixed $\epsilon > 0$. On taking the limit as $\epsilon \to 0$, we need to reconsider the boundedness of all terms. The following result clarifies the situation and leads to a better understanding of the formation of the singularity in the $v-$component of the solution.*

Lemma 3.3.8. *If $h(S_+) > 0$, then $c_\epsilon \to 0$ and $\int_{\mathbb{R}} (v_\epsilon')^2 dz \to \infty$ as $\epsilon \to 0$.*

Proof. Similar to the proof of Lemma 3.3.3, from the $u-$equation in (3.1), it follows that

$$c_\epsilon \int_{\mathbb{R}} (u_\epsilon')^2 dz = -\int_0^1 f(\sigma, P_\epsilon(\sigma)) d\sigma.$$

As detailed in the proof of Theorem 3.3.6, it follows that if $h(S_+) > 0$ then the right hand side tends to zero as $\epsilon \to 0$. Also, by Lemma 8 in [5] equation (2.3) , and following arguments similar to those in the proof of Lemma 7 in [5], for any closed interval $D \subset \mathbb{R} \setminus z^*$,

$$\int_{\mathbb{R}} (u_\epsilon')^2 dz \geq \int_D (u_\epsilon')^2 dz \to \int_D (u_0')^2 dz > 0,$$

with positivity following directly from the construction of u_0. This implies $c_\epsilon \to 0$. Moreover, from the $v-$equation in (3.1), it follows that

$$c_\epsilon \int_{\mathbb{R}} (v_\epsilon')^2 dz = \int_0^1 g(Q_\epsilon(\tau), \tau) d\tau.$$

Again, the proof of Theorem 3.3.6 reveals that the limit of the right hand side is strictly positive. Thus,

$$\int_{\mathbb{R}} (v_\epsilon')^2 dz > \frac{K}{c_\epsilon}$$

for some $K > 0$, independent of ϵ. The result follows on taking the limit as $\epsilon \to 0$.

□

Finally, the above results can be summarised as follows. This theorem links the energy function derived in [34] for the reduced problem (3.2) to the direction of travelling waves in the general problem (3.1), at least for ϵ sufficiently small. Recall that given any problem of the form (3.1), the energy function $h(S_+)$ can be computed directly from the kinetics and does not require *a priori* knowledge of the solutions.

Theorem 3.3.9. *Let $(u_\epsilon, v_\epsilon, c_\epsilon)$ be a component-wise monotone solution of* (3.1)*.*
(i) If $h(S_+) < 0$ then for ϵ sufficiently small, $c_\epsilon < 0$ and $c_\epsilon \to c_0 < 0$ as $\epsilon \to 0$.
(ii) If $h(S_+) > 0$ then for ϵ sufficiently small $c_\epsilon > 0$ and $c_\epsilon \to 0$ as $\epsilon \to 0$, and $\lim_{\epsilon \to 0} \|v_\epsilon'\|_{L^2(\mathbb{R})} = \infty$.

Remark 3.3.10. *In the case that $h(S_+) = 0$, numerical integration suggests that $H_\epsilon(S_+) > 0$ and hence $c_\epsilon > 0$ for $0 < \epsilon << 1$. However a proof of this result has yet to be obtained and remains an open problem.*

3.4 Non-monotone nullclines

In this section we relax condition (4) of Assumption 0.0.1 to include a class of non-monotone functions g. In particular, we replace (4) by

(4*) The non-trivial solutions (u, v) of $g(u, v) = 0$ are given by $u = \Gamma(v)$, for a continuous function $\Gamma : [0, 1] \to [0, \infty)$ with $\Gamma(1) = 0$ and $\Gamma(0) = \hat{u}$, where $0 < \hat{u} < 1$. Moreover, $\Gamma'(v) = 0$ implies Γ has a local maximum.

This case is also considered in [34] and we follow the constructions given there. The assumptions on f are unchanged (note that f could also be similarly non-monotone). A sketch of a typical g-nullcline satisfying (4*) is given in Figure 3.3, where the points u_1 and v_1 are identified by

$$u_1 = \min\left\{1, \sup_{\tau\in(0,1)} \Gamma(\tau)\right\}, \quad v_1 := \gamma_m(u_1),$$

where γ_m is the unique maximal inverse of Γ, *i.e.* $\gamma_m(0) = 1$ and

$$\gamma_m(\sigma) := \max_{\tau\in(0,1)} \{\Gamma(\tau) = \sigma\}.$$

Note that γ_m is monotone decreasing on $(0, u_1)$.

Clearly, functions that satisfy (4*) also satisfy (4). As the latter case has already been covered, in the following we focus on kinetics for which Γ is non-monotone, *i.e.* $u_1 > \hat{u}$.

In [34], a functional $A(u)$ is defined by

$$\begin{aligned} A(u) &:= h(1,0) - h(u,0) + h(u,\gamma_m(u)) \\ &= -\int_0^u f(\sigma,\gamma_m(\sigma))d\sigma - \int_u^1 f(\sigma,0)d\sigma. \end{aligned} \tag{3.14}$$

Proof. Using the definition of $h(u, v)$ stated in (3.4),

$$\begin{aligned} A(u) &= -\int_0^1 f(\sigma,0)d\sigma - \int_0^1\int_0^{\Gamma(\tau)} f_v(\sigma,\tau)d\sigma d\tau + \int_0^u f(\sigma,0)d\sigma \\ &\quad + \int_0^1\int_0^{\Gamma(\tau)} f_v(\sigma,\tau)d\sigma d\tau - \int_0^u f(\sigma,\gamma_m(u))d\sigma - \int_{\gamma_m(u)}^1\int_0^{\Gamma(\tau)} f_v(\sigma,\tau)d\sigma d\tau \\ &= -\int_u^1 f(\sigma,0)d\sigma - \int_0^u f(\sigma,\gamma_m(u))d\sigma - \underbrace{\int_{\gamma_m(u)}^1\int_0^{\Gamma(\tau)} f_v(\sigma,\tau)d\sigma d\tau}_{\mathbf{I}}. \end{aligned}$$

We need to solve the double integral **I** separately.

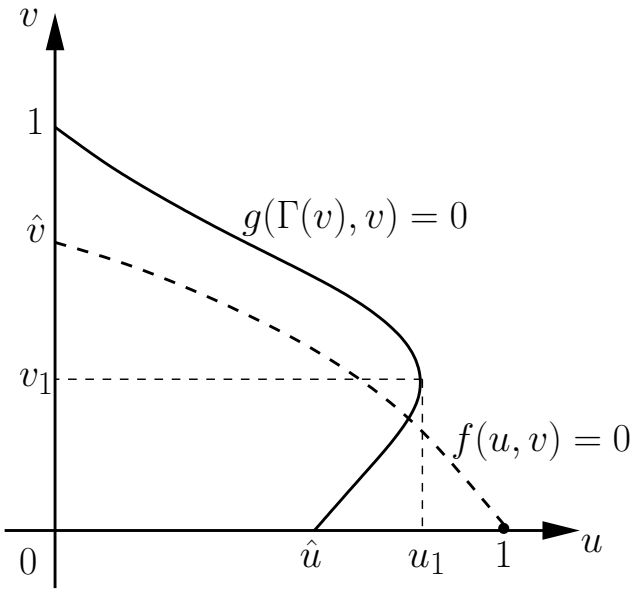

Figure 3.3: Schematic representation of the nullcline $f = 0$ and $g = 0$ satisfying Assumption 0.0.1 with (4) replaced by (4*). The maximum of Γ occurs at v_1 with $u_1 = \Gamma(v_1) > \hat{u}$.

$$\mathbf{I} = \int_{\gamma_m(u)}^{1} \int_{0}^{\Gamma(\tau)} f_v(\sigma, \tau) d\sigma d\tau,$$

with aid of Figure 3.4, we change the order of the integrals, then we obtain

$$\begin{aligned} \mathbf{I} &= \int_0^u \int_{\gamma_m(u)}^{\gamma_m(\sigma)} f_v(\sigma, \tau) d\tau d\sigma \\ &= \int_0^u f(\sigma, \gamma_m(\sigma)) d\sigma - \int_0^u f(\sigma, \gamma_m(u)) d\sigma. \end{aligned}$$

Hence,

$$\begin{aligned} A(u) &= -\int_u^1 f(\sigma, 0) d\sigma - \int_0^u f(\sigma, \gamma_m(u)) d\sigma - \int_0^u f(\sigma, \gamma_m(\sigma)) d\sigma \\ &\quad + \int_0^u f(\sigma, \gamma_m(u)) d\sigma \\ &= -\int_0^u f(\sigma, \gamma_m(\sigma)) d\sigma - \int_u^1 f(\sigma, 0) d\sigma. \end{aligned}$$

□

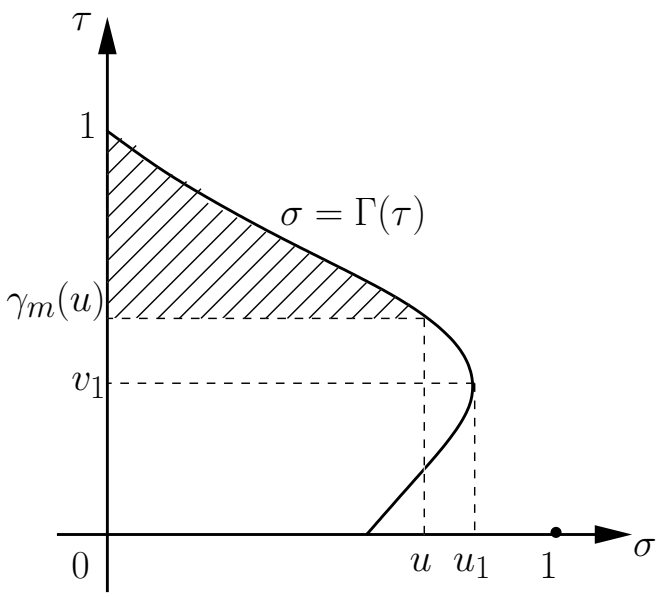

Figure 3.4: Schematic representation of the nullcline g satisfying Assumption 0.0.1 with condition (4^*). The dashed area where we change the order of integrals of **I**.

To assist the reader and for ease of reference, we include the key results concerning such solutions. The proofs can be found in [33] and [34].

Theorem 3.4.1. [33, 34] *Suppose f and g satisfy Assumption 0.0.1.*

(i) If $A(u_1) < 0$, then there exists a monotone solution (u_0, v_0, c_0) to (3.2) with $c_0 < 0$ and $(u_0, v_0) \in C^2(\mathbb{R}) \times C^1(\mathbb{R})$. If $c_0 > 0$, then no monotone solution to (3.2) exists.

(ii) If $A(u_1) \geq 0$, then there exists a monotone solution (u_0, v_0, c_0) to (3.2) with $c_0 = 0$. In this case, $u_0 = \gamma(v_0)$, v_0 has a unique singularity at z^*, say, and hence whilst $u_0 \in C^1(\mathbb{R})$, v_0 is only continuous if $A(u_1) = 0$ and only bounded if $A(u_1) > 0$. However, away from this point, (u_0, v_0) is in $[C^2(\mathbb{R} \setminus z^*)]^2$. If $c_0 \neq 0$, then no monotone solution to (3.2) exists.

Note that if Γ is monotone decreasing in v, then $u_1 = \hat{u}$, $v_1 = 0$ and $A(u_1) =$

$h(1,0) = h(S_+)$. Hence, Theorem 3.4.1 holds with $A(u_1)$ replaced by $h(S_+)$ and the result recovers the physically intuitive notion that the direction of the wave is mediated by the relative energies of the asymptotic states $S_\pm$, *i.e.* the wave direction is determined by the sign of $h(S_+) - h(S_-) = h(S_+)$.

A key point here is that for any given kinetics f and g, the potential $h(S_+)$ and therefore the functional A can be directly computed without knowledge of the solutions.

If $u_1 = 1$, then

$$A(1) = A(u_1) = -\int_0^1 f(\sigma, \gamma_m(\sigma))d\sigma > 0.$$

With (4*) replacing (4), all the results in Theorem 3.1.1 hold with $A(u_1)$ replacing $h(S_+)$. (Note that under condition (4), $u_1 = \hat{u}$, $v_1 = 0$ and $A(u_1) = h(1,0) = h(S_+)$.) Thus in the case $A(u_1) < 0$, the solution (u_0, v_0, c_0) is classical and $c_0 < 0$. In the case $A(u_1) \geq 0$, the solution (u_0, v_0, c_0) has $c_0 = 0$ and a unique discontinuity at $(u_0, v_0)(z^*) = (u^*, v^*)$, with $u^* \leq u_1$ for $u_1 < 1$. The value u^* is the unique positive solution to $A(u^*) = 0$. Finally, as shown in [34], $A'(u) > 0$.

It is straightforward to show that the convergence results proved in Theorem 3.2.1 here also hold with (4*) replacing (4). (In [5] Lemmas 6-9 follow without alteration. Lemma 10 requires extra cases to be considered but the method of proof and results are unaltered.) Similarly, the definition of the energy function H_ϵ given in (3.8) and the relationship between $H_\epsilon(S_+)$ and the wave speed c_ϵ as detailed in Theorem 3.3.4 are unaltered.

It remains to discuss the relationship between the energy function H_ϵ defined here and that defined in [34]. This result requires one further definition.

Definition 3.4.2. *Define* $\underline{u} \in (\hat{u}, 1]$ *by* $\underline{u} := \min\{s, 1\}$ *where* s *is the unique*

solution of $G(s) = 0$, *where*

$$G(u) := \int_0^{\gamma_m(u)} g(u,\tau)d\tau.$$

Remark 3.4.3. *It is clear by the definition of* $\hat{u}$, *conditions (3) and* (4^*) *in Assumption 0.0.1, that* $G(\hat{u}) > 0$, *and the existence of the unique value* $\underline{u}$ *follows by the continuity of* g *and for* $u \in (\hat{u}, u_1)$,

$$\begin{aligned} G'(u) &= \gamma_m'(u)g(u,\gamma_m(u)) + \int_0^{\gamma_m(u)} g_u(u,\tau)d\tau \\ &= \int_0^{\gamma_m(u)} g_u(u,\tau)d\tau < 0. \end{aligned}$$

Note also that the definition of $\underline{u}$ *does not require a formal extension of the definition of* g *for values of* $s > 1$. *For if* $G(1) > 0$, *then* $\underline{u} = 1$ *and the value of* s *is redundant.*

We now have the following result that replaces Theorem 3.3.6 above.

Theorem 3.4.4. *Suppose that Assumption 0.0.1 holds with* (4) *replaced by* (4^*). *Let* $H_\epsilon(S_+)$ *be given as in* (3.8). *Then there exists a number* $H_0(S_+)$ *such that* $\lim_{\epsilon\to 0} H_\epsilon(S_+) = H_0(S_+)$. *Moreover,*
(i) If $A(\underline{u}) < 0$ *then* $H_0(S_+) < 0$,

(ii) If $A(\underline{u}) = 0$ *then* $H_0(S_+) = 0$,

(iii) If $A(\underline{u}) > 0$ *then* $H_0(S_+) > 0$.

Proof. Case *(i)*: $A(\underline{u}) < 0$. We have two cases to consider. (a) Suppose $A(u_1) \geq 0$. Then as $A'(u) > 0$ and $A(u^*) = 0$, by definition $\underline{u} < u^* \leq u_1$. Since $G(\underline{u}) = 0$ and $G'(u) < 0$, it follows that $G(u^*) < 0$ and applying the arguments in the proof of Theorem 3.3.6*(i)* yields $H_0(S_+) < 0$. (b) Suppose $A(u_1) < 0$, then the arguments in the proof of Theorem 3.3.6*(i)* can be applied unaltered and again $H_0(S_+) < 0$.

Case *(ii)*: $A(\underline{u}) = 0$. Then $\underline{u} = u^* < u_1$ and $G(u^*) = 0$. We can apply the

arguments in the proof of Theorem 3.3.6*(ii)* to yield $H_0(S_+) = 0$.
Case *(iii)*: $A(\underline{u}) > 0$. Then as $A'(u) > 0$, if follows that $\underline{u} > u^*$ and thus $G(u^*) > 0$ and again we can apply the arguments in the proof of Theorem 3.3.6*(iii)* to yield $H_0(S_+) > 0$. □

In one easily-verified case, the sign of the limit is straightforward to compute. The proof follows from similar arguments to those used in Case *(ii)* above.

Corollary 3.4.5. *If* $G(1) \geq 0$ *then* $H_0(S_+) > 0$.

Finally, we can relate the value of the energy function for the degenerate problem to the wave speed of the problem considered here. The proof follows directly from the arguments in the proof of Theorem 3.4.4.

Theorem 3.4.6. *Let* $(u_\epsilon, v_\epsilon, c_\epsilon)$ *be be a component-wise monotone solution of* (3.1). *If* ϵ *is sufficiently small and*
(i) $A(\underline{u}) < 0 \leq A(u_1)$ *then* $c_\epsilon < 0$ *and* $c_\epsilon \to 0$ *as* $\epsilon \to 0$.
(ii) $0 < A(\underline{u}) \leq A(u_1)$ *then* $c_\epsilon > 0$ *and* $c_\epsilon \to 0$ *as* $\epsilon \to 0$.
(iii) $A(u_1) < 0$ *then* $c_\epsilon < 0$ *and* $c_\epsilon \to c_0 < 0$ *as* $\epsilon \to 0$.

An alternative formulation to Theorem 3.4.6 that directly uses the definition of G given above is as follows:

Theorem 3.4.7. *Let* $(u_\epsilon, v_\epsilon, c_\epsilon)$ *be a component-wise monotone solution of* (3.1).
(i) If $A(u_1) < 0$ *then for* ϵ *sufficiently small,* $c_\epsilon < 0$ *and* $c_\epsilon \to c_0 < 0$ *as* $\epsilon \to 0$.
(ii) If $A(u_1) \geq 0$ *and* $G(u^*) > 0$ *then for* ϵ *sufficiently small,* $c_\epsilon > 0$ *and* $c_\epsilon \to 0$ *as* $\epsilon \to 0$.
(iii) If $A(u_1) \geq 0$ *and* $G(u^*) < 0$ *then for* ϵ *sufficiently small,* $c_\epsilon < 0$ *and* $c_\epsilon \to 0$ *as* $\epsilon \to 0$.

3.5 Conclusion

We conclude that the values $\underline{u}, u_1$ and u^* and thus the values $A(\underline{u})$, $A(u_1)$ and $G(u^*)$ can be directly computed using only the properties of the reaction terms f and g. Thus, as with the monotone case, the sign of the wave speed of the full problem can be directly computed using only knowledge of these kinetics, at least for ϵ sufficiently small. However, as in the monotone case, the sign of the wave speed c_ϵ in the critical case $A(\underline{u}) = 0$ (alt. $G(u^*) = 0$) remains an open question.

The function F defined in (3.5) provides a measure of the energy associated with system (3.1). (A similar expression can be formulated for the system (1).) From the proof of Lemma 3.3.1, it follows that if $c_\epsilon \to 0$ as $\epsilon \to 0$ (*i.e.* in the case where v_0 has a discontinuity at $z = z^*$), then $F'_\epsilon \to 0$ pointwise on $\mathbb{R}\backslash z^*$. Therefore, as $\epsilon \to 0$, the total change in the energy F (given by $H_\epsilon(S_+)$) over $\mathbb{R}$ is compressed to a discontinuous jump at the point z^*. The size of this discontinuity is equal to $H_0(S_+) = G(u^*)$.

Note that in the case Γ is monotone decreasing, $G(u^*) \geq 0$ and therefore, the results (i) and (ii) here are direct generalisations of the monotone cases covered in Theorem 3.4.1 (i) and (ii). Theorem 3.4.7 (iii) relates only to the non-monotone case. The critical cases $h(S_+) = 0$ (resp. $G(u^*) = 0$) will be discussed in the next chapter.

Chapter 4

Reversing Invasion in Bistable Systems

The results in this chapter form the work in [4]. In this chapter, we will consider a particular problem with relevance to many applications in population dynamics. Essentially, we study how the interplay of relative motility and competitive strength can cause waves of invasion to be halted and reversed.

The energy function (3.7) computed in Chapter 3 for the general problem (2.3) and the energy function (3.3) for the reduced problem (3.2) play an important role in determining the wave direction as we have seen in the last chapter.

These results suggest that as we increase ϵ, the regions for which right travelling wave (RTW) and left travelling wave (LTW) exist are separated by what we call the "Maxwell Curve" $H_\epsilon(S_+) = 0$ on which standing waves exist. We will further investigate this threshold standing wave (SW) case by means of numerical simulations of certain particular examples.

In Subsection 4.1.1, we will build a better understanding of how the wave speeds associated with solutions to (3.1) relate to those of (3.2) using the singular perturbation method.

In Subsection 4.1.2, we compute for the CLV problem the energy function

$h(S_+)$. Moreover, we show that $h(S_+)$ depends essentially on the competition rates α and β and hence we can study the effect of varying $h(S_+)$ by varying either α or β. Numerical results suggest that points in the $h(S_+) - \epsilon^2$ which correspond to SW, form a curve which asymptotes as ϵ^2 gets large. Hence, in Subsection 4.1.3, we discuss the wave behaviour for CLV where ϵ is large, *i.e.* D^2 is small in equations (4.13), by first calculating $k(S_+)$ in the CLV case.

4.1 Building a Picture of Motility vs Competition

The results in the previous chapter detail a rigorous way of relating wave direction of the full problem (3.1) to that associated with the degenerate system (3.2) in the case where ϵ is sufficiently small. We now show that the degenerate problem and a related mirror problem seem to completely determine the wave direction in the general case.

4.1.1 Singular Perturbation

We start by using singular perturbation arguments to provide a rough, but more readily accessible understanding of how the wave speeds associated with solutions to (3.1) relate to those of (3.2).

A singular perturbation is a modification of a given partial differential equation obtained by adding a small multiple ϵ times a higher order term. In accordance with the informal principle that the behaviour of solutions is governed primarily by the highest order terms, a solution u_ϵ of the perturbed problem will often behave analytically quite differently from a solution u of the original problem. More precisely, a singular perturbation problem is a problem containing a small parameter that cannot be approximated by setting the parameter value to

zero. This is in contrast to regular perturbation problems, for which an approximation can be obtained by simply setting the small parameter to zero, see [23, 37] for more details. The overall procedure for doing singular perturbation work is always

1. Develop an appropriate scaling for the equations and identify the small parameters.

2. Find the outer solution.

3. Find the inner solution.

4. Match up the two solutions in an intermediate time range.

Thus, taking $\epsilon \to 0$ changes the very nature of the problem. In the case of differential equations, for example, boundary conditions cannot be satisfied or the regularity of the solution changes, for further reading see [35].

These formal arguments follow along similar lines to those presented in [75], which were applied to a different problem, and [39, 42] for the system under consideration. Of particular importance is that they shine some light on the special case $h(S_+) = 0$ (resp. $G(u^*) = 0$) for monotone (resp. non-monotone) kinetics. It has been established that solutions of the type $(u_0, v_0, 0)$ exist for a range of kinetic functions f and g, in fact all such functions for which the condition $A(u_1) \geq 0$ is satisfied. Moreover, it has been shown that $c_\epsilon \to 0$ as $\epsilon \to 0$ again for all kinetics provided $A(u_1) \geq 0$ (and provided $G(u^*) \neq 0$). Hence, the following question arises. How do the solutions $(u_\epsilon, v_\epsilon, c_\epsilon = 0)$ relate to the solutions $(u_0, v_0, 0)$? In particular, as ϵ gets small, what form do the solutions $(u_\epsilon, v_\epsilon, c_\epsilon = 0)$ take?

Standing wave solutions $(u_\epsilon, v_\epsilon, c_\epsilon)$ of (3.1) satisfy $c_\epsilon = 0$ and

$$\begin{aligned} 0 &= u'' + f(u,v), \\ 0 &= \epsilon^2 v'' + g(u,v), \\ (u,v)(-\infty) &= S_-, \quad (u,v)(\infty) = S_+. \end{aligned} \tag{4.1}$$

For ϵ small, the solutions undergo a rapid change in the region around the point z^*, which marks the discontinuity of the $\epsilon = 0$ solution. Away from this region, the solutions changes smoothly. Following a standard approach, we therefore seek solutions close to and away from this boundary layer.

Let us first consider the outer region, which is to the right of the discontinuity. Let $(u, v, c) = (u_0^r + \epsilon u_1^r + O(\epsilon^2), v_0^r + \epsilon v_1^r + O(\epsilon^2), 0)$. Then, on substitution into (4.1), and equating zeroth order terms immediately yields $g(u_0^r, v_0^r) = 0$. Therefore, $v_0^r = 0$ or $v_0^r = \gamma(u_0^r)$. The right asymptotic condition requires $(u_0^r, v_0^r)(z) \to (1, 0)$ as $z \to \infty$. It follows from the definition of Γ and monotonicity that $v_0^r(z) \equiv 0$.

Hence, u_0^r must satisfy

$$\begin{aligned} \frac{d^2 u_0^r}{dz^2} + f(u_0^r, 0) = 0, \quad z > z^*, \\ \lim_{z\to\infty} u_0^r(z) = 1 \end{aligned} \tag{4.2}$$

and hence $u_0^r = u_0$ on $[z, \infty)$ for any $z > z^*$. On multiplying the first equation in (4.2) by du_0/dz, integrating over $[z, \infty)$ and applying the right boundary condition yields

$$-\frac{1}{2}\left(\frac{du_0}{dz}(z)\right)^2 + \int_{u_0^r(z)}^1 f(u, 0)du = 0. \tag{4.3}$$

In a similar manner, a left outer solution $(u, v, c) = (u_0^l + \epsilon u_1^l + O(\epsilon^2), v_0^l + \epsilon v_1^l + O(\epsilon^2), 0)$ can be constructed and shown to satisfy $g(u_0^l, v_0^l) = 0$. The left asymptotic condition requires $(u_0^l, v_0^l)(z) \to (0, 1)$ as $z \to -\infty$. Therefore following

similar arguments to above, $v_0^l = \Gamma^{-1}(u_0^l)$ and u_0^l satisfies

$$\begin{aligned} \frac{d^2u_0^l}{dz^2} + f(u_0^l, \Gamma^{-1}(u_0^l)) = 0, \quad z < z^*, \\ \lim_{z\to-\infty} u_0^l(z) = 0 \end{aligned} \tag{4.4}$$

and hence $u_0^l = u_0$ on $(-\infty, z]$ for any $z < z^*$. Making this substitution and following similar procedures as above, we get

$$\frac{1}{2}\left(\frac{du_0}{dz}(z)\right)^2 + \int_0^{u_0^l(z)} f(u, \Gamma^{-1}(u))du = 0. \tag{4.5}$$

We now consider the behaviour close to the singularity. Let $z - z^* = \epsilon y$. Then, it is straightforward to show that (4.1) can be rewritten in terms of the new independent variable y as

$$\begin{aligned} 0 &= \frac{d^2u}{dy^2} + \epsilon^2 f(u, v), \\ 0 &= \frac{d^2v}{dy^2} + g(u, v). \end{aligned} \tag{4.6}$$

We now seek an inner solution of the form $(u, v, c) = (U_0 + \epsilon U_1 + O(\epsilon^2), V_0 + \epsilon V_1 + O(\epsilon^2), 0)$. Substituting into (4.6) and equating coefficients of ϵ^0 yields

$$\frac{d^2U_0}{dy^2} = 0, \quad U_0 \geq 0, \quad y \in \mathbb{R}.$$

Therefore, $U_0(y) = U_2 y + U_1$, so we take $U_2 = 0$ to prevent $U_0(y) \to \pm\infty$ as $y \to \pm\infty$ because of the asymptotic conditions on u. Hence, $U_0(y) \equiv U_1$ is some constant (to be determined later). Using this result and by equating coefficients in the second equation in (4.6), we get

$$\begin{aligned} \frac{d^2V_0}{dy^2} + g(U_1, V_0) = 0, \quad y \in \mathbb{R}, \\ \lim_{y\to-\infty} V_0(y) = V_1, \quad \lim_{y\to\infty} V_0(y) = V_2, \end{aligned} \tag{4.7}$$

for constants V_1 and V_2, again to be determined by matching.

As $u_0(z)$ is continuous at z^*, matching the outer solutions to the inner reveals that

$$\lim_{z\to z^*} u_0^l(z) = \lim_{z\to z^*} u_0^r(z) = U_1 = u_0(z^*) = u^*,$$

$$\lim_{z\to z^*} v_0^l(z) = \Gamma^{-1}(u^*) = v^* = V_1 = \lim_{y\to-\infty} V_0(y)$$

and

$$\lim_{z\to z^*} v_0^r(z) = 0 = V_2 = \lim_{y\to\infty} V_0(y).$$

Hence, comparing (4.3) and (4.5) gives

$$\int_{u^*}^{1} f(u,0)du + \int_{0}^{u^*} f(u,\Gamma^{-1}(u))du = 0 \tag{4.8}$$

and on multiplying the first equation in (4.7) by dV_0/dy, integrating over $\mathbb{R}$ and applying the boundary conditions yields

$$\int_{0}^{v^*} g(u^*,v)dv = 0. \tag{4.9}$$

Equation (4.8) is equivalent to the condition $A(u^*) = 0$ as discussed above. Thus, we see that matching of the left and right outer solutions is equivalent to the reduced problem (3.2) having a solution $(u_0, v_0, c_0) = (u_0, v_0, 0)$.

If Γ is monotone, then by condition (2) in Assumption 0.0.1, $g > 0$ in the region of integration and therefore (4.9) can hold if and only if $v^* = 0$. This represents the case where the solution (u_0, v_0) is continuous (but not differentiable) at $z = z^*$. Thus, the inner solution in this case is given by the solution of (3.1) for which $c_0 = 0$ and $v^* = 0$.

If Γ is not monotone, then the solution $(u_0, v_0, 0)$ has a discontinuity in v_0 at z^*. By definition, if $G(u^*) = 0$, then $u^* \in (\hat{u}, u_1)$ and since G is invertible in this interval, the value u^* is uniquely determined by $u^* = G^{-1}(0)$ and in turn, v^* is uniquely given by $v^* = \gamma_m(G^{-1}(0))$. Notice that, these definitions only require knowledge of the function g. Thus, the inner solution in this case is given by the solution of (3.1) for which $c_0 = 0$ and (u^*, v^*) is prescribed as above.

We see then that singularly perturbed standing wave solutions, for which $c_\epsilon \equiv 0$, cannot be formed from any solution (3.2) of the type $(u_0, v_0, 0)$. Rather,

the solutions that form the "birth points" for standing wave solutions of the non-degenerate problem (3.1) are uniquely determined the condition $G(u^*) = 0$. Moreover, by following similar arguments, it can be shown that singularly perturbed solutions for which $c \neq 0$, must have wave speeds of the form $c_\epsilon = \epsilon c_1 + \mathcal{O}(\epsilon^2)$ where $\text{sign}(c_1) = \text{sign}(G(u^*))$.

4.1.2 Some Specific Examples

The CLV kinetics as detailed in (5) are monotone and thus pertain to the energy function h, (3.3), as given in Chapter 3 and the results of Theorem 3.3.6. In this case, the energy function can be computed as follows

$$\begin{aligned} h(u,v) &= -\int_0^u f(\sigma,v)d\sigma - \int_v^1 \int_0^{\Gamma(\tau)} f_v(\sigma,\tau)d\sigma d\tau \\ &= -\int_0^u [\sigma - \sigma^2 - \alpha\sigma v]d\sigma - \int_v^1 \int_0^{\Gamma(\tau)} (-\alpha\sigma)d\sigma d\tau \\ &= -\left(\frac{u^2}{2} - \frac{u^3}{3} - \frac{\alpha u^2 v}{2}\right) + \frac{\alpha}{2}\int_v^1 \left(\frac{1-\tau}{\beta}\right)^2 d\tau \\ &= -\frac{1}{2}u^2\left(1 - \frac{2}{3}u - \alpha v\right) - \frac{\alpha}{6\beta^2}(v-1)^3 \end{aligned}$$

and hence

$$h(S_+) = \frac{1}{6\beta^2}(\alpha - \beta^2). \tag{4.10}$$

By Theorem 3.1.1, it follows that the sign of the wave speed, c_0, for system (3.2) is thus determined by the sign of $\alpha - \beta^2$. Moreover, by Theorem 3.3.6, this relationship continues to hold for the wave speed, c_ϵ in system (3.1), for ϵ sufficiently small. By fixing β, we can therefore consider how the sign of the wave speed varies in the $\alpha - \epsilon^2$ plane (ϵ^2 is used for easier comparison with the system of equations). If we assume that the condition $H_\epsilon(S_+) = 0$ defines a graph in the $\alpha - \epsilon^2$ plane then by the results detailed above, this curve emanates from $(\beta^2, 0)$. We now present some results obtained by numerical integration that help determine the behaviour of this graph.

The accurate numerical integration of the ODE system (3.1) is problematic as the asymptotic states $S_\pm$ are saddles. Moreover, as will be seen, determining the direction of the wave front reduces to a two-parameter (α and ϵ) continuation of standing wave solutions. Therefore, we opted to integrate the PDE (1) directly using a suitably large domain with no-flux boundary conditions and initial data composed of exponentials chosen to give an approximation to the wave form. Integrating the PDE has the added benefit that only stable solutions are resolved and we can find zero and non-zero speed travelling waves using the same procedure. Our integrator of choice was MATLAB's *pdepe*. All the usual checks were applied to ensure that grids were fine enough to ensure no measurable difference in wave speeds could be induced by further refinement. Particular care had to be taken when ϵ was chosen to be large and rescaling of the equations ensured that reliable wave behaviour could be observed free from interference with the computationally imposed boundaries. Wave speed was measured by tracking the position of a given point on the wave front, namely, $x_f(t) := x(t)|_{u(x,t)=0.5}$.

Figure 4.1(i)-(ii) shows the locus of the $c_\epsilon = 0$ solutions of (1) in the $\alpha - \epsilon^2$ plane. For parameter values to the right (resp. left) of the curve, right travelling waves (resp. left travelling waves) are observed. Here, $\beta = 2$ and $\delta = 1$. Notice that the locus of $c_\epsilon = 0$ solutions is a graph (as speculated above) which emanates from $\alpha = \beta^2$ and passes through the point $(\alpha, \epsilon^2) = (\beta, 1)$. Most interestingly, this graph appears to have a vertical asymptote at $\alpha = \sqrt{\beta}$ (more on this later).

Moreover, it can be seen also from Figure 4.1(iii)-(iv) the locus of the $c_\epsilon = 0$ solutions of (1) in the $h(S_+) - \epsilon^2$ plane. We also found right travelling wave solutions to the right of the curve and left travelling wave solutions to the left. We observed that the locus of $c_\epsilon = 0$ solutions emanates from $h(S_+) = \frac{1}{6\beta^2}(\alpha - \beta^2) = 0$ (*i.e.* $\alpha = \beta^2$) and passes through the point $(h(S_+), \epsilon^2) = (\frac{1}{6\beta^2}(\beta - \beta^2), 1)$ and has a vertical asymptote at $h(S_+) = \frac{1}{6\beta^2}(\sqrt{\beta} - \beta^2)$, which will be discussed later.

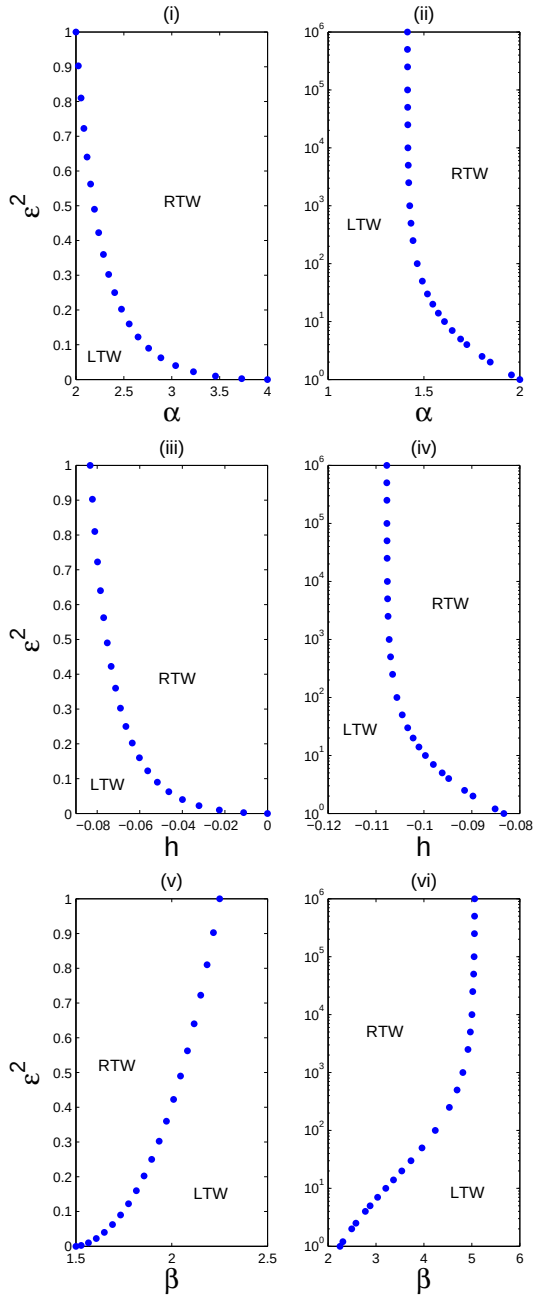

Figure 4.1: Travelling wave direction for the CLV problem (1) and (5). Locus of the $c_\epsilon = 0$ solutions is indicated by the dots. To the left (resp. right) of this curve, $c_\epsilon < 0$ (resp. $c_\epsilon > 0$) in plots (i)-(iv) and vice versa in plots (v)-(vi). In (i), (iii) and (v) $0 < \epsilon \leq 1$, (ii), (iv) and (vi) $1 \leq \epsilon \leq 1000$. Here, $\beta = 2$ in plots (i)-(iv), $\alpha = 2.25$ in plots (v)-(vi) and $\delta = 1$.

Here, $\beta = 2$ and $\delta = 1$.

In the $\beta - \epsilon^2$ plane, the solutions of the locus of the $c_\epsilon = 0$ are shown in Figure 4.1(v)-(vi). Here, left travelling waves to the right of the curve and inversely right travelling waves to the left of the curve are found. Here, $\alpha = 2.25$ and $\delta = 1$. These solutions of $c_\epsilon = 0$ emanate from $\beta = \sqrt{\alpha}$ and pass through the point $(\beta, \epsilon^2) = (\alpha, 1)$ and vertically asymptote at $\beta = \alpha^2$ (more details come later).

Apparently, the behaviour detailed above for the CLV case is not peculiar to that specific example. For it is easy to reproduce qualitatively similar results for other (monotone) kinetics. For example, consider the equations

$$\begin{aligned} u_t &= u_{xx} + u(1 - u^2 - \alpha v), \\ v_t &= \epsilon^2 v_{xx} + \delta v(1 - v^2 - \beta u). \end{aligned} \tag{4.11}$$

It is straightforward to show that $(1, 0)$ and $(0, 1)$ are uniform stable steady states and the kinetics satisfy all conditions in Assumption 0.0.1. The nullclines of (4.11) are represented in Figure 1.

We compute the energy function as follows:

$$\begin{aligned} h(u,v) &= -\int_0^u f(\sigma, v)d\sigma - \int_v^1 \int_0^{\Gamma(\tau)} f_v(\sigma, \tau)d\sigma d\tau \\ &= -\int_0^u \left(\sigma - \sigma^3 - \alpha\sigma v\right) d\sigma - \int_v^1 \int_0^{\Gamma(\tau)} (-\alpha\sigma)d\sigma d\tau \\ &= -\left(\frac{u^2}{2} - \frac{u^4}{4} - \frac{\alpha u^2 v}{2}\right) - \int_v^1 \left(\frac{-\alpha(\Gamma(\tau))^2}{2}\right) d\tau \\ &= -\frac{1}{4}u^2\left(2 - u^2 - 2\alpha v\right) + \frac{\alpha}{30\beta^2}\left(8 - 15v + 10v^3 - 3v^5\right). \end{aligned}$$

Hence,

$$h(S_+) = \frac{1}{4\beta^2}(\frac{16}{15}\alpha - \beta^2). \tag{4.12}$$

Results for this case are shown in Figure 4.2. Again, the locus of $c_\epsilon = 0$ solutions forms a graph in the $\alpha - \epsilon^2$ plane, which emanates from $\alpha = 15\beta^2/16$ ($h(S_+) = 0$) and again has a vertical asymptote (at $\alpha = \sqrt{16\beta/15}$ as will be

confirmed shortly). We now analyse this asymptotic behaviour and hence discuss further the shape of the $c_\epsilon = 0$ solution locus.

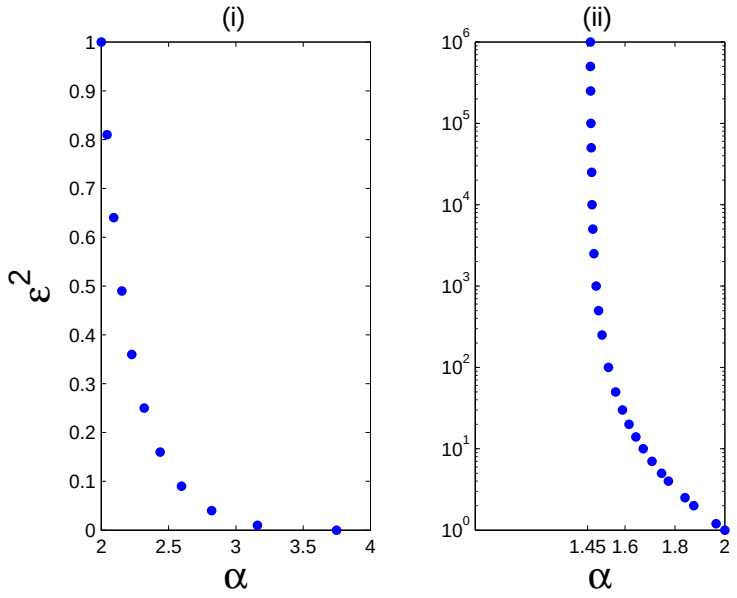

Figure 4.2: Travelling wave direction for the problem (4.11). Locus of the $c_\epsilon = 0$ solutions is indicated by the dots. To the left (resp. right) of this curve, $c_\epsilon < 0$ (resp. $c_\epsilon > 0$). (i) $0 < \epsilon \leq 1$, (ii) $1 \leq \epsilon \leq 1000$. Here, $\beta = 2$ and $\delta = 1$.

4.1.3 The Mirror Problem

We now consider the related *mirror* problem $\epsilon \to \infty$, in order to illuminate the asymptotic behaviour illustrated above. To this end, let $\hat{x} = x/\epsilon$. Then (1) becomes

$$\begin{aligned} u_t &= D^2 u_{xx} + f(u,v), \\ v_t &= v_{xx} + g(u,v), \end{aligned} \tag{4.13}$$

where $D^2 = 1/\epsilon^2$ and for ease of exposition, we have dropped the hats. The related travelling wave system is

$$\begin{aligned} -\hat{c}u' &= D^2u'' + f(u,v), \\ -\hat{c}v' &= v'' + g(u,v), \\ (u,v)(-\infty) = S_-, &\quad (u,v)(\infty) = S_+, \end{aligned} \tag{4.14}$$

Clearly, if $\epsilon \to \infty$, then $D \to 0$. Hence, we have a parallel problem to that detailed above, with D replacing ϵ. Thus, following parallel arguments to those detailed above, we can define energy functions and relate the travelling waves of the D-small system to those of the degenerate system

$$\begin{aligned} -cu' &= f(u,v), \\ -cv' &= v'' + g(u,v), \\ (u,v)(-\infty) = S_-, &\quad (u,v)(\infty) = S_+. \end{aligned} \tag{4.15}$$

To draw a direct parallel with system (3.2), we insist the follow additional assumption holds for f:

(4f) The non-trivial solutions (u,v) of $f(u,v) = 0$ are given by $v = \Xi(u)$ for a continuous function $\Xi : [0,1] \to [0,\infty)$ with $\Xi(1) = 0$ and $\Xi(0) = \hat{v}$, where $0 < \hat{v} < 1$. Moreover, $\Xi'(u) = 0$ implies Ξ has a local maximum.

A sketch of a typical f-nullcline satisfying $(4f)$ is given in Figure 4.3, where the points u^1 and v^1 are identified by

$$v^1 = \min\left\{1, \sup_{\sigma\in(0,1)} \Xi(\sigma)\right\}, \quad u^1 := \xi_m(u^1),$$

where ξ_m is the unique maximal inverse of Ξ, *i.e.* $\xi_m(0) = 1$ and

$$\xi_m(\tau) := \max_{\sigma\in(0,1)} \{\Xi(\sigma) = \tau\}.$$

Note that ξ_m is monotone decreasing on $(0, v^1)$ and if Ξ is monotone decreasing then $v^1 = \hat{v}$ and $u^1 = 0$.

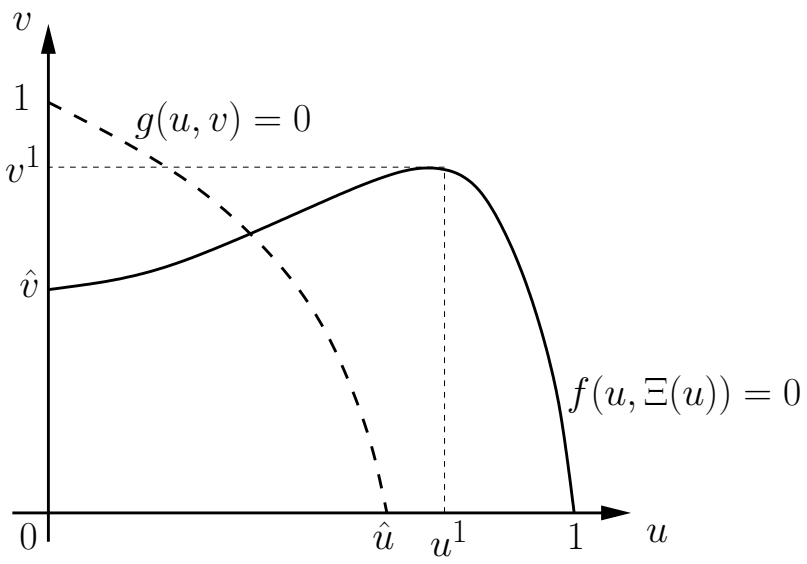

Figure 4.3: Schematic representation of the nullclines $f = 0$ and $g = 0$ satisfying Assumption 0.0.1 with condition (4f).

Following [64], we define an energy function for (4.15) of the form

$$[k(u,v)](z) := \int_{v(z)}^{1} g(u(z),\tau)d\tau - \int_{0}^{u(z)} \int_{\Xi(\sigma)}^{1} g_u(\sigma,\tau)d\tau d\sigma \quad z \in \mathbb{R}. \tag{4.16}$$

It follows directly that $[k(0,1)](z) \equiv k(S_-) = 0$ and that $[k(1,0)](z) \equiv k(S_+)$ given by (4.16) with the appropriate substitution. Similar to above, in the Ξ-monotone case and after a little manipulation, it can be shown that

$$k(S_+) = \int_{\hat{v}}^{1} g(0,\tau)d\tau + \int_{0}^{\hat{v}} g(\xi_m(\tau),\tau)d\tau. \tag{4.17}$$

Furthermore, for all $v \in [0, v^1]$, define

$$\begin{aligned} B(v) &:= k(1,0) + k(0,v) - k(\xi_m(v),v) \\ &= \int_{v}^{1} g(0,\tau)d\tau + \int_{0}^{v} g(\xi_m(\tau),\tau)d\tau. \end{aligned} \tag{4.18}$$

Proof. Using the definition of $k(u,v)$ stated in (4.16),

$$\begin{aligned} B(v) &= \int_0^1 g(1,\tau)d\tau - \int_0^1 \int_{\Xi(\sigma)}^1 g_u(\sigma,\tau)d\tau d\sigma + \int_v^1 g(0,\tau)d\tau \\ &\quad - \int_0^0 \int_{\Xi(\sigma)}^1 g_u(\sigma,\tau)d\tau d\sigma - \int_v^1 g(\xi_m(v),\tau)d\tau + \int_0^{\xi_m(v)} \int_{\Xi(\sigma)}^1 g_u(\sigma,\tau)d\tau d\sigma \\ &= \int_0^1 g(1,\tau)d\tau + \int_v^1 g(0,\tau)d\tau - \int_v^1 g(\xi_m(v),\tau)d\tau \\ &\quad \underbrace{- \int_{\xi_m(v)}^1 \int_{\Xi(\sigma)}^1 g_u(\sigma,\tau)d\tau d\sigma}_{\mathbf{I}}. \end{aligned}$$

We need to solve the double integral **I** separately.

$$\mathbf{I} = \int_{\xi_m(v)}^1 \int_{\Xi(\sigma)}^1 g_u(\sigma,\tau)d\tau d\sigma,$$

with aid of Figure 4.4, we change the order of the integrals, then we obtain

$$\begin{aligned} \mathbf{I} &= \int_0^v \int_{\xi_m(\tau)}^1 g_u(\sigma,\tau)d\sigma d\tau + \int_v^1 \int_{\xi_m(v)}^1 g_u(\sigma,\tau)d\sigma d\tau \\ &= \int_0^v g(1,\tau)d\tau - \int_0^v g(\xi_m(\tau),\tau)d\tau + \int_v^1 g(1,\tau)d\tau - \int_v^1 g(\xi_m(v),\tau)d\tau. \end{aligned}$$

Hence,

$$\begin{aligned} B(v) &= \int_0^1 g(1,\tau)d\tau + \int_v^1 g(0,\tau)d\tau - \int_v^1 g(\xi_m(v),\tau)d\tau - \int_0^v g(1,\tau)d\tau \\ &\quad + \int_0^v g(\xi_m(\tau),\tau)d\tau - \int_v^1 g(1,\tau)d\tau + \int_v^1 g(\xi_m(v),\tau)d\tau \\ &= \int_0^v g(\xi_m(\tau),\tau)d\tau + \int_v^1 g(0,\tau)d\tau. \end{aligned}$$

□

Then, using similar arguments to those in [34], it can be shown that the existence of a solution $(u_0, v_0, c = 0)$ to (4.15) is equivalent to the existence of a solution $v_* \in (0, v^1)$ of $B(v) = 0$. Now,

$$B(0) = \int_0^1 g(0,\tau)d\tau > 0,$$

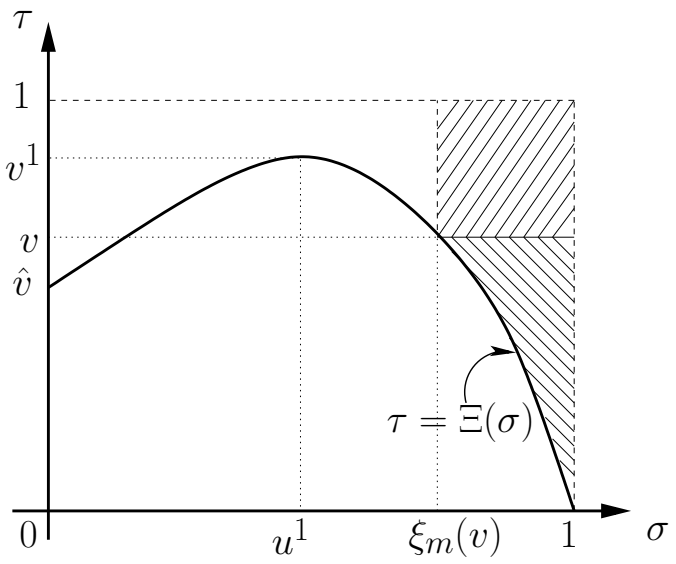

Figure 4.4: Schematic representation of the nullcline f satisfying Assumption 0.0.1 with condition (4f). The dashed area where we change the order of integrals of **I**.

by Assumption 0.0.1. Moreover, $B'(v) = -g(0, v) + g(\xi_m(v), v) < 0$ and so the existence of a solution v_* is assured iff $B(v^1) \leq 0$. Finally, we require the following definition, which parallels the definition of G given above.

Definition 4.1.1. *for $v \in [0, v^1]$, define the functional $F(v)$ by*

$$F(v) := \int_0^{\xi_m(v)} f(\sigma, v) d\sigma.$$

We have the following theorems that are analogous to Theorem 3.4.1 and 3.4.7. The proofs follow by essentially identical arguments

Theorem 4.1.2. *Suppose f and g satisfy Assumptions 0.0.1 and let B be defined as in* (4.18)*.*

(i) If $B(v^1) > 0$, then there exists a monotone solution (u_0, v_0, c_0) to (4.15) *with $c_0 > 0$ and $(u_0, v_0) \in C^1(\mathbb{R}) \times C^2(\mathbb{R})$. If $c_0 < 0$, then no monotone solution to* (3.2) *exists.*

(ii) If $B(v^1) \leq 0$*, then there exists a monotone solution* (u_0, v_0, c_0) *to* (4.15) *with* (3.2) *with* $c_0 = 0$*. In this case,* $v_0 = \xi(u_0)$*,* u_0 *has a unique singularity at* z_**, say, and hence whilst* $v_0 \in C^1(\mathbb{R})$*,* u_0 *is only bounded. However, away from this point,* (u_0, v_0) *is in* $[C^2(\mathbb{R} \setminus z_*)]^2$*. If* $c_0 \neq 0$*, then no monotone solution to* (4.15) *exists.*

Theorem 4.1.3. *Suppose* f *and* g *satisfy Assumptions 0.0.1 and (4f) and let* B *be defined as in* (4.18)*. Let* (u_D, v_D, c_D) *be a component-wise monotone solution of* (4.14)*.*
(i) If $B(v^1) < 0$ *then for* D *sufficiently small,* $c_D < 0$ *and* $c_D \to c_0 < 0$ *as* $D \to 0$*.*
(ii) If $B(v^1) \geq 0$ *and* $F(v_*) > 0$ *then for* D *sufficiently small,* $c_D > 0$ *and* $c_D \to 0$ *as* $D \to 0$*.*
(iii) If $B(v^1) \geq 0$ *and* $F(v_*) < 0$ *then for* D *sufficiently small,* $c_D < 0$ *and* $c_D \to 0$ *as* $D \to 0$*.*

Similar to above, if Ξ is monotone decreasing in u, then $v^1 = \hat{v}$, $u^1 = 0$ and $B(u^1) = k(1, 0) = k(S_+)$. Hence, Theorem 4.1.3 holds with $B(u^1)$ replaced by $k(S_+)$ and the wave direction is determined by the sign of $k(S_+) - k(S_-) = k(S_+)$.

Note also the singular perturbation arguments outlined in the beginning of this chapter can also be transcribed to the D-case and by following similar procedures, it can be shown that the "birth points" of the zero-speed ($c_D = 0$) solutions of (4.14) are determined by our new functional equation $F(v_*) = 0$. Similar to above, given kinetics f and g, the solution of this equation is directly computable.

4.2 Relating the Original and Mirror Problems

4.2.1 Monotone Nullclines

Returning first to the CLV case, it is now clearer why the $c_\epsilon = 0$ locus has a vertical asymptote at $\alpha = \sqrt{\beta}$. From (4.16), it follows that

$$\begin{aligned} k(u,v) &= -\int_1^v g(u,\tau)d\tau + \int_0^u \int_1^{\Xi(\sigma)} g_u(\sigma,\tau)d\tau d\sigma \\ &= -\int_1^v [\delta\tau - \delta\tau^2 - \delta\beta u\tau]d\tau + \int_0^u \int_1^{\Xi(\sigma)} (-\delta\beta\tau)d\tau d\sigma \\ &= -\frac{\delta}{6}\left(3v^2 - 2v^3 - 3\beta uv^2 + 3\beta u - 1\right) - \frac{\delta\beta}{2\alpha^2}\int_0^u \left((1-\sigma)^2 - \alpha^2\right)d\sigma \\ &= -\frac{\delta}{6}\left(3v^2 - 2v^3 - 3\beta uv^2 + 3\beta u - 1\right) + \frac{\delta\beta}{6\alpha^2}\left((1-u)^3 + 3\alpha^2 u - 1\right). \end{aligned}$$

Hence, $k(S_+) = \delta(\alpha^2 - \beta)/6\alpha^2$. Therefore, for the mirror problem (4.13), we anticipate that the $c_D = 0$ locus will emanate from the point $(\sqrt{\beta}, 0)$ in the $\alpha - D^2$ plane and pass through the point $(\beta, 1)$ (for $\delta = 1$). Numerical simulations confirm this, see Figure 4.5(i)-(ii). Here, it is seen that the $c_D = 0$ locus is again a graph, which indeed emanates from $\alpha = \sqrt{\beta}$ (*i.e.* where $k(S_+) = 0$) and passes through $(\beta, 1)$. Moreover, this locus has a vertical asymptote at $\alpha = \beta^2$. But this mirrors exactly the original problem, for which the $c_\epsilon = 0$ locus emanates from $\alpha = \beta^2$ and has vertical asymptote $\alpha = \sqrt{\beta}$. Furthermore, for the mirror problem (4.13) we expect that the $c_D = 0$ locus will emanate from the point $\left(\frac{1}{6\beta^2}(\sqrt{\beta} - \beta^2), 0\right)$ (where $\alpha = \sqrt{\beta}$) in the $k(S_+) - D^2$ plane and pass through the point $\left(\frac{\delta}{6\beta^2}(\beta^2 - \beta), 1\right)$ (for $\delta = 1$). Figure 4.5(iii)-(iv) confirms this result and shows that the locus of $c_D = 0$ emanates from $k(S_+) = \frac{\delta}{6\alpha^2}(\alpha^2 - \beta) = 0$ (where $\beta = \alpha^2$) and passes through $\left(\frac{\delta}{6\beta^2}(\beta^2 - \beta), 1\right)$ and has a vertical asymptote at $k(S_+) = \frac{\delta}{6\beta^2}(\beta^4 - \beta)$ (where $\beta = \alpha^2$). This also mirrors the original problem, for which the locus of $c_\epsilon = 0$ emanates from $h(S_+) = \frac{1}{6\beta^2}(\alpha - \beta^2)$ and has the vertical asymptote $h(S_+) = \frac{\delta}{6\beta^2}\left(\sqrt{\beta} - \beta^2\right)$. Now we can see why the $c_\epsilon = 0$ locus has a vertical asymptote at $h(S_+) = \frac{\delta}{6\beta^2}\left(\sqrt{\beta} - \beta^2\right)$. What is more, for

the mirror problem (4.13), we predict also that the locus of $c_D = 0$ will emanate from the point $(\alpha^2, 0)$ in the $\beta - D^2$ plane and pass through the point $(\alpha, 1)$ (for $\delta = 1$). It can be seen from Figure 4.5(v)-(vi) that numerical simulations confirm this picture. Here it is seen that the $c_D = 0$ locus is again a graph, which indeed emanates from $\beta = \alpha^2$ (*i.e.* where $k(S_+) = 0$) and passes through $(\alpha, 1)$. Moreover, this locus has a vertical asymptote at $\beta = \sqrt{\alpha}$. But this mirrors exactly the original problem, for which the $c_\epsilon = 0$ locus emanates from $\beta = \sqrt{\alpha}$ and has vertical asymptote at $\beta = \alpha^2$. Thus, we can view Figures 4.1 and 4.5 as being images of the same graph: each details the appropriate small parameter behaviour (ϵ and D^2 respectively) with the small parameter behaviour of one determining the asymptotic behaviour of the other. From Assumption 0.0.1, $\beta > 1$ it follows that $\alpha|_{h(S_+)=0} = \beta^2 > \sqrt{\beta} = \alpha|_{k(S_+)=0}$.

This coupling is not unique to CLV kinetics. Considering again the kinetics given in system (4.11), the energy function is

$$\begin{aligned} k(u,v) &= -\int_1^v g(u,\tau)d\tau + \int_0^u \int_1^{\Xi(\sigma)} g_u(\sigma,\tau)d\tau d\sigma \\ &= -\int_1^v \left(\tau - \tau^3 - \beta u\tau\right) d\tau + \int_0^u \int_1^{\Xi(\sigma)} (-\beta\tau)d\tau d\sigma \\ &= -\left(\frac{v^2}{2} - \frac{v^4}{4} - \frac{\beta u v^2}{2} - \frac{1}{2} + \frac{1}{4} + \frac{\beta u}{2}\right) - \frac{\beta}{2}\int_0^u \left((\Xi(\sigma))^2 - 1\right) d\sigma \\ &= \frac{1}{4}\left(v^4 - 1\right) - \frac{1}{2}(1-\beta u)(v^2-1) - \frac{\beta}{2}\left(\frac{1}{\alpha^2} - 1\right) u + \frac{\beta}{3\alpha^2}u^3 - \frac{\beta}{10\alpha^2}u^5. \end{aligned}$$

It follows that,

$$k(S_+) = \frac{\delta}{4\alpha^2}(\alpha^2 - \frac{16}{15}\beta).$$

Therefore $k(S_+) = 0$ when $\alpha = \sqrt{\frac{16}{15}\beta}$. This locates the vertical asymptote of the original system in this case, see Figure 4.6. Moreover, recalling that $h(S_+) = \frac{1}{4\beta^2}(\frac{16}{15}\alpha - \beta^2)$, then again, $\alpha|_{h(S_+)=0} > \alpha|_{k(S_+)=0}$ and so we retain the same qualitative picture as for the CLV case. So for these simple examples, the dependence of the wave direction on system parameters is clear. The curve on

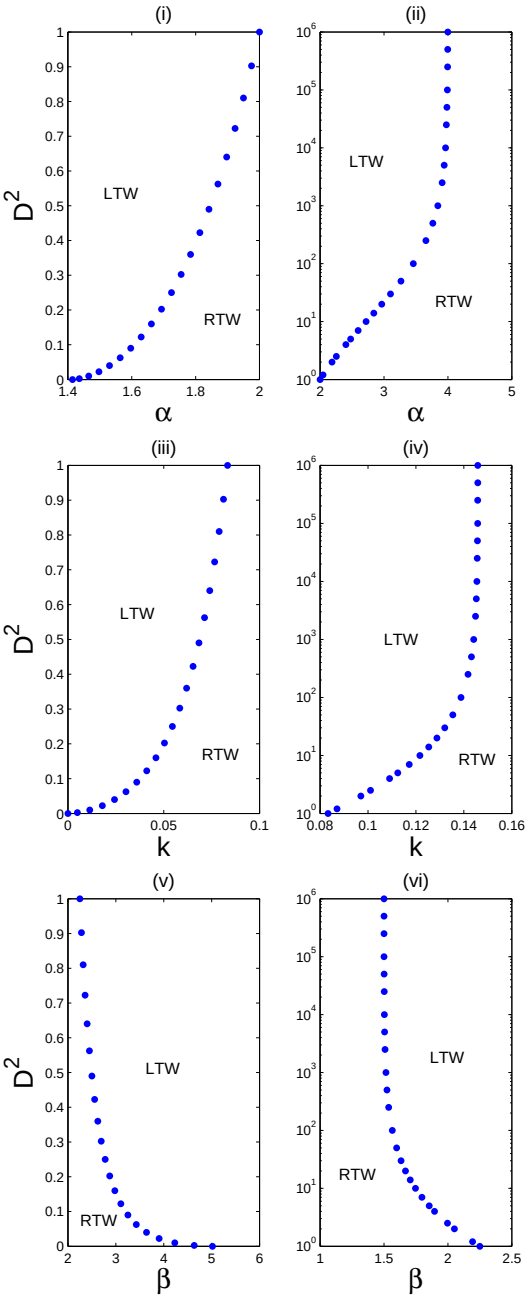

Figure 4.5: Travelling wave direction for the mirror of CLV problem (4.13) and (5). Locus of the $c_D = 0$ solutions is indicated by the dots. To the left (resp. right) of this curve, $c_D < 0$ (resp. $c_D > 0$) in plots (i)-(iv) and vice versa in plots (v)-(vi). In (i), (iii) and (v) $0 < D \leq 1$, (ii), (iv) and (vi) $1 \leq D \leq 1000$. Here, $\beta = 2$ in plots (i)-(iv), $\alpha = 2.25$ in plots (v)-(vi) and $\delta = 1$.

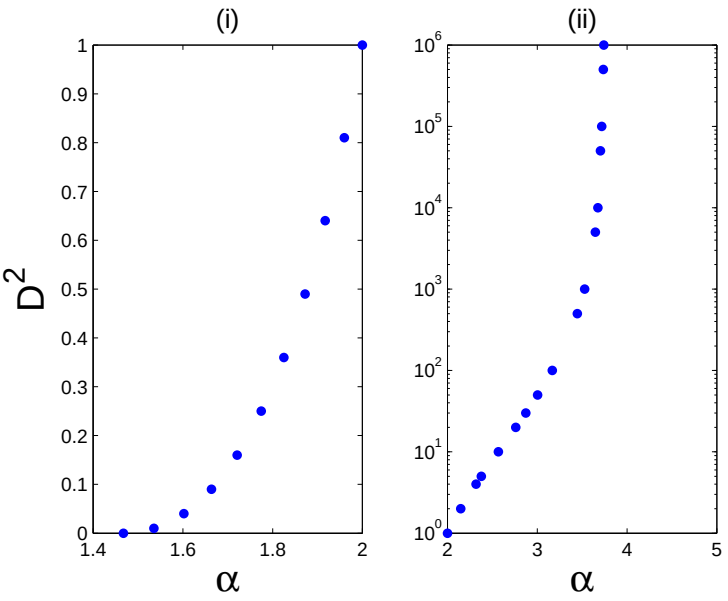

Figure 4.6: Travelling wave direction for the mirror of problem (4.11). Locus of the $c_D = 0$ solutions is indicated by the dots. To the left (resp. right) of this curve, $c_D < 0$ (resp. $c_D > 0$). (i) $0 < D \leq 1$, (ii) $1 \leq D \leq 1000$. Here, $\beta = 2$ and $\delta = 1$.

which $c_\epsilon = 0$ is a graph in the (α, ϵ^2)-plane and $\alpha|_{k(S_+)=0} < \alpha|_{h(S_+)=0}$. Hence, increasing ϵ can only change the direction of the travelling wave solution in the favour of the v-component. That is, with all other parameters fixed, increasing ϵ can only change the wave direction from left to right (and not *vice versa*). However, for $\alpha \notin [\alpha|_{k(S_+)=0}, \alpha|_{h(S_+)=0}]$, the wave direction is set by the degenerate ($\epsilon = 0$) problem and is thus independent of ϵ ($c > 0$ for $\alpha > \alpha|_{h(S_+)=0}$ and $c < 0$ for $\alpha < \alpha|_{k(S_+)=0}$).

It is of interest to speculate whether this qualitative behaviour holds for an extended class of similar kinetics. Of particular importance is the preservation of the ordering of the end points of the $c = 0$ locus. For if it were not preserved, then for certain values of $\alpha > \alpha|_{h(S_+)=0}$, increasing ϵ would decrease the wave speed and reverse the direction of the front from right to left. Consider therefore

the class of kinetics of the form

$$f(u,v) = u(\mathcal{F}(u) - \alpha v), \quad g(u,v) = \delta v(\mathcal{G}(v) - \beta u), \tag{4.19}$$

where $\mathcal{F}$ and $\mathcal{G}$ are monotone decreasing and chosen so that Assumption 0.0.1 is satisfied. A standard calculation yields that the bistable assumption requires $\mathcal{F}(0) < \alpha$ and $\mathcal{G}(0) < \beta$. Using the definition (3.3),

$$\begin{aligned} h(S_+) &= -\int_0^1 \sigma\mathcal{F}(\sigma)d\sigma - \int_0^1 \int_0^{\frac{\mathcal{G}(\tau)}{\beta}} (-\alpha\sigma)d\sigma d\tau \\ &= -\int_0^1 \sigma\mathcal{F}(\sigma)d\sigma + \frac{\alpha}{2\beta^2}\int_0^1 (\mathcal{G}(\tau))^2 d\tau \end{aligned} \tag{4.20}$$

and using (4.16)

$$\begin{aligned} k(S_+) &= \int_0^1 \delta\tau(\mathcal{G}(\tau) - \beta)d\tau - \int_0^1 \int_{\frac{\mathcal{F}(\sigma)}{\alpha}}^1 (-\delta\beta\tau)d\tau d\sigma \\ &= \delta\int_0^1 \tau\mathcal{G}(\tau)d\tau - \delta\frac{\beta}{2\alpha^2}\int_0^1 (\mathcal{F}(\sigma))^2 d\sigma. \end{aligned} \tag{4.21}$$

Setting

$$K = \int_0^1 \sigma\mathcal{F}(\sigma)d\sigma,\ L = \int_0^1 (\mathcal{G}(\tau))^2 d\tau,\ M = \int_0^1 \tau\mathcal{G}(\tau)d\tau,\ N = \int_0^1 (\mathcal{F}(\sigma))^2 d\sigma,$$

yields the critical values

$$\alpha|_{h(S_+)=0} = \frac{2K}{L}\beta^2 \quad \text{and} \quad \alpha|_{k(S_+)=0} = \sqrt{\frac{N}{2M}}\beta. \tag{4.22}$$

Clearly, for any (fixed) values of the constants K to N, if β is chosen sufficiently large, then $\alpha|_{h(S_+)=0} > \alpha|_{k(S_+)=0}$. So the ordering in parameter space of the birth point and the vertical asymptote of the $c_\epsilon = 0$ locus is indeed the same as for the specific examples detailed above. Moreover,

$$\alpha|_{h(S_+)=0} = \alpha|_{k(S_+)=0} \quad \text{iff} \quad \beta = \beta_0 := \left(\frac{NL^2}{8K^2M}\right)^{1/3}.$$

We have been unable to establish any general result that ensures the existence or otherwise of this value β_0 with $\beta_0 > \mathcal{G}(0)$ and $\alpha|_{h(S_+)=0} = \alpha|_{k(S_+)=0} > \mathcal{F}(0)$

at β_0. Indeed, a test of a large range of examples revealed that in each case $\alpha|_{h(S_+)=0} > \alpha|_{k(S_+)=0}$ for values of $\beta > \mathcal{G}(0)$. These results lead us to propose that the partition of parameter space illustrated for the CLV kinetics in Figure 4.1 is qualitatively unaltered for all kinetics of the form (4.19).

4.2.2 Non-Monotone Nullclines

One might reasonably suppose that the ordering of parameter space detailed above is a consequence of the monotone nullclines. However, we now discuss examples in which the kinetics are not monotone and yet show that the $c_\epsilon = 0$ curve behaves as above. To start with, consider the specific example

$$f(u,v) = u(1-u-\alpha v), \quad g(u,v) = v\left((\frac{1}{2}+v)(1-v)-\beta u\right). \tag{4.23}$$

With these kinetics, system (1) satisfies all conditions in Assumption 0.0.1, provided $\alpha > 1$, $\beta > \frac{1}{2}$. As the $g-$nullcline is non-monotone as shown in Figure 4.7,

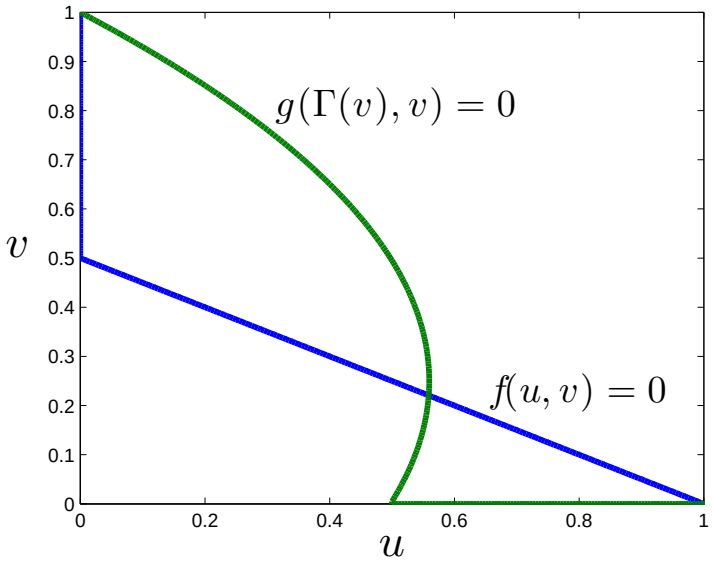

Figure 4.7: The nullclines $f = 0$ and $g = 0$ for the kinetics in system (1) and (4.23).

in order to position the birth point of the $c_\epsilon = 0$ locus, we have to consider the functionals A and G. In particular, the singular perturbation results in Section 4.1.1 suggest that the birth point is defined by the condition $G(u^*) = 0$. From (4.23), it follows directly that $\hat{u} = 1/(2\beta)$, $u_1 = 9/(16\beta)$ and that

$$\gamma_m(u) = \frac{1}{4}\left(1 + \sqrt{9 - 16\beta u}\right)$$

for $u \in [0, u_1]$. Therefore,

$$\begin{aligned} G(u) &= \int_0^{\gamma_m(u)} g(u,\tau)d\tau \\ &= -\frac{1}{1024}\left(1+\sqrt{9-16\beta u}\right)^4 + \frac{1}{384}\left(1+\sqrt{9-16\beta u}\right)^3 \\ &\quad +\frac{1}{32}\left(\frac{1}{2}-\beta u\right)\left(1+(\sqrt{9-16\beta u}\right)^2 \end{aligned}$$

and hence $G(u^*) = 0$ when $u^* = 5/(9\beta)$. Note that $\hat{u} < u^* < u_1$ as required. Now,

$$\begin{aligned} A(u) &= -\int_0^u f(\sigma, \gamma_m(\sigma))d\sigma - \int_u^1 f(\sigma, 0)d\sigma \\ &= -\int_0^u \left(\sigma - \sigma^2 - \alpha\sigma\frac{1}{4}\left(1+\sqrt{9-16\beta\sigma}\right)\right)d\sigma - \int_u^1 \left(\sigma-\sigma^2\right)d\sigma \\ &= -\frac{1}{6} + \frac{\alpha}{8}u^2 - \frac{\alpha}{5120\beta^2}\left(30(9-16\beta u)^{3/2} - 2(9-16\beta u)^{5/2} - 324\right). \end{aligned}$$

Hence,

$$A(u^*) = \frac{247}{2430\beta^2}\left(\alpha - \frac{405}{247}\beta^2\right)$$

and $A(u^*) = 0 \iff \alpha = \frac{405}{247}\beta^2$, see Figure 4.8. This marks the birth-point of the $c_\epsilon = 0$ locus in the $\alpha - \epsilon^2$ plane.

Following the arguments above, the asymptotic behaviour of this curve is determined by the degenerate mirror problem (4.15) with f and g given in (4.23). As the f-nullcline is monotone, we need only consider the energy function k. In

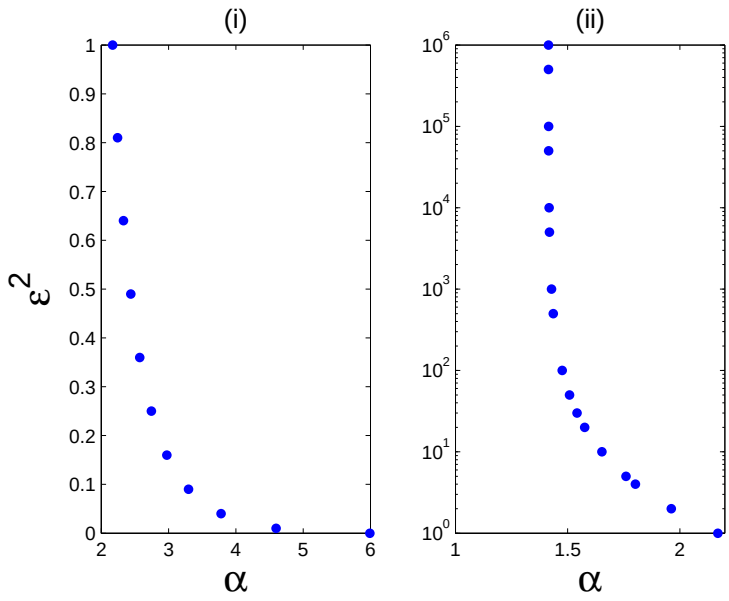

Figure 4.8: Travelling wave direction for the problem (1), (4.23). Locus of the $c_\epsilon = 0$ solutions is indicated by the dots. To the left (resp. right) of this curve, $c_\epsilon < 0$ (resp. $c_\epsilon > 0$). (i) $0 < \epsilon \leq 1$, (ii) $1 \leq \epsilon \leq 1000$. Here, $\beta = 2$.

this case,

$$\begin{aligned} k(u,v) &= \int_v^1 g(u,\tau)d\tau - \int_0^u \int_{\Xi(\sigma)}^1 g_u(\sigma,\tau)d\tau d\sigma \\ &= \int_v^1 \left(\tau(\frac{1}{2}+\tau)(1-\tau) - \beta u\tau\right) d\tau - \int_0^u \int_{\frac{1}{\alpha}(1-\sigma)}^1 (-\beta\tau)d\tau d\sigma \\ &= \frac{1}{12\alpha^2}\left(2\alpha^2 + 3v^4\alpha^2 - 2v^3\alpha^2 + 6\alpha^2\beta uv^2 - 3\alpha^2v^2 - 2\beta u^3 + 6u^2\beta - 6\beta u\right). \end{aligned}$$

It follows directly that $k(S_+) = \frac{1}{6\alpha^2}(\alpha^2 - \beta)$ and hence the position of the vertical asymptote is given by $\alpha = \sqrt{\beta}$. Numerical simulations confirm this, see Figure 4.9. Note that

$$\alpha|_{k(S_+)=0} < \alpha|_{A(u^*)=0}$$

for all $\beta > 1/2$ and once more we have shown that the ordering of these critical points is preserved. Numerical results for system (1) with kinetics (4.23) confirm that the $c_\epsilon = 0$ locus is once more a graph, which this time emanates from $\alpha|_{A(u^*)=0}$ and has a vertical asymptote at $\alpha|_{k(S_+)=0}$.

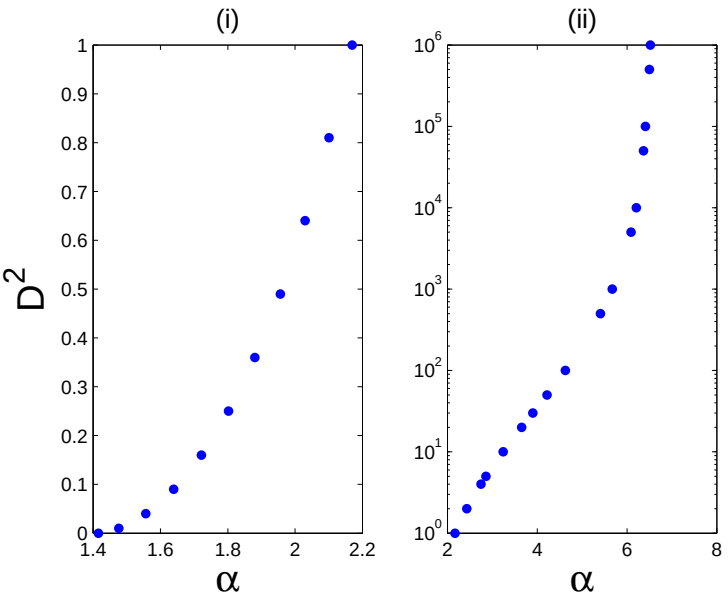

Figure 4.9: Travelling wave direction for the mirror of problem (4.13), (4.23). Locus of the $c_D = 0$ solutions is indicated by the dots. To the left (resp. right) of this curve, $c_D < 0$ (resp. $c_D > 0$). (i) $0 < D \leq 1$, (ii) $1 \leq D \leq 1000$. Here, $\beta = 2$.

The calculations can be repeated for a range of examples, in particular,

Example(1):

$$f(u,v) = u\left((\frac{1}{2}+u)(1-u) - \alpha v\right), \quad g(u,v) = v(1-v-\beta u). \tag{4.24}$$

System (1) with the kinetics in (4.24) satisfy all conditions in Assumption 0.0.1, provided $\alpha > \frac{1}{2}$ and $\beta > 1$.

It can be seen from Figure 4.10 that the g-nullcline is monotone, in order to position the birth point of the $c_\epsilon = 0$ locus, we only need consider the energy function h. From (4.24), it follows that $\hat{u} = \frac{1}{\beta}$. In this case, from (3.4), the energy function

$$\begin{aligned} h(S_+) &= -\int_0^{\frac{1}{\beta}} \sigma\left((\frac{1}{2}+\sigma)(1-\sigma) - \alpha(1-\beta u)\right) d\sigma - \int_{\frac{1}{\beta}}^1 \sigma(\frac{1}{2}+\sigma)(1-\sigma)d\sigma \\ &= \frac{1}{6\beta^2}\left(\alpha - \beta^2\right) \end{aligned}$$

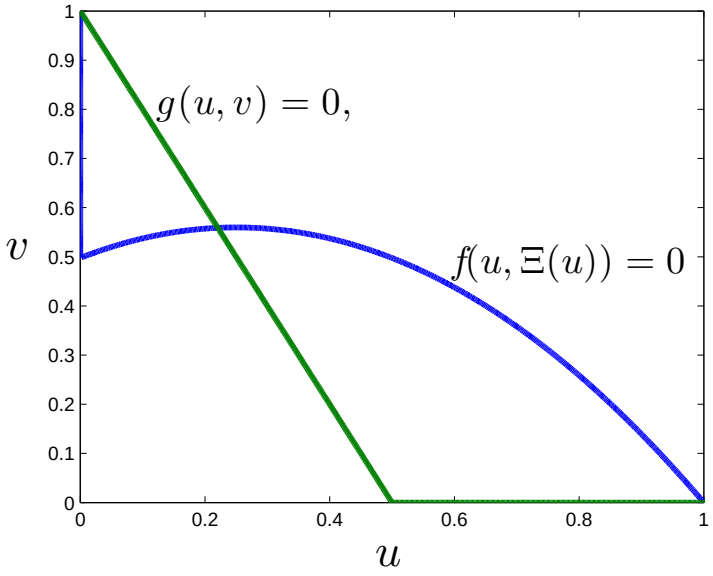

Figure 4.10: The nullclines $f = 0$ and $g = 0$ for the kinetics in system (1) and (4.24).

and hence $h(S_+) = 0 \iff \alpha = \beta^2$. This marks the birth-point of the $c_\epsilon = 0$ locus in the $\alpha - \epsilon^2$ plane, as shown in Figure 4.11. Following the arguments above, the asymptotic behaviour of this curve is determined by the degenerate problem (4.15) with f and g given in (4.24). As the f-nullcline is non-monotone, we have to consider the functionals B and F. The birth point is defined by the condition $F(v_*) = 0$. From (4.24), it is straightforward to show that $\hat{v} = \frac{1}{2\alpha}$, $v_1 = \frac{9}{16\alpha}$ and that

$$\xi_m(v) = \frac{1}{4}\left(1 + \sqrt{9 - 16\alpha v}\right)$$

for $v \in [0, v_1]$. Therefore,

$$\begin{aligned} F(v) &= \int_0^{\xi_m(v)} f(\sigma, v)\, d\sigma \\ &= -\frac{1}{1024}\left(1 + \sqrt{9 - 16\alpha v}\right)^4 + \frac{1}{384}\left(1 + \sqrt{9 - 16\alpha v}\right)^3 \\ &\quad + \frac{1}{32}\left(\frac{1}{2} - \alpha v\right)\left(1 + \sqrt{9 - 16\alpha v}\right)^2 \end{aligned}$$

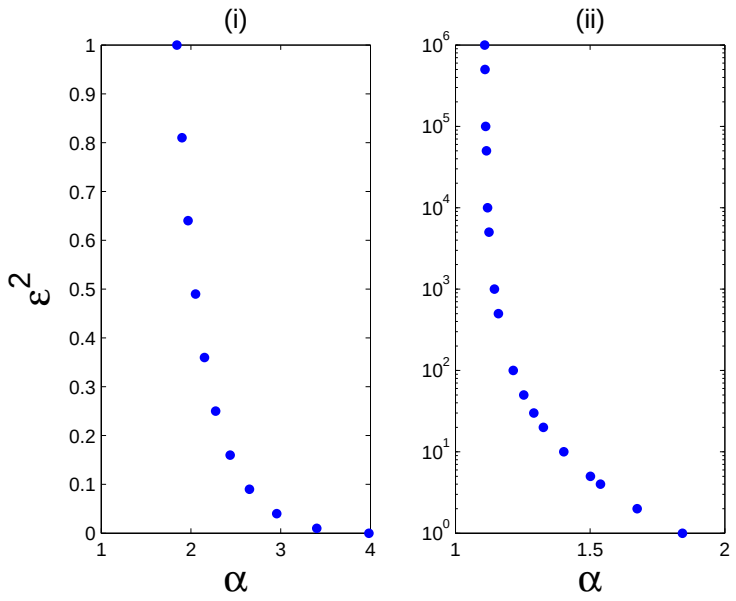

Figure 4.11: Travelling wave direction for the problem (1), (4.24). Locus of the $c_\epsilon = 0$ solutions is indicated by the dots. To the left (resp. right) of this curve, $c_\epsilon < 0$ (resp. $c_\epsilon > 0$). (i) $0 < \epsilon \leq 1$, (ii) $1 \leq \epsilon \leq 1000$. Here, $\beta = 2$.

and hence $F(v_*) = 0$ when $v_* = 5/(9\alpha)$. Note that $\hat{v} < v_* < v_1$ as required. Now,

$$\begin{aligned} B(v) &= \int_0^v g(\xi_m(\tau), \tau) d\tau + \int_v^1 g(0, \tau) d\tau \\ &= \int_0^v \left(\tau - \tau^2 - \beta\tau . \frac{1}{4}(1 + \sqrt{9 - 16\alpha\tau}) \right) d\tau + \int_v^1 (\tau - \tau^2) d\tau \\ &= \frac{1}{6} - \frac{\beta}{8} v^2 + \frac{\beta}{5120\alpha^2} \left(30(9 - 16\alpha v)^{3/2} - 2(9 - 16\alpha v)^{5/2} - 324 \right). \end{aligned}$$

Hence,

$$B(v_*) = \frac{405}{2430\alpha^2} \left(\alpha^2 - \frac{247}{405}\beta \right)$$

and $B(v_*) = 0 \iff \alpha = \sqrt{\frac{247}{405}\beta}$. Thus, the position of the vertical asymptote is given by $\alpha = \sqrt{\frac{247}{405}\beta}$ as shown in Figure 4.12. Note that,

$$\alpha|_{B(v_*)=0} < \alpha|_{h(S_+)=0}$$

for all $\alpha > \frac{1}{2}$.

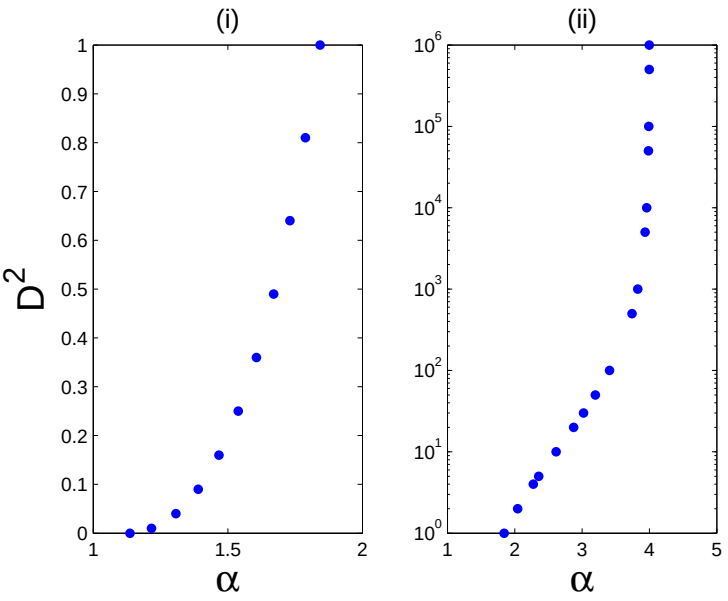

Figure 4.12: Travelling wave direction for the mirror of problem (4.13), (4.24). Locus of the $c_D = 0$ solutions is indicated by the dots. To the left (resp. right) of this curve, $c_D < 0$ (resp. $c_D > 0$). (i) $0 < D \leq 1$, (ii) $1 \leq D \leq 1000$. Here, $\beta = 2$.

Example(2):

$$f(u,v) = u\left((\frac{1}{2}+u)(1-u) - \alpha v\right), \quad g(u,v) = v\left((\frac{1}{2}+v)(1-v) - \beta u\right). \tag{4.25}$$

With these kinetics, system (1) satisfies all conditions in Assumption 0.0.1, provided $\alpha > \frac{1}{2}$ and $\beta > \frac{1}{2}$.

As the g-nullcline is monotone which can be seen from Figure 4.13, in order to position the birth point of the $c_\epsilon = 0$ locus, we have to find the functionals A and G. The birth point is defined by the condition $G(u^*) = 0$ that is suggested in Section 3.4 by the singular perturbation results. From (4.25), it follows directly that $\hat{u} = \frac{1}{2\beta}$, $u_1 = \frac{9}{16\beta}$ and that

$$\gamma_m(u) = \frac{1}{4}\left(1 + \sqrt{9 - 16\beta u}\right)$$

for $u \in [0, u_1]$. Therefore,

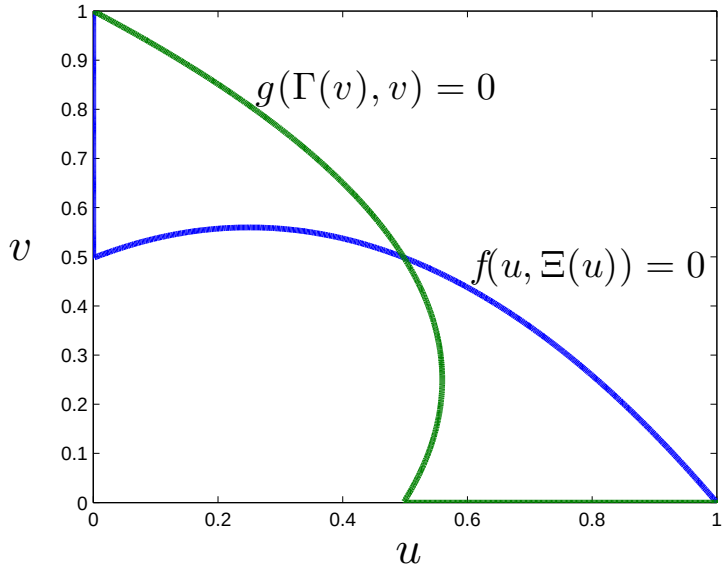

Figure 4.13: The nullclines $f = 0$ and $g = 0$ for the kinetics in system (1) and (4.25).

$$\begin{aligned} G(u) &= \int_0^{\gamma_m(u)} g(u,\tau)d\tau \\ &= -\frac{1}{1024}\left(1+\sqrt{9-16\beta u}\right)^4 + \frac{1}{384}\left(1+\sqrt{9-16\beta u}\right)^3 \\ &\quad +\frac{1}{32}\left(\frac{1}{2}-\beta u\right)\left(1+(\sqrt{9-16\beta u}\right)^2 \end{aligned}$$

and hence $G(u^*) = 0$ when $u^* = 5/(9\beta)$. Note that $\hat{u} < u^* < u_1$ as required. Now,

$$\begin{aligned} A(u) &= -\int_0^u f(\sigma,\gamma_m(\sigma))d\sigma - \int_u^1 f(\sigma,0)d\sigma \\ &= -\int_0^u \sigma\left((\frac{1}{2}+\sigma)(1-\sigma) - \alpha.\frac{1}{4}\left(1+\sqrt{9-16\beta\sigma}\right)\right)d\sigma - \int_u^1 \sigma(\frac{1}{2}+\sigma)(1-\sigma)d\sigma \\ &= -\frac{1}{6}+\frac{\alpha}{8}u^2 - \frac{\alpha}{5120\beta^2}\left(30(9-16\beta u)^{3/2} - 2(9-16\beta u)^{5/2} - 324\right). \end{aligned}$$

Hence,

$$A(u^*) = \frac{247}{2430\beta^2}\left(\alpha - \frac{405}{247}\beta^2\right)$$

and $A(u^*) = 0 \iff \alpha = \frac{405}{247}\beta^2$. This marks the birth-point of the $c_\epsilon = 0$ locus in the $\alpha - \epsilon^2$ plane. Numerical simulations confirms this result as seen in Figure 4.14. Following the arguments above, the asymptotic behaviour of this curve

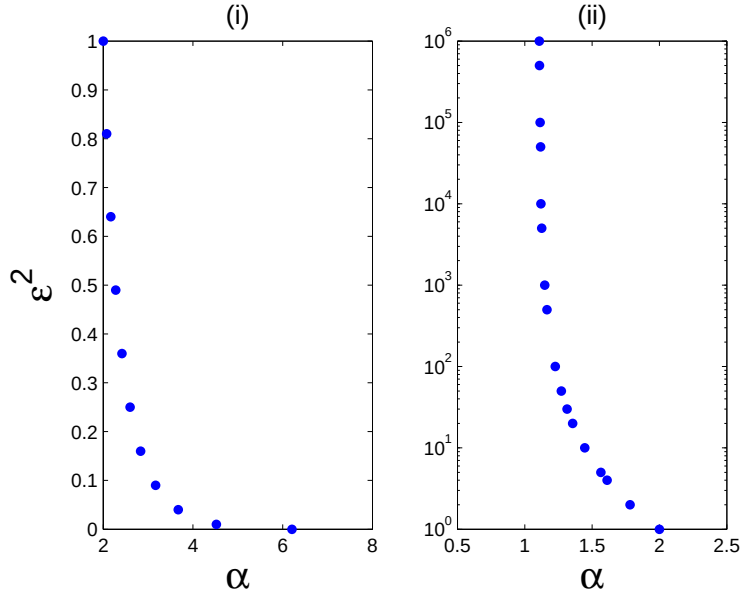

Figure 4.14: Travelling wave direction for the problem (1), (4.25). Locus of the $c_\epsilon = 0$ solutions is indicated by the dots. To the left (resp. right) of this curve, $c_\epsilon < 0$ (resp. $c_\epsilon > 0$). (i) $0 < \epsilon \leq 1$, (ii) $1 \leq \epsilon \leq 1000$. Here, $\beta = 2$.

is determined by the degenerate problem (4.15) with f and g given in (4.25). As the f-nullcline is non-monotone, we have to consider the functionals B and F. The birth point is defined by the condition $F(v_*) = 0$. From (4.25), it is straightforward to show that $\hat{v} = \frac{1}{2\alpha}$, $v_1 = \frac{9}{16\alpha}$ and that

$$\xi_m(v) = \frac{1}{4}\left(1 + \sqrt{9 - 16\alpha v}\right)$$

for $v \in [0, v_1]$. Therefore,

$$\begin{aligned} F(v) &= \int_0^{\xi_m(v)} f(\sigma, v)d\sigma \\ &= -\frac{1}{1024}\left(1 + \sqrt{9 - 16\alpha v}\right)^4 + \frac{1}{384}\left(1 + \sqrt{9 - 16\alpha v}\right)^3 \\ &\quad + \frac{1}{32}\left(\frac{1}{2} - \alpha v\right)\left(1 + \sqrt{9 - 16\alpha v}\right)^2 \end{aligned}$$

and hence $F(v_*) = 0$ when $v_* = 5/(9\alpha)$. Note that $\hat{v} < v_* < v_1$ as required. Now,

$$\begin{aligned} B(v) &= \int_0^v g(\xi_m(\tau), \tau) d\tau + \int_v^1 g(0, \tau) d\tau \\ &= \int_0^v \tau \left((\frac{1}{2} + \tau)(1 - \tau) - \beta . \frac{1}{4} \left(1 + \sqrt{9 - 16\alpha\tau} \right) \right) d\tau + \int_v^1 \tau \left(\frac{1}{2} + \tau \right) (1 - \tau) d\tau \\ &= \frac{1}{6} - \frac{\beta}{8} v^2 + \frac{\beta}{5120\alpha^2} \left(30(9 - 16\alpha v)^{3/2} - 2(9 - 16\alpha v)^{5/2} - 324 \right). \end{aligned}$$

Hence,

$$B(v_*) = \frac{405}{2430\alpha^2} \left(\alpha^2 - \frac{247}{405} \beta \right)$$

and $B(v_*) = 0 \iff \alpha = \sqrt{\frac{247}{405}\beta}$. Thus, the position of the vertical asymptote is given by $\alpha = \sqrt{\frac{247}{405}\beta}$ as shown in Figure 4.15. Note that

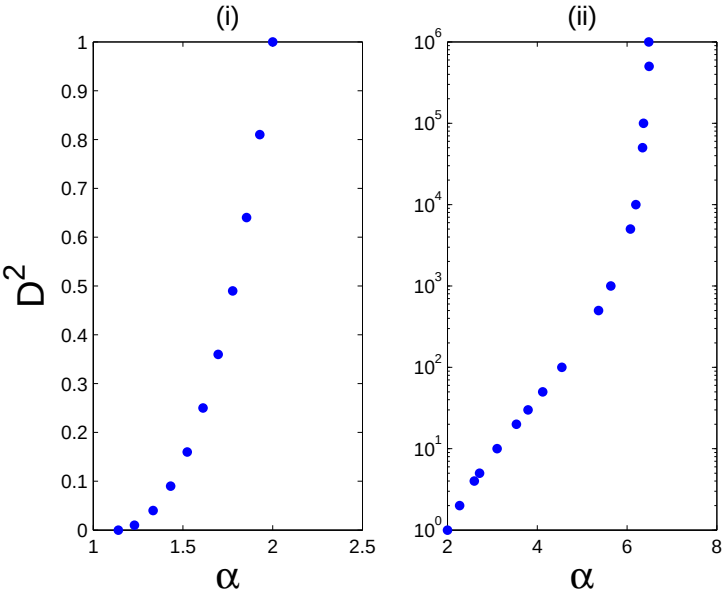

Figure 4.15: Travelling wave direction for the mirror of problem (4.13), (4.25). Locus of the $c_D = 0$ solutions is indicated by the dots. To the left (resp. right) of this curve, $c_D < 0$ (resp. $c_D > 0$). (i) $0 < D \leq 1$, (ii) $1 \leq D \leq 1000$. Here, $\beta = 2$.

$$\alpha|_{B(v_*)=0} < \alpha|_{A(u^*)=0}$$

for all $\alpha > \frac{1}{2}$ and $\beta > \frac{1}{2}$.

We deduce from both examples above that the ordering remains preserved and the qualitative structure of the division of parameter space remains the same. Other similar examples display the same qualitative behaviour.

4.2.3 General remarks

We note that the mirror problem also plays a role in determining the asymptotic wave speed in the general case: clearly, fixing α and letting $\epsilon \to \infty$ is equivalent to letting $D \to 0$ in the mirror problem, as detailed above. Moreover, in Chapter 2 a bound on the wave speed of the form $-K < c_\epsilon < K\epsilon$, for some positive constant K was established. Thus, the c_ϵ remains bounded for each fixed $\epsilon \geq 0$ and the sign of the wave speed for large ϵ is determined via Theorem 4.1.2. Moreover, the solution $(u_\epsilon, v_\epsilon, c_\epsilon)$ of (3.1) tends uniformly to the solution of the degenerate mirror problem (4.15) on all compact intervals in $\mathbb{R} \setminus \{z_*\}$.

4.3 Conclusions and Open Questions

The above results detail how properties of relative motility and competitive strength interact to determine the direction of invasive waves in competition models. For the range of examples detailed here (and other similar systems not reported here), the rigorous results concerning degenerate and near-degenerate systems in both the "original" and "mirror" problems appear to completely determine the interaction behaviour for the general case. In particular, critical points (given by $G(u^*) = 0 = A(u^*)$ and $F(v_*) = 0 = B(v_*)$) determined by the degenerate systems, provide the end points of the locus of standing waves.

That standing waves exist at all is in itself noteworthy: recall that in the absence of motility (setting both diffusion coefficients to zero) the coexistence state is unstable. However, an appropriate balance of competitive strength and

relative motility produces a spatial region in which the species coexist in a stable (modulo translation) state. The results above detail how standing waves and thus stable coexistence can be maintained as these parameters are changed.

The monotone nature of this locus of standing waves induces a separation of the motility *versus* competitive strength parameter space into three distinct zones: a central zone, in which selecting any fixed competition rate then increasing the motility causes the wave to slow, halt and reverse; to the right of this zone, the species v is too strong a competitor and the wave travels to the right, irrespective of the relative motilities; to the left, the species v is too weak a competitor and the wave travels to the left, again irrespective of the relative motilities. In summary, we speculated in the Introduction that increased motility could have a detrimental "thinning out" effect on the invasive strength of a species. From the results presented above, we are lead to conclude that this is not the case for competition models of the type considered here. Therefore, we (somewhat boldly) conjecture that this ordering of parameter space is a generic feature of models that satisfy Assumption 0.0.1. However, we have been unable to produce a proof of this result: the key components are the ordering of the standing wave locus endpoints and the proof that the locus is a graph. The numerical results in the previous section strongly suggest that the $c_\epsilon = 0$ locus is a graph in (α, ϵ)-space. In general, this locus is defined by $H_\epsilon(S_+)(\Lambda, \epsilon) = 0$ where Λ is some measure of the strength of the competition terms. That this equation defines a graph is equivalent to showing that there exists a unique solution $H_\epsilon(S_+)(\Lambda, \epsilon(\Lambda)) = 0$ (or $H_\epsilon(S_+)(\Lambda(\epsilon), \epsilon) = 0$ through each point that satisfies $H_\epsilon(S_+)(\Lambda_0, \epsilon_0) = 0$, *i.e.* that we can apply the Implicit Function Theorem to $H_\epsilon(S_+)$. However this requires differentiating the $H_\epsilon(S_+)$ with respect to either ϵ or Λ. Differentiating wrt ϵ yields

$$\frac{\partial}{\partial \epsilon}\left\{H_\epsilon(S_+)\right\} = -\int_0^1 f_v(\sigma, P_\epsilon(\sigma))\left[\frac{\partial}{\partial \epsilon}\left\{P_\epsilon\right\}\right](\sigma)d\sigma + \int_0^1 g_u(Q_\epsilon(\tau), \tau)\left[\frac{\partial}{\partial \epsilon}\left\{Q_\epsilon\right\}\right](\tau)d\tau.$$

and so to make progress here we require some knowledge of how the standing wave solutions change with ϵ. Similarly, differentiating with respect to Λ leads to an expression involving $\left[\frac{\partial}{\partial \Lambda}\{P_\epsilon\}\right]$ and $\left[\frac{\partial}{\partial \Lambda}\{Q_\epsilon\}\right]$ and again to make progress requires knowledge of the solution behaviour. However, it is exactly this dependence that we are trying to establish and so this appears to be a circular approach. An alternative method of proof would be to establish monotonicity of the wave speed c_ϵ with respect to ϵ. In all the examples detailed above, this was indeed the case. If monotonicity could be rigorously established, then the structure of the division of parameter space would follow directly from the results for the limiting cases presented above. Monotonicity with respect to the diffusion ratio of the wave speed in bistable Lotka-Volterra competition models remains to be proved. A mini-max formula for the wave speed for bistable systems is presented on p255 of [102]. However, this formula has not yielded relevant results. Moreover, monotonicity of (minimal) wave speeds in reaction-diffusion systems is a topic that has attracted recent interest, albeit in scalar problems with monostable kinetics and in the case of vanishing motility ([18]). Finally, a class of near-degenerate systems of which the model discussed here is an example, is considered in [24]. There, certain similar results to those established in [33] are presented, but for a wider class of systems. Again the boundedness of c_ϵ is established, but monotonicity does not seem to readily follow from the results presented there either. Despite the lack of a complete proof, the rigorous results for the limiting problems coupled to the numerical experiments presented here are compelling and lead us to speculate that for bistable competition models for which the kinetics satisfy Assumption 0.0.1, the wave speed c_ϵ is a monotonically increasing function of the diffusion ratio ϵ.

Chapter 5

Effects of Domain Size in 2-D Spatially Extended Lotka-Volterra Competition Models

5.1 2-D Spatially Extended Lotka-Volterra Models

Although a 1-dimensional spatial domain can be a useful modelling tool in certain circumstances (*e.g.* modelling long, thin regions) normally, we would expect spatial domains to be in 2- or 3-dimensions. In this chapter as a first step, we therefore consider the following 2-D spatially extended Lotka-Volterra system:

$$\begin{aligned} u_t &= (u_{xx} + u_{yy}) + f(u, v), \\ v_t &= \epsilon^2 (v_{xx} + v_{yy}) + g(u, v), \end{aligned} \tag{5.1}$$

where $(x, y) \in \Omega \subseteq \mathbb{R}^2$, for some set Ω. We now present extensions of our work in Chapters 3-4 but also some results that are only manifested in 2-D.

To avoid computational errors on the boundary, it is necessary to rescale space in system (5.1) as it is explained for the one spatial dimensional case in Chapter 1. Moreover, we will consider the CLV kinetics (5) and also $\epsilon = 1$ throughout this chapter.

5.2 Radially Symmetric Solutions

First, we consider radially symmetric solutions. The relationship between plane polar coordinates and cartesian coordinates is given by

$$\begin{aligned} x &= r\cos\theta, \\ y &= r\sin\theta, \end{aligned}$$

where

$$\begin{aligned} r &= \sqrt{x^2+y^2}, \\ \theta &= \tan^{-1}\left(\frac{y}{x}\right). \end{aligned}$$

Hence, the Laplacian in polar coordinates can be written as

$$\frac{\partial^2}{\partial x^2} + \frac{\partial^2}{\partial y^2} = \frac{\partial^2}{\partial r^2} + \frac{1}{r}\frac{\partial}{\partial r} + \frac{1}{r^2}\frac{\partial^2}{\partial \theta^2}. \tag{5.2}$$

We seek radially symmetric solutions, *i.e.* solutions for which $u(r,\theta) = u(r)$ and hence $\frac{\partial^2}{\partial\theta^2} = 0$. Therefore, using (5.2), equations (5.1) become

$$\begin{aligned} u_t &= \frac{1}{r}u_r + u_{rr} + f(u,v), \\ v_t &= \frac{1}{r}v_r + v_{rr} + g(u,v), \end{aligned} \tag{5.3}$$

for $(r,t) \in \mathbb{R}^+ \times \mathbb{R}^+$. To ensure symmetry at $r = 0$, we require that $\frac{\partial u}{\partial r} = \frac{\partial v}{\partial r} = 0$. We would expect a similar condition to hold at "$r = \infty$". Since, for reasonable solutions we expect u_r and v_r to be bounded, for r sufficiently large, (5.3) can

therefore be approximated a large r by the system

$$\begin{aligned} u_t &= u_{rr} + f(u,v), \\ v_t &= v_{rr} + g(u,v). \end{aligned} \tag{5.4}$$

Thus, we would expect solutions of (5.3) to be well-approximated by solutions to (5.4), for large r in any case. But (5.4) is identical to (1), in particular, as was discussed above, travelling wave solutions to (5.4) exist and thus we would expect solutions of (5.3) to approximate travelling wave solution for large r. However, if we make the substitution $z = r - ct$, then (5.3) becomes

$$\begin{aligned} u_t - cu_z &= u_{zz} + \frac{1}{z+ct}u_z + f(u,v), \\ v_t - cv_z &= v_{zz} + \frac{1}{z+ct}v_z + g(u,v), \end{aligned} \tag{5.5}$$

and clearly, no solutions of (5.5) of the form $(u(z), v(z))$ exists because the coefficients of u_z and v_z depend on time (and $u_z \not\equiv 0$ and $v_z \not\equiv 0$). Notwithstanding this, the relationship between (5.3) and (5.4) ensures that if a travelling wave solution of the latter exists, then the front provides an approximate solution for (5.3), at large r at least, as shown in Figure 5.1(i)-(ii). Indeed, numerically, it is difficult to distinguish between the 1-D wave solution of (5.4) and the corresponding front solution of (5.3). It can be seen from Figure 5.1(iii) that the speed of the right travelling waves of problem 1-D is greater than the speed of the radially symmetric solutions. This is due to the slowing effect of the $\frac{1}{r}u_r$ term in (5.3). If diffusion is combined with an advective process, this provides a mechanism for maintaining a slow speed wave, for similar problem, see Lika and Hellam in [61]. We noticed also from Figure 5.1(iii) that blue and red lines appear straight, which reflect approximately constant speed in both cases.

In the previous chapters, we discussed standing waves extensively. We had a standing wave in 1-D for the CLV system provided $\epsilon^2 = 1$, $\alpha = \beta$ and $\delta = 1$. Do we still get the same behaviour for radially symmetric solutions? The answer

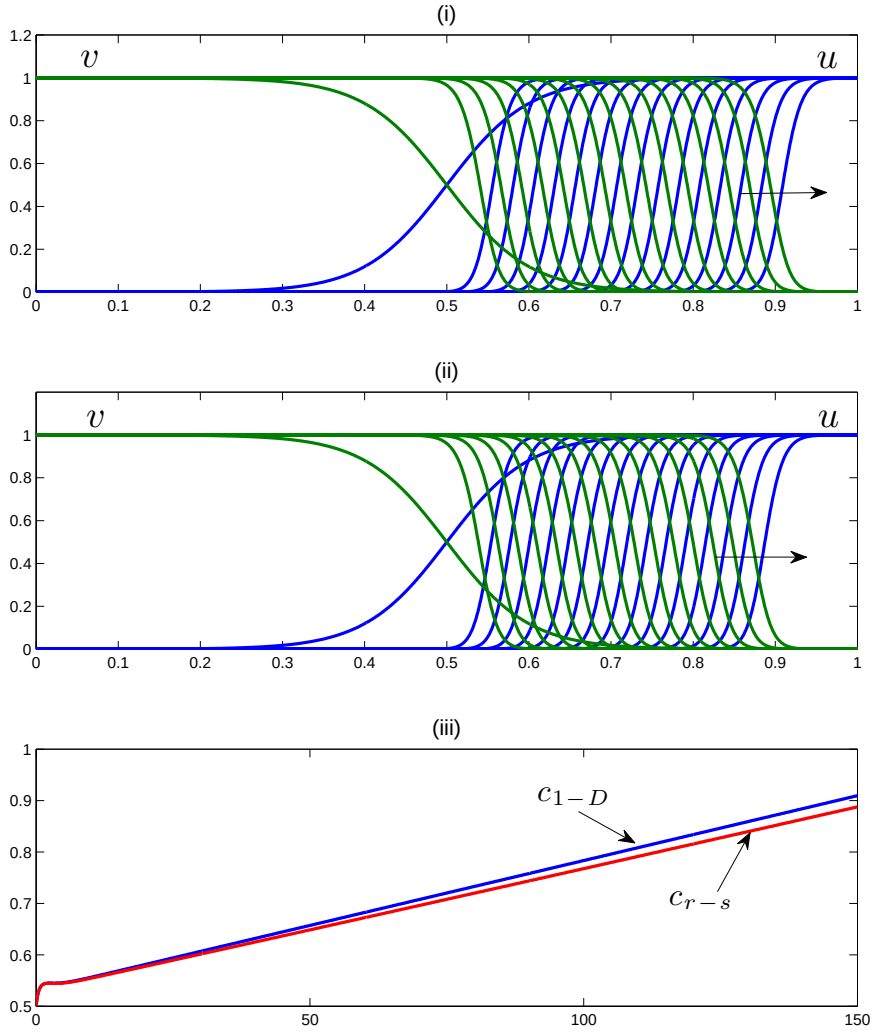

Figure 5.1: (i) Right travelling wave solutions for the CLV system (1), (5), (ii) Right front solutions for the CLV system (5.3), (5), (iii) The blue line represents the position of the front of 1-D problem (1) and the red line the position of the front for radially symmetric solutions of (5.3). Here, $\alpha = 3$, $\beta = 2$, $\delta = 1$, $\epsilon = 1$ and $t = [0, 150]$ with rescaling factor $\gamma = 10^{-4}$.

is yes if r is chosen sufficiently large, see Figure 5.2(a). On the other hand, if r is small, no standing wave is obtainable (for $\alpha = \beta$ in any case) as shown in Figure 5.2(b). Each line in the latter figure represents solutions at different time for u (in blue) and v (in green). We see then that even in this most simple case,

going from 1 to 2 spatial dimensions can have a significant effect on the predicted interfaces.

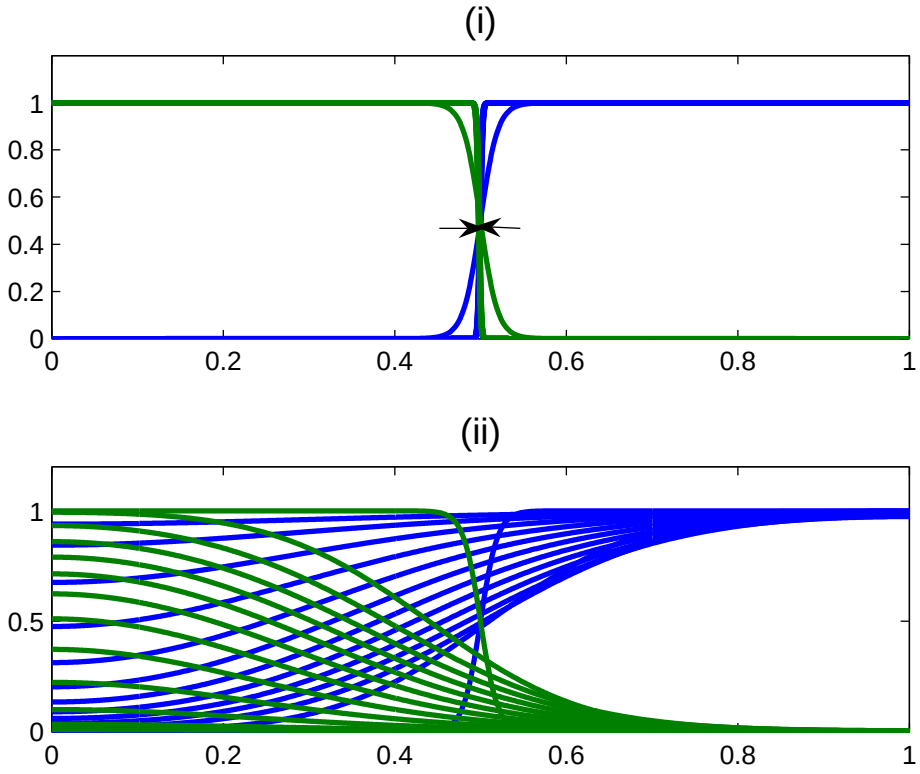

Figure 5.2: Numerical solutions of system (5.3). Here, $\alpha = \beta = 2$, $\delta = 1$ and $\epsilon = 1$. u and v are represented by the blue and green lines, respectively. (i) Standing wave solutions exist for r large (*i.e.* system (5.3) is rescaled by the factor $\gamma = 10^{-6}$) and for $t = [0, 1000]$, (ii) No standing wave solutions exist for r small (*i.e.* system (5.3) is rescaled by the factor $\gamma = 10^{-2}$) and for $t = [0, 15]$.

5.3 Planar and Non-Planar Interfaces

In this section, we will discuss the situations where we solve the system (5.2), first for a given initial data which is represented by the planar interface and then for a non-planar interface.

We solved the CLV system (5.1) numerically using the COMSOL package,

which uses the finite element technique. Triangular basis elements and Lagrange quadratic basis functions along with a backward Euler time-stepping method for integrating the equations were used in all simulations. Further details on COMSOL may be found online [108]. We solved system (5.1) on a square domain $-1 \leq x, y \leq 1$ and used zero flux boundary conditions for all simulations presented.

(i) *Smooth Planar Interface*:

As we discussed in the previous chapters, in 1-D for fixed ϵ ($\epsilon = 1$) we observed three different behaviours dependent on the competition rates α and β. We are interested here in additional behaviour that may arise from setting the problem in 2-D. To begin we used planar initial data for u (v is identically the opposite), as shown in Figure 5.3(a). It can be seen from Figure 5.3 for the parameter values used, that we have a right planar wave solution. This is entirely as we expected and reflects the behaviour found in 1-D. Results, corresponding to the 1-D analogues can be obtained, with right, left and standing fronts obtainable for the equivalent parameter value ranges.

(ii) *Small Oscillations*:

Now, we want to choose initial conditions represented by a planar interface with small oscillations (see Figure 5.4(a)) to test if instabilities can be generated in the front. As is seen in Figure 5.4, the waves start travelling to the right and the surface oscillations present in the initial conditions level off. By $t = 175$ (Figure 5.4(c)), it is clear that a planar right travelling wave is obtained, again mimicking the 1-D case.

This smoothing of initial data was observed in all other cases corresponding to the 1-D analogues. It appears then, that planar fronts are stable, to small perturbations at least.

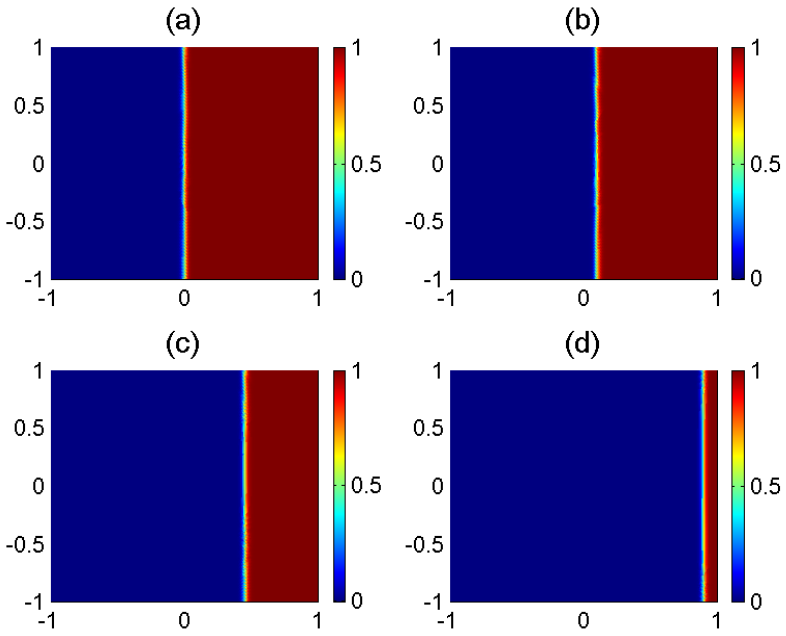

Figure 5.3: Right travelling wave solution for the CLV problem (5.1), (5). u and v are represented by the red and blue colours, respectively. Here, $\alpha = 3$, $\beta = 2$, $\delta = 1$, $\epsilon = 1$ and $t = [0, 350]$ with rescaling factor $\gamma = 10^{-4}$. (a) $t = 0$, (b) $t = 35$, (c) $t = 175$ and (d) $t = 350$.

(iii) *Large Oscillations*:

Finally, we choose non-planar initial conditions with large oscillations (see Figure 5.5(a)) to test if instabilities can be generated in the front. It is shown in Figure 5.5 that even large perturbations to the front smoothed out. Again, the previous behaviour is consistent with 1-D case.

5.3.1 Domain Size and Curvature

The above simulations were all conducted using a fixed domain size. In this section, we consider the effects of changing the domain size. Alternatively, this can be viewed as studying the role that curvature plays in the stability of the interface, as will be explained. Increasing the domain size for (5.1) is equivalent to decreasing the scaling factor γ as discussed in Chapter 1. Figures 5.6 and

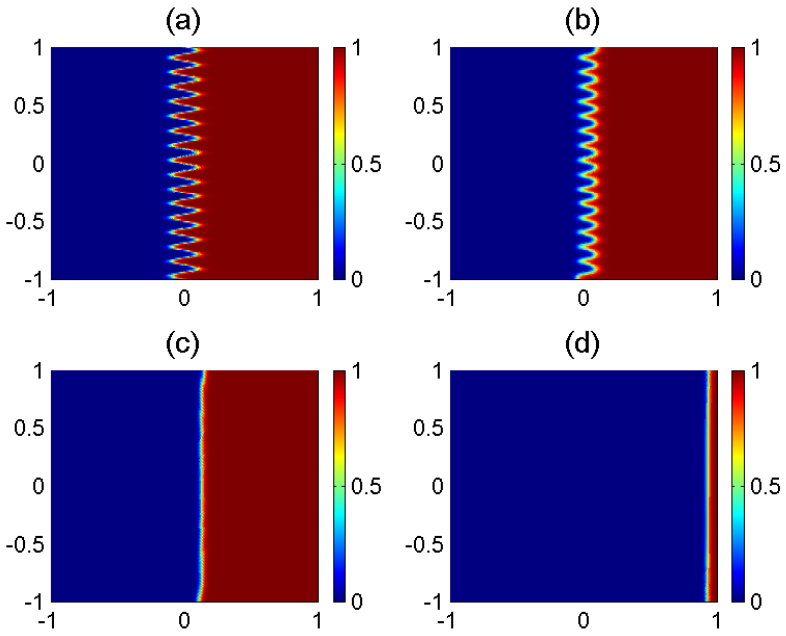

Figure 5.4: Right travelling wave solution for the CLV problem (5.1), (5). u and v are represented by the red and blue colours, respectively. Here, $\alpha = 3$, $\beta = 2$, $\delta = 1$, $\epsilon = 1$ and $t = [0, 350]$ with rescaling factor $\gamma = 10^{-4}$. (a) $t = 0$, (b) $t = 35$, (c) $t = 175$ and (d) $t = 350$.

5.7 show simulations with γ reduced by a factor of 10 and 100 respectively. Comparing Figures 5.5 and 5.6, we see that increasing the domain size causes the large oscillations with interface to persist for a much larger time. For significantly increased domain size, as illustrated in Figure 5.7, the spatial oscillations in the interface now appear fixed and stable, (as solutions of the numerical scheme at least). At the very worst, this suggests that these large-scale patterns are *meta-stable* solutions of the PDE.

So why does increasing the domain size stabilize the non-planar interface? The answer appears to lie in geometry. Note that the number of oscillations is fixed in each case (6 "peaks"). Therefore, if we decrease γ then each peak becomes wider. For very small γ (very large domain) if we zoom in to the interface, each segment is approximately planar. So it seems that locally, the interface is identical to

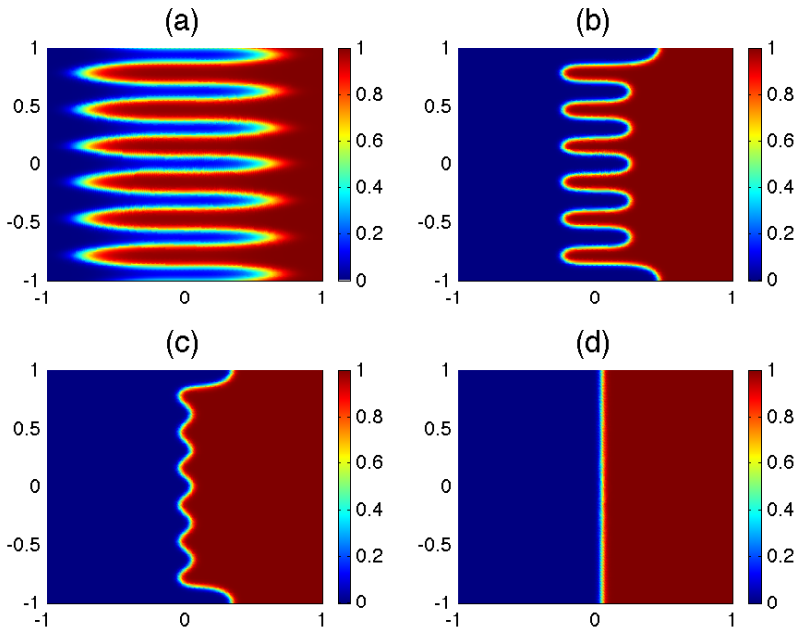

Figure 5.5: Stable standing wave for the CLV problem (5.1), (5). u and v are represented by the red and blue colours, respectively. Here, $\alpha = \beta = 2$, $\delta = 1$, $\epsilon = 1$ and $t = [0, 50000]$ with rescaling factor $\gamma = 10^{-4}$. (a) $t = 0$, (b) $t = 200$, (c) $t = 300$ and (d) $t = 50000$.

the planar case. As we have selected parameter values that result in stationary planar interfaces, this is then the resultant "local" behaviour. In summary the numerical scheme "sees" each part of the interface as planar and a (meta-) stable standing non-planar interface is obtained (of the numerical scheme at least).

To check this hypothesis, we conducted two further simulations. Figures 5.8 and 5.9 show the effect of fixing the domain size but choosing interfaces with different local curvatures. Large curvatures influence the interactions at the interface as illustrated in Figure 5.8. On the contrary, with identical parameter values and domain size, the lower curvatures in the interface shown in Figure 5.9 have a much smaller effect. Moreover, we notice from the Figure 5.8 that the interface smoothed out faster than the interface in Figure 5.9 when the number of oscillations are reduced.

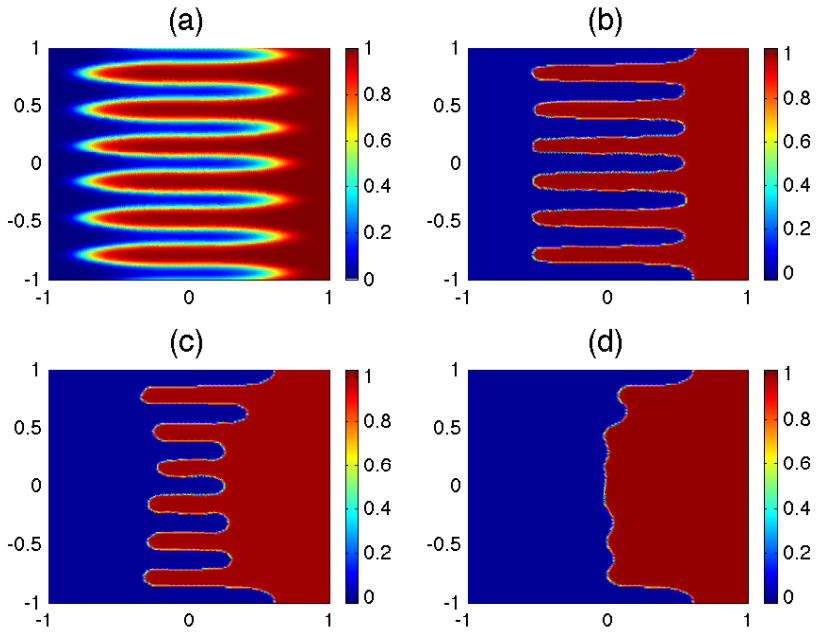

Figure 5.6: Meta-stable wave solution for the CLV problem (5.1), (5). u and v are represented by the red and blue colours, respectively. Here, $\alpha = \beta = 2$, $\delta = 1$, $\epsilon = 1$ and $t = [0, 50000]$ with rescaling factor $\gamma = 10^{-5}$. (a) $t = 0$, (b) $t = 500$, (c) $t = 2500$ and (d) $t = 50000$.

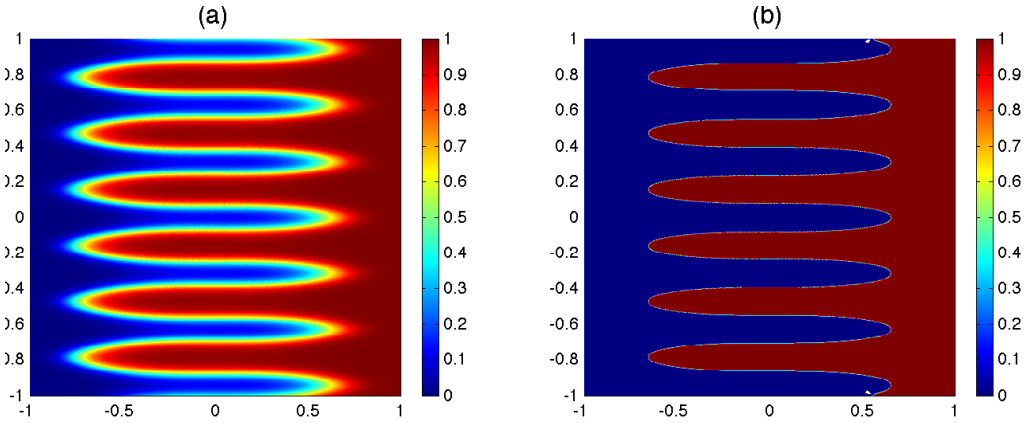

Figure 5.7: Meta-stable wave solution for the CLV problem (5.1), (5). u and v are represented by the red and blue colours, respectively. Here, $\alpha = \beta = 2$, $\delta = 1$, $\epsilon = 1$ and $t = [0, 50000]$ with rescaling factor $\gamma = 10^{-6}$. (a) $t = 0$ and (b) $t = 50000$.

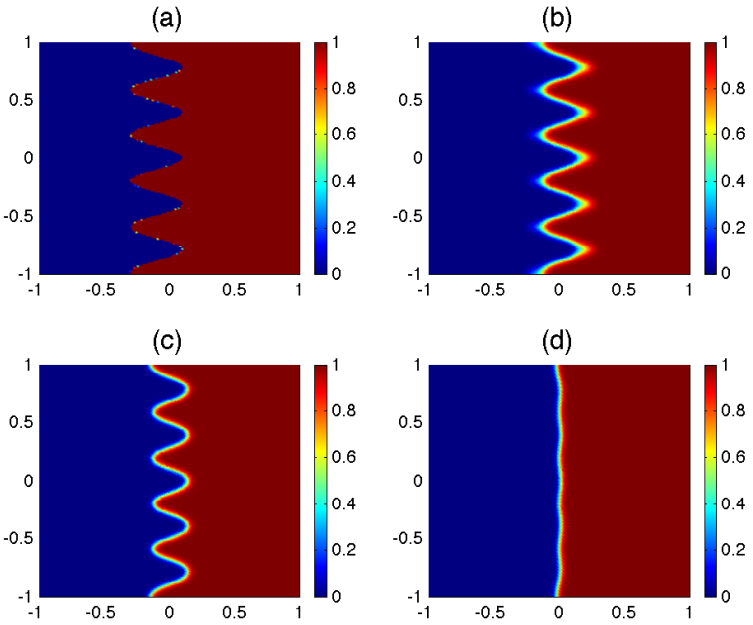

Figure 5.8: Not fully smoothed interface solutions at final output for the CLV problem (5.2), (5). u and v are represented by the red and blue colours, respectively. Here, $\alpha = \beta = 2$, $\delta = 1$, $\epsilon = 1$ and $t = [0, 150]$ with rescaling factor $\gamma = 10^{-4}$. (a) $t = 0$, (b) $t = 7.5$, (c) $t = 15$ and (d) $t = 150$.

5.3.2 Further Examples

In this section, we investigate further the effects of the geometry of the interface on the competitive outcome.

(i) *Circular initial condition:*

We first start with the initial conditions that are circular as shown in Figure 5.10(a) for u only and v is the opposite of it. Figure 5.10 shows that a travelling wave front moving inwards when $\alpha = \beta = 2$. As shown in Figure 5.11, we observed an outward travelling wave front when $\alpha = 1.5$ and $\beta = 2$. While in Figure 5.12 a standing wave is achieved for $\alpha = 1.9545$ and $\beta = 2$, which is somewhat different from the behaviour found in 1-D case for CLV problem when $\alpha = \beta$. This highlights again the effect of curvature and in particular the $\frac{1}{r}\frac{\partial u}{\partial r}$

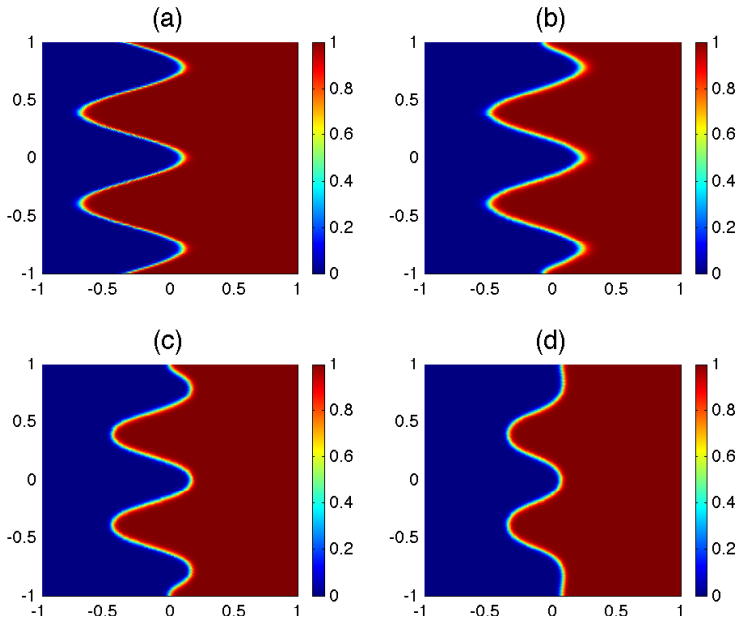

Figure 5.9: Nonsmoothed interface at final output solution for the CLV problem (5.2), (5). u and v are represented by the red and blue colours, respectively. Here, $\alpha = \beta = 2$, $\delta = 1$, $\epsilon = 1$ and $t = [0, 150]$ with rescaling factor $\gamma = 10^{-4}$. (a) $t = 0$, (b) $t = 12$, (c) $t = 45$ and (d) $t = 150$.

term in system (5.4), which is relevant to this case.

(ii) *Diamond initial condition:*

We consider now the case where we have four spots or diamonds. By solving the problem (5.1) for the 4-diamond initial conditions as shown in Figure 5.13 and setting $\alpha = \beta = 2$, results in wave fronts moving inwards in each spot. This behaviour reflects what we observed in 1-D case such $\alpha > \beta$, where we had a right travelling wave solutions. On the other hand, we obtained a wave front moving outwards for given $\alpha < \beta$ as shown in Figure 5.14. It reflects the behaviour found in 1-D that results in right travelling wave solutions. As for the case where $\alpha = 1.91204$ and $\beta = 2$ as is seen in Figure 5.15, we observed a stable standing pattern similar to what we got in 1-D, but with slightly different conditions in terms of α and β. We see also that starting with diamond initial conditions we

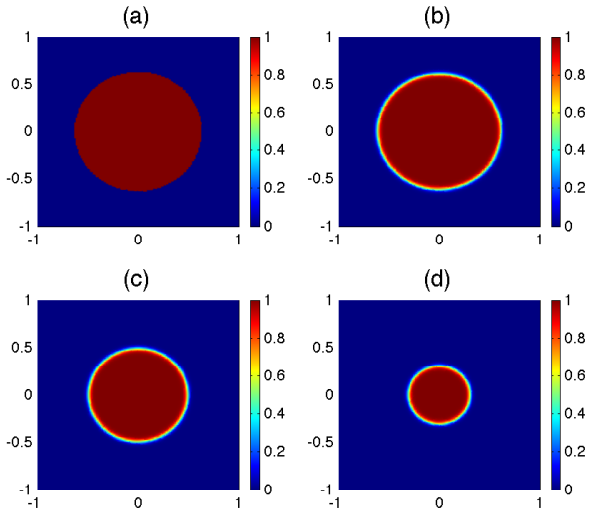

Figure 5.10: Travelling wave solutions moving inwards for the CLV problem (5.1), (5). u and v are represented by the red and blue colours, respectively. Here, $\alpha = \beta = 2$, $\delta = 1$, $\epsilon = 1$ and $t = [0, 1500]$ with rescaling factor $\gamma = 10^{-4}$. (a) $t = 0$, (b) $t = 75$, (c) $t = 750$ and (d) $t = 1500$.

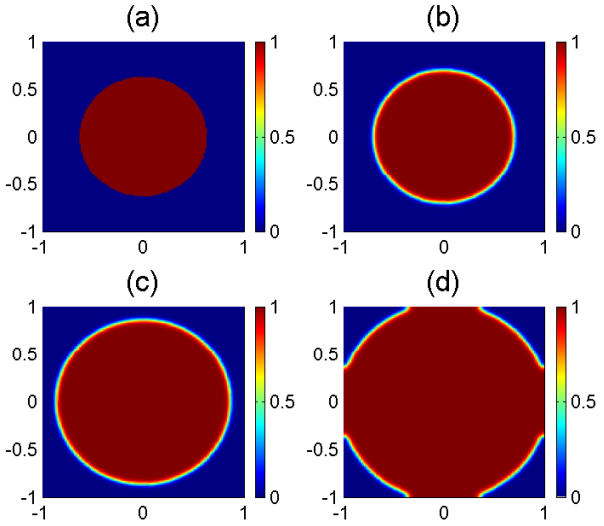

Figure 5.11: Travelling wave solutions moving outwards for the CLV problem (5.1), (5). u and v are represented by the red and blue colours, respectively. Here, $\alpha = 1.5$, $\beta = 2$, $\delta = 1$, $\epsilon = 1$ and $t = [0, 200]$ with rescaling factor $\gamma = 10^{-4}$. (a) $t = 0$, (b) $t = 40$, (c) $t = 120$ and (d) $t = 200$.

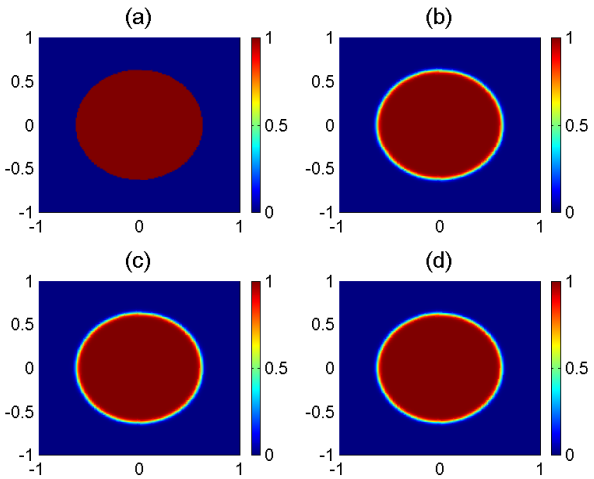

Figure 5.12: Standing wave solutions for the CLV problem (5.1), (5). u and v are represented by the red and blue colours, respectively. Here, $\alpha = 1.9545$, $\beta = 2$, $\delta = 1$, $\epsilon = 1$ and $t = [0, 10000]$ with rescaling factor $\gamma = 10^{-4}$. (a) $t = 0$, (b) $t = 100$, (c) $t = 1000$ and (d) $t = 10000$.

end up with circular ones. This is because the greater curvatures at the points locally accelerate the interfaces causing them to smooth out.

5.4 Conclusion

In this chapter, we considered the effects of setting the competition model in a two dimensional spatial domain. We first discussed the radially symmetric case in which the geometry plays an important role. It was established that, the travelling wave solutions for the 1-D case travel faster than the wave fronts in the radially symmetric solutions. Furthermore, it was noted that the form of the radially symmetric fronts approaches that of the 1-D travelling wave for large r.

Next, we discussed the case where a planar interface is considered with smooth planar interface and with small oscillations in a small size domain. In both cases we obtained smooth surfaces either travel to the right, left or remaining still matching exactly the behaviour of the 1-D waves.

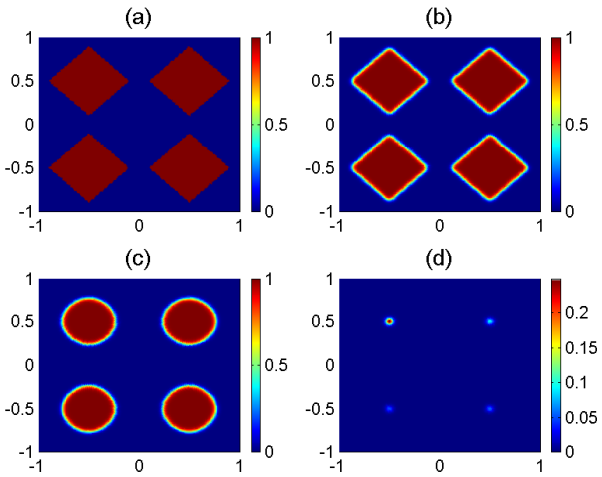

Figure 5.13: Wave fronts solutions moving inwards for the CLV problem (5.1), (5). u and v are represented by the red and blue colours, respectively. Here, $\alpha = \beta = 2$, $\delta = 1$, $\epsilon = 1$ and $t = [0, 500]$ with rescaling factor $\gamma = 10^{-4}$. (a) $t = 0$, (b) $t = 5$, (c) $t = 150$ and (d) $t = 500$.

Moreover, we showed that the curvature of the interface plays an important role in determining the competitive outcome. By choosing the domain size sufficiently large and/or the curvature of the interface sufficiently small, locally, the competitive interaction "sees" the interface as planar and hence the competitive outcome is determined exactly as it is in the 1-D case. Increasing the curvature (decreasing the domain size) perturbs this balance and the geometry effects influence the final outcome.

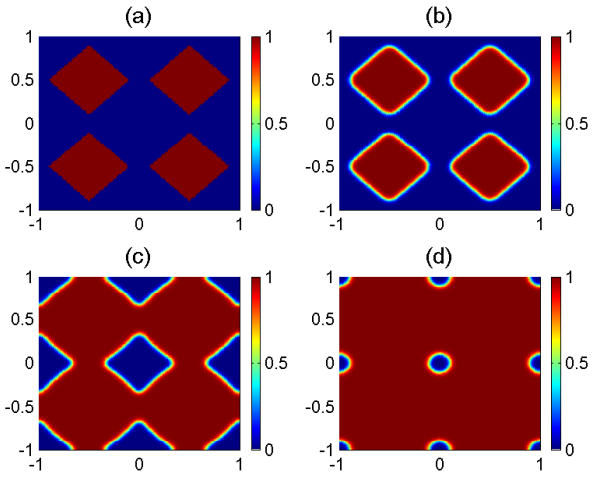

Figure 5.14: Wave fronts solutions moving outwards for the CLV problem (5.1), (5). u and v are represented by the red and blue colours, respectively. Here, $\alpha = 1.5$, $\beta = 2$, $\delta = 1$, $\epsilon = 1$ and $t = [0, 150]$ with rescaling factor $\gamma = 10^{-4}$. (a) $t = 0$, (b) $t = 15$, (c) $t = 90$ and (d) $t = 150$.

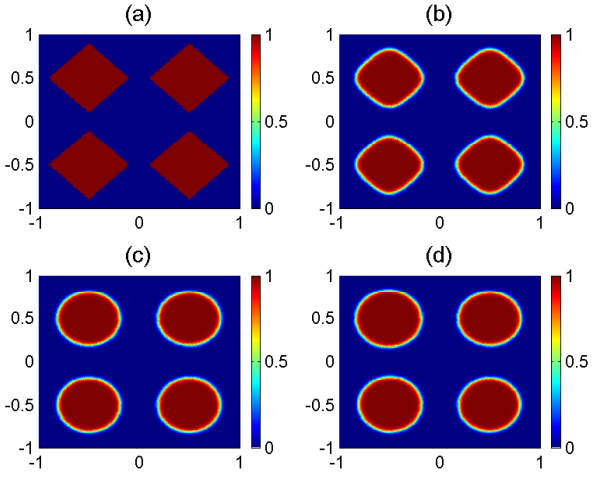

Figure 5.15: Standing wave solutions for the CLV problem (5.1), (5). u and v are represented by the red and blue colours, respectively. Here, $\alpha = 1.91204$, $\beta = 2$, $\delta = 1$, $\epsilon = 1$ and $t = [0, 7000]$ with rescaling factor $\gamma = 10^{-4}$. (a) $t = 0$, (b) $t = 70$, (c) $t = 700$ and (d) $t = 7000$.

Chapter 6

Wave Behaviour in Tristable Competition Models

6.1 3-Species Competition Lotka-Volterra Model

In this chapter, we are interested in what happens if we introduce a third species, w, to system (1). Given that we have established how u and v compete, can the third species alter this interaction, *e.g.* can it stop or even reverse a wave of invasion? If it can, this third species could be viewed as a *bio-control agent* or a *bio-buffer agent*. These questions will be partially addressed in this chapter.

Consider the Lotka-Volterra model for three competing species

$$\begin{aligned} u_t &= D_1 u_{xx} + f(u,v,w), \\ v_t &= D_2 v_{xx} + g(u,v,w), \\ w_t &= D_3 w_{xx} + h(u,v,w), \end{aligned} \tag{6.1}$$

where for definiteness, we will consider $f(u,v,w) = u(1-u-\alpha_1 v-\alpha_2 w)$, $g(u,v,w) = \delta_1 v(1-v-\beta_1 u-\beta_2 w)$ and $h(u,v,w) = \delta_2 w(1-w-\gamma_1 u-\gamma_2 v)$. Let $u(x,t)$, $v(x,t)$ and $w(x,t)$ denote the population densities of the species at time t and position x. Here, D_i $(i=1,2,3)$ are the diffusion rates and α_i, β_i and γ_i

$(i = 1, 2)$ represent the interspecific competition rates and δ_i $(i = 1, 2)$ represent the net birth rates. All of the coefficients are assumed to be positive constants.

In Section 6.2, we will discuss initial conditions that represent a third species being introduced as a bio-control agent (Type I). This section will be divided into two subscetions, where the third species is either annihilated or persistent. In Section 6.3, we discuss the most important cases for initial conditions where the third species is introduced as a bio-buffer (Type II).

6.1.1 Tristability

First, we consider the behaviour of the kinetic system associated with (6.1). Thus, we study the following ODE system:

$$\begin{aligned} \frac{du}{dt} &= u(1 - u - \alpha_1 v - \alpha_2 w), \\ \frac{dv}{dt} &= \delta_1 v(1 - v - \beta_1 u - \beta_2 w), \\ \frac{dw}{dt} &= \delta_2 w(1 - w - \gamma_1 u - \gamma_2 v). \end{aligned} \tag{6.2}$$

Here and below we have set $\delta_1 = \delta_2 = 1$. This models the case where the intrinsic birth rate of all three species is approximately the same. The result could be derived for $\delta_1 \neq \delta_2 \neq 1$, but for clarity of exposition, we investigate the former case.

System (6.2) has eight steady states. After straightforward but lengthy calculations, it can be shown that these are

$$
\begin{aligned}
&(u_*, v_*, w_*) = (0,0,0); \quad (u_*, v_*, w_*) = (1,0,0);\\
&(u_*, v_*, w_*) = (0,1,0); \quad (u_*, v_*, w_*) = (0,0,1);\\
&(u_*, v_*, w_*) = (\frac{1-\alpha_1}{1-\alpha_1\beta_1}, \frac{1-\beta_1}{1-\alpha_1\beta_1}, 0);\\
&(u_*, v_*, w_*) = (\frac{1-\alpha_2}{1-\alpha_2\gamma_1}, 0, \frac{1-\gamma_1}{1-\alpha_2\gamma_1});\\
&(u_*, v_*, w_*) = (0, \frac{1-\beta_2}{1-\beta_2\gamma_2}, \frac{1-\gamma_2}{1-\beta_2\gamma_2})\\
&(u_*, v_*, w_*) = (\frac{1-\alpha_1-\alpha_2+\alpha_1\beta_2+\alpha_2\gamma_2-\beta_2\gamma_2}{1-\alpha_1\beta_1-\alpha_2\gamma_1-\beta_2\gamma_2+\alpha_1\beta_2\gamma_1+\alpha_2\beta_1\gamma_2},\\
&\qquad \frac{1-\beta_1-\beta_2+\alpha_2\beta_1-\alpha_2\gamma_1+\beta_2\gamma_1}{1-\alpha_1\beta_1-\alpha_2\gamma_1-\beta_2\gamma_2+\alpha_1\beta_2\gamma_1+\alpha_2\beta_1\gamma_2},\\
&\qquad \frac{1-\gamma_1-\gamma_2-\alpha_1\beta_1+\alpha_1\gamma_1+\beta_1\gamma_2}{1-\alpha_1\beta_1-\alpha_2\gamma_1-\beta_2\gamma_2+\alpha_1\beta_2\gamma_1+\alpha_2\beta_1\gamma_2}).
\end{aligned}
\tag{6.3}
$$

For these steady states to be biologically relevant, they have to be nonnegative and we will assume the parameters to be chosen so that this is the case.

As is standard, the linear (asymptotic) stability of these steady states is determined by the eigenvalues of the Jacobian matrix, which for (6.2) is

$$
\begin{aligned}
&J(u_*, v_*, w_*)\\
&= \begin{pmatrix}
1-2u_*-\alpha_1 v_*-\alpha_2 w_* & -\alpha_1 u_* & -\alpha_2 u_*\\
-\beta_1 v_* & 1-2v_*-\beta_1 u_*-\beta_2 w_* & -\beta_2 v_*\\
-\gamma_1 w_* & -\gamma_2 w_* & 1-2w_*-\gamma_1 u_*-\gamma_2 v_*
\end{pmatrix}.
\end{aligned}
$$

Using $J(u_*, v_*, w_*)$, we find that system (6.2) has an unstable node $(0,0,0)$ and three stable nodes $(1,0,0)$, $(0,1,0)$ and $(0,0,1)$ and all other steady states are unstable. Hence, we will refer to system (6.1) as being ***tristable***. Note, these steady states represent uniform steady states of the spatially extended system (6.1), which in this case we will also refer to as ***tristable***. The term tristable is not reserved for systems of the form (6.1) and has been applied to quite different systems of equations (see [31, 88, 109]).

6.1.2 Initial Conditions

We will consider smooth initial conditions for ease of numerical computations. We have two different types of initial conditions, which are depicted in Figure 6.1.

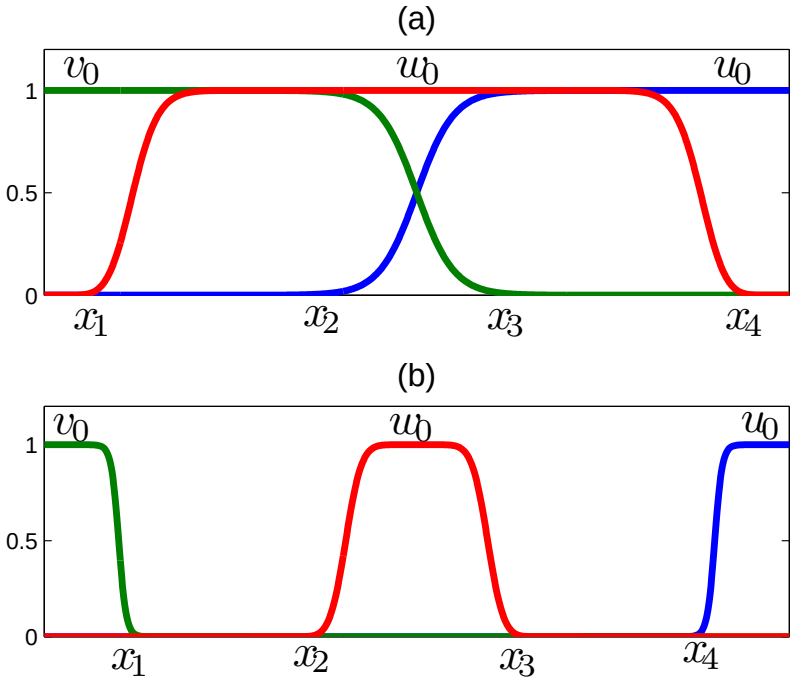

Figure 6.1: The species are given by u (blue), v (green) and w (red). (a) Type I initial conditions for system (6.1) shows that w_0 represents as a bio-control for u_0 and v_0. (b) Type II initial conditions for system (6.1) where w_0 is plugged in between u_0 and v_0 as a bio-buffer.

Type I:

This type of initial conditions has the form that is sketched in Figure 6.1(a). We consider in this case that u and v are already interacting so we expect either stationary, left or right travelling wave and we introduce a third species w as a bio-control agent to see if we can alter the dynamics, *i.e.* slow, stop or reverse the $u - v$ interaction. For example, change a left travelling wave to the right or

the wave stops. We will discuss this type of the initial conditions in Section 6.2 in more details.

Type II:

We suppose here that the species u and v are not interacting yet and we place w in between them as a bio-buffer agent as shown in Figure 6.1(b). This type will be discussed in Section 6.3 in further detail aiming to see if we can prevent, reverse or stop the interaction of u and v when we know that parameters are such that u or v will win and we do not want this to occur.

6.2 Type I initial conditions: bio-control

We divide this section into two parts according to the final wave front we obtain: one where w is annihilated and the other one where w is persistent.

6.2.1 Annihilation of w

In this section we will see that w is annihilated and we find that u and v go on to interact as before. We will obtain the same behaviours discussed in Chapters 3-4. This section is going to detail two possible results, where w dies out immediately or vanishes after exerting a transient response.

LTW in the $u - v$ system

Solving system (6.1) results in existence of left travelling wave solutions (LTW) in terms of u and v only, where the third species w vanishes completely after initial interaction with u and v. We obtain this behaviour if

$$\alpha_1 < \beta_1, \tag{6.4}$$

besides the following conditions

$$\alpha_2 < \gamma_1 \quad \text{and} \quad \beta_2 < \gamma_2. \tag{6.5}$$

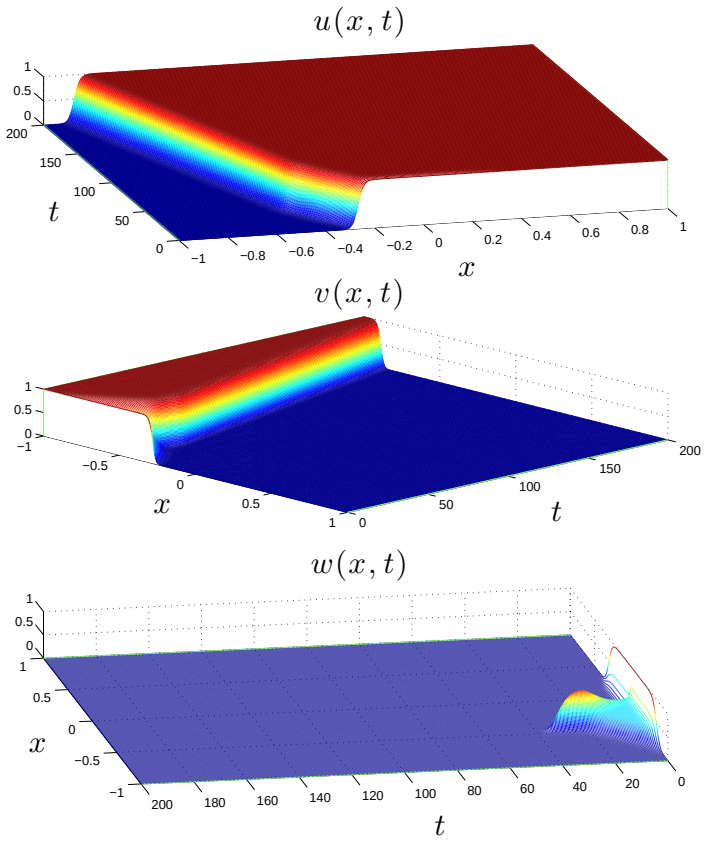

Figure 6.2: Numerical solutions of system (6.1). For the following parameter set, $\alpha_1 = 2$, $\alpha_2 = 1.5$, $\beta_1 = 3$, $\beta_2 = 2$, $\gamma_1 = 3$ and $\gamma_2 = 2$ at $t = [0, 200]$, a left travelling wave solution is observed for species u and v while the third species w is annihilated.

In Figure 6.2, species u initially outcompetes w due to $\alpha_2 < \gamma_1$ and left travelling wave solutions are obtained for very limited time. Simultaneously, v outcompetes w because of $\beta_2 < \gamma_2$ which leads to initial right travelling wave solutions. It is apparent that propagating waves move towards each other for

limited time (t), which results in the annihilation of the third species w. Afterwards, in the long-term, the solution of system (6.1) soon settles to a travelling wave solution as $u - v$ system. Because of $\alpha_1 < \beta_1$, this travelling wave goes to the left involving u and v only as seen in Chapters 3-4.

RTW in the $u - v$ system

This case happens when

$$\alpha_1 > \beta_1, \tag{6.6}$$

and conditions (6.5) are satisfied.

In this case, we also observe that the third species w vanishes as in the previous case. This happens by both the wave (u, w) travel to the left and (v, w) to the right causing w collapsing and because of $\alpha_1 > \beta_1$, that results in a right travelling wave (RTW) involving u and v only.

SW in the $u - v$ system

This case happens when

$$\alpha_1 = \beta_1, \tag{6.7}$$

in addition to conditions (6.5).

This case is similar to the previous cases. Here, we also find that w vanishes and we are left with the interaction between u and v only, which from these parameter values, produces a standing wave (SW).

In the above three cases, the annihilation of w means that the long-term behaviour is essentially determined by the (u, v) system alone.

Temporarily left moving 3-species interaction wave

The initial conditions ensure that a natural order for the species is, in the positive x-direction, v, w and u. Hence, we introduce the following notation:

Definition 6.2.1. Assume that the interaction waves of (u, w) and (v, w) are travelling both to the left. We call (v, w) a *leading wave* and (u, w) a *rear wave*. For interaction waves (u, w) and (v, w) are travelling to the right we call (u, w) a *leading wave* and (v, w) a *rear wave*.

If

$$\alpha_2 < \gamma_1 \qquad \text{and} \qquad \beta_2 > \gamma_2 \tag{6.8}$$

and one of the conditions (6.4), (6.6) and (6.7) holds, then, in this case the rear wave (u, w) travels faster than the leading one (v, w).

In general, under conditions (6.8) we obtain a transient behaviour moving to the left, which results in vanishing w. In the long-term, we may observe a left travelling wave, a right travelling wave or a standing wave, depending on the relative values of α_1 and β_1.

One of the most interesting cases discussed above is the transient reversal wave direction as we now explain. For $\alpha_1 > \beta_1$, then in the absence of w, u and v travel to the right (see Chapter 3). On introducing w as detailed above, we observed that both waves (u, w) and (v, w) initially travel to the left. Moreover, the rear wave (u, w) propagates faster than the leading one, so it caught up the wave of (v, w) leading to w vanishing. Subsequently, the (u, v) fronts to the right, see Figure 6.3.

Temporarily right moving 3-species interaction wave

This case is opposite to the above and occurs when

$$\alpha_2 > \gamma_1 \qquad \text{and} \qquad \beta_2 < \gamma_2. \tag{6.9}$$

After w vanishes, one of the conditions (6.4), (6.6) and (6.7) holds, we expect either LTW, RTW or SW respectively in the u and v only.

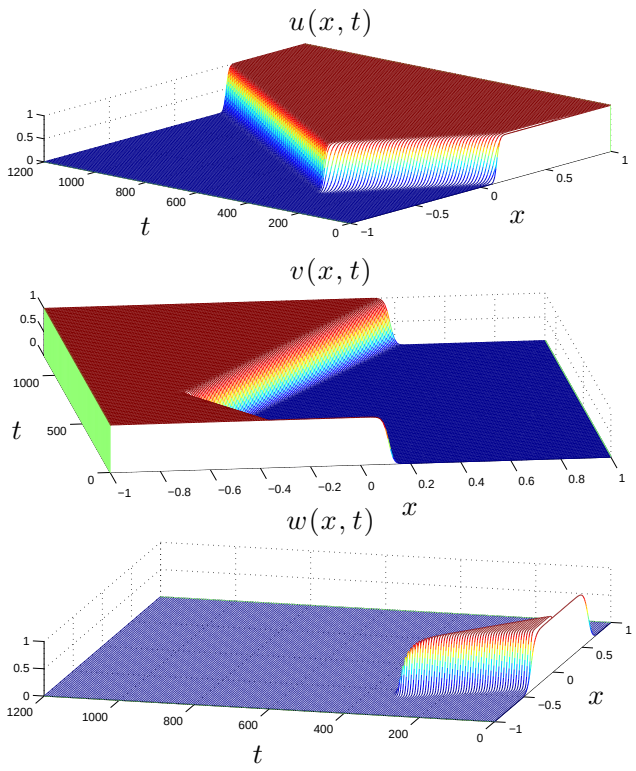

Figure 6.3: Numerical solutions of system (6.1). For the following parameter set, $\alpha_1 = 3$, $\alpha_2 = 1.2$, $\beta_1 = 2.5$, $\beta_2 = 2.3$, $\gamma_1 = 1.5$ and $\gamma_2 = 2$ at $t = [0, 1200]$, a right travelling wave exists in the long-term involving u and v only and a left transient behaviour is observed.

6.2.2 Persistence of w

We again discuss cases in turn.

Fixed region of separation moving to the left

This case happens if both leading and rear waves travel with constant speed to the left. This case can be obtained if the following conditions are satisfied:

$$\alpha_2 = \gamma_2, \quad \beta_2 = \gamma_1 \quad \text{and} \quad \gamma_1 > \gamma_2. \tag{6.10}$$

In fact, the behaviour observed here shows that there are two different "travelling waves" glued together to form a new type of solution, which is moving to the left

with constant speed. Furthermore, in absence of v, u outcompetes w and travel to the left and at the same time w dominates v. Both waves propagate with the same speed, as shown in Figure 6.4.

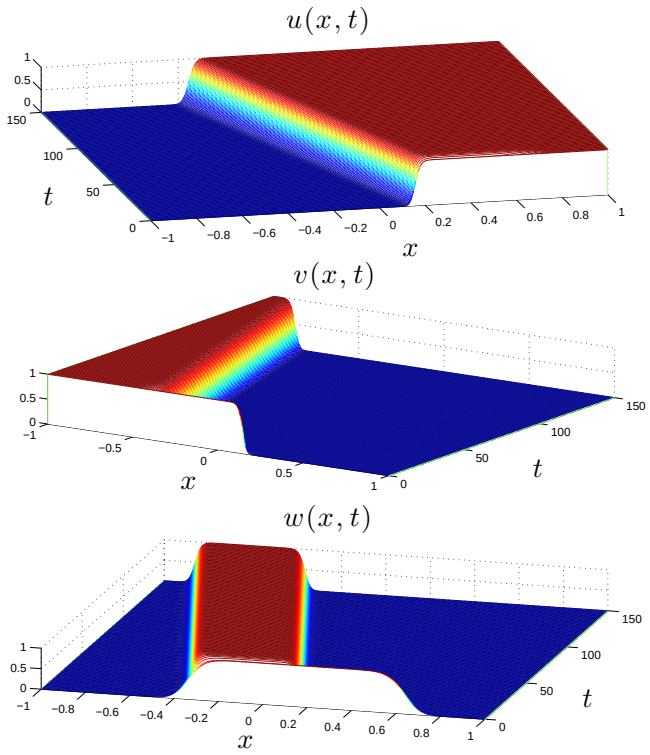

Figure 6.4: Numerical solutions of system (6.1). Both the leading wave (v, w) and the rear wave (u, w) travel to the left with constant speed. Here, $\alpha_1 = 3$, $\alpha_2 = 1.5$, $\beta_1 = 2$, $\beta_2 = 2.5$, $\gamma_1 = 2.5$ and $\gamma_2 = 1.5$ at $t = [0, 150]$.

Fixed region of separation moving to the right

Both leading and rear waves travel with constant speed to the right. This case can be obtained if the following conditions hold:

$$\alpha_2 = \gamma_2, \quad \beta_2 = \gamma_1 \quad \text{and} \quad \gamma_1 < \gamma_2. \tag{6.11}$$

We observe that both waves the leading (u, w) and the rear (v, w) travelling to the right with the same speed forming a fixed region separating u and v with the

third species w.

Expanding region of separation moving to the left

This behaviour is obtained if the leading wave travels faster than the rear wave. To have this behaviour we require

$$\gamma_2 \leq \alpha_2 < \gamma_1 \quad \text{and} \quad \beta_2 \geq \gamma_1. \tag{6.12}$$

We observe from Figure 6.5 that the leading wave (v, w) travels faster than the rear wave (u, w), which results in forming an expanding region that increases with time.

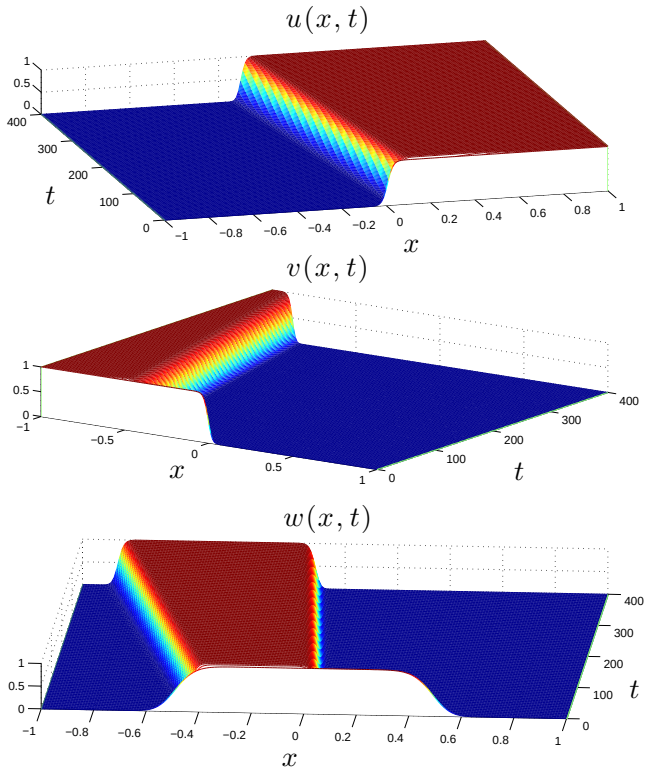

Figure 6.5: Numerical solutions of system (6.1). Left wave fronts, where the leading wave travels faster then the rear one forming an expanding region. The parameters are $\alpha_1 = 2$, $\alpha_2 = 2.8$, $\beta_1 = 2$, $\beta_2 = 3$, $\gamma_1 = 3$ and $\gamma_2 = 2.5$ at $t = [0, 400]$.

Expanding region of separation moving to the right

In the opposite direction of the latter case, the leading wave (u, w) travels faster than the rear wave (v, w) if

$$\alpha_2 \geq \gamma_2 \quad \text{and} \quad \gamma_1 \leq \beta_2 < \gamma_2. \tag{6.13}$$

Both waves (u, w) and (v, w) propagate to the right with different speeds such that the leading wave travels faster than the rear wave. We find that an expanding region is formed.

Expanding region of separation

This behaviour can be generally obtained by the following conditions:

$$\alpha_2 > \gamma_1 \quad \text{and} \quad \beta_2 > \gamma_2. \tag{6.14}$$

It can be shown from Figure 6.6 that the wave front of u and w travel to the right because of $\alpha_2 > \gamma_1$ while v and w propagate to the left due to $\beta_2 > \gamma_2$. In the long-term, an expanding region of separation is formed.

Expanding region of separation from left

Here, the waves (v, w) propagates to the left while the rear wave of (u, w) stands still if the system (6.1) satisfies the conditions:

$$\alpha_2 = \gamma_1 \quad \text{and} \quad \beta_2 > \gamma_2. \tag{6.15}$$

For example, we can reverse a right travelling wave obtained from solving 1-D case by inserting the bio-control agent w. This results in a left travelling wave consisting from (v, w) only and a standing wave (u, w) is observed as seen in Figure 6.7. We noticed also that an expansion of region separating u and v is formed and moving to the left.

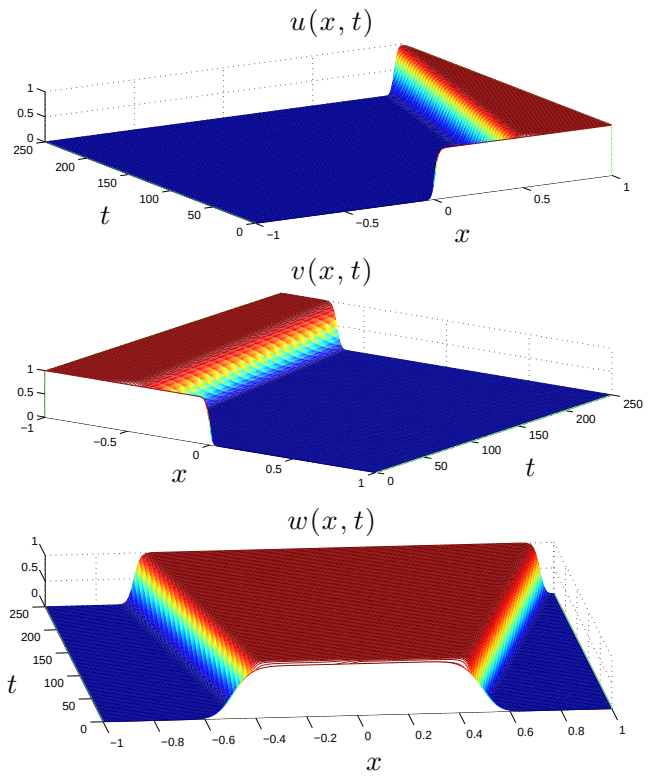

Figure 6.6: Numerical solutions of system (6.1). LTW of (v, w) and RTW of (u, w) are forming an expanding region in the long-term. Here, $\alpha_1 = 3$, $\alpha_2 = 3.5$, $\beta_1 = 3$, $\beta_2 = 2.3$, $\gamma_1 = 2.5$ and $\gamma_2 = 2$ at $t = [0, 250]$.

Expanding region of separation from right

The species u and w propagate to the right while v and w stand still if they satisfy

$$\alpha_2 > \gamma_1 \quad \text{and} \quad \beta_2 = \gamma_2. \tag{6.16}$$

In this case, we can reverse a wave, for example, a left travelling wave which results from solving the $(u-v)$ case and we observed from solving the problem (6.1) that a right travelling wave of (u, w) and standing wave of (v, w) are discovered. An expanding region is obtained and only expands from right.

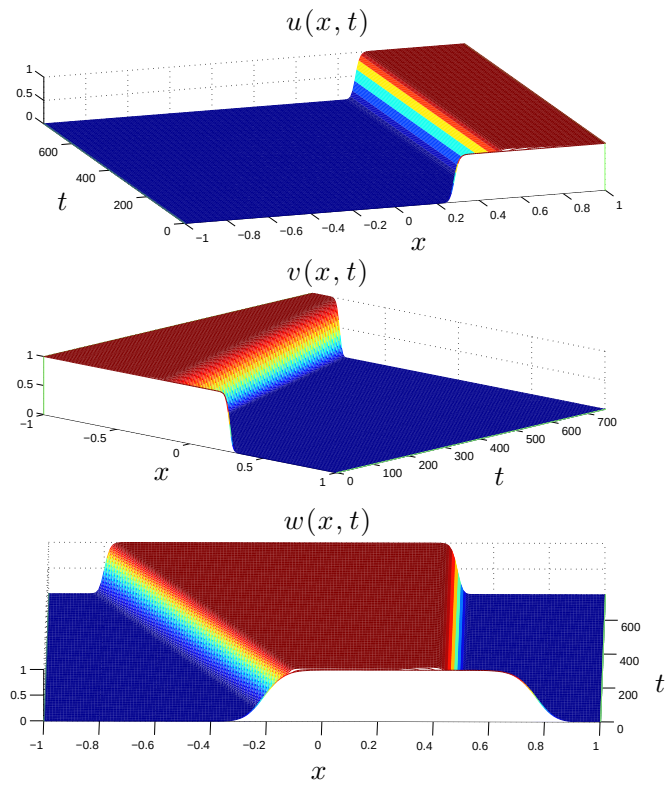

Figure 6.7: Numerical solutions of system (6.1). LTW involving (v, w) only and SW of (u, w), where $\alpha_1 = 3$, $\alpha_2 = 3$, $\beta_1 = 2$, $\beta_2 = 3.5$, $\gamma_1 = 3$ and $\gamma_2 = 3$ at $t = [0, 750]$.

Fixed region of separation

If

$$\alpha_2 = \gamma_1 \quad \text{and} \quad \beta_2 = \gamma_2. \tag{6.17}$$

Then a fixed region of separation is formed, see Figure 6.8. This illustrates an interesting difference to the (u, v)-system: for the two-species interaction model, with ϵ fixed, a standing wave could be obtained only for a unique choice of parameter values ($\alpha = \beta$ in the CLV case). Here we see that the introduction of w essentially decouples the (u, v) interaction and so standing waves can be formed for any values of the $u - v$ interaction parameters (α_1, β_1 here).

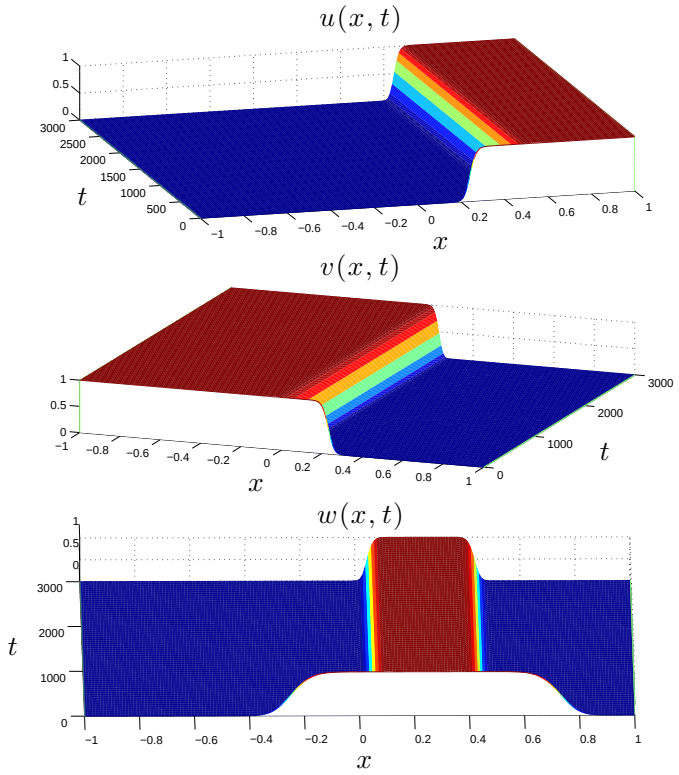

Figure 6.8: Numerical solutions of system (6.1). SW in both waves (u, w) and (v, w) for the parameter set, $\alpha_1 = 2$, $\alpha_2 = 2.5$, $\beta_1 = 1.5$, $\beta_2 = 3$, $\gamma_1 = 2.5$ and $\gamma_2 = 3$ at $t = [0, 3000]$.

6.3 Type II initial conditions: bio-buffers

Similarly to Type I, it is possible to observe the kinds of interaction which have been discussed above. Furthermore, such behaviour can be divided into two main sets in terms of the wave behaviour of w, which is either annihilated or persistent. However, we focus here on three important cases, which are related to applications to ecology. We now discuss in more detail how the initial data affects these special cases.

Suppose the parameters are known to be set such that u would win if u and v interact. We wish to study the scenario under which a similar invasion could be prevented by the introduction of a third species w to the common spatial

habitat that lies between the u and v populations. In the following sections, we will discuss the most important cases, where the movements of the species u and v are reversed or stopped by inclusion of a third species, w.

In the following examples below, we use the following initial conditions (ICs) for the species u, v and w, respectively.

$$\text{ICs} = [0.5e^{100(x-0.7)}sech(100(x-0.7)), 0.5e^{-100(x+0.7)}sech(100(x+0.7)), sech((10x)^4)].$$

6.3.1 Wave stalling

We obtain this behaviour under the same conditions stated in (6.17), which are

$$\alpha_2 = \gamma_1 \quad \text{and} \quad \beta_2 = \gamma_2.$$

For the same reason discussed in the previous case, we initially started with the species u and v far apart from each other. For competition strengths chosen such that $\beta_1 > \alpha_1$, we know that the outcome would be u invading v. To stop this occuring, we introduced a third species w as a bio-buffer stuck in between u and v. We successfully found a fixed region occupied fully by w as shown in Figure 6.9 preventing u from outcompeting v.

6.3.2 Species removal

Similarly to the case of expanding region of separation discussed in the previous section, this case is obtained if

$$\alpha_2 > \gamma_1 \quad \text{and} \quad \beta_2 > \gamma_2.$$

Initially, we assume species u and v are localised in such a way that there is a distance separating them (see Figure 6.1(b)). Competition rates are given so that u would compete v, *i.e.* $\beta_1 > \alpha_1$, producing a left travelling wave. We introduced a third species w, in order to prevent u from invading v. From Figure 6.10, it

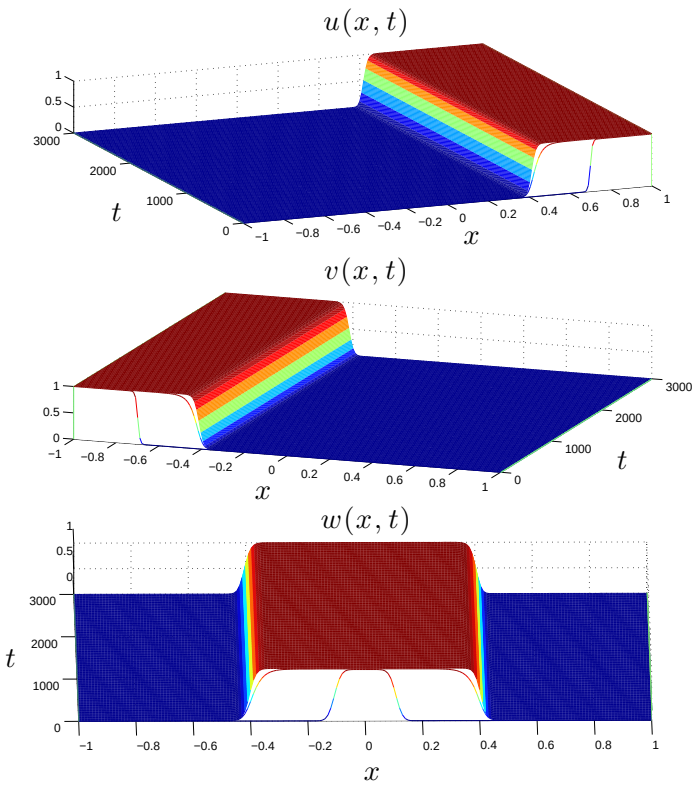

Figure 6.9: Numerical solutions of system (6.1). Both waves (u, w) and (v, w) are segregated for the parameter set, $\alpha_1 = 2$, $\alpha_2 = 3$, $\beta_1 = 3$, $\beta_2 = 2.5$, $\gamma_1 = 3$ and $\gamma_2 = 2.5$ at $t = [0, 3000]$.

can be seen that right travelling waves consist of (u, w) and left travelling waves of (v, w). We observed a change in direction of species u and v upon introducing species w. More precisely, the initial direction of u and v was reversed.

6.3.3 Wave reversal

This case happens when

$$\alpha_2 \geq \gamma_2 \quad \text{and} \quad \gamma_1 \leq \beta_2 < \gamma_2.$$

For $\alpha_1 < \beta_1$, we expect that species u invades v in absence of the third species w. In the case of introducing w as a bio-buffer we observed that the initial behaviours of the species u and v consist of propagation to the right, as seen in Figure 6.11.

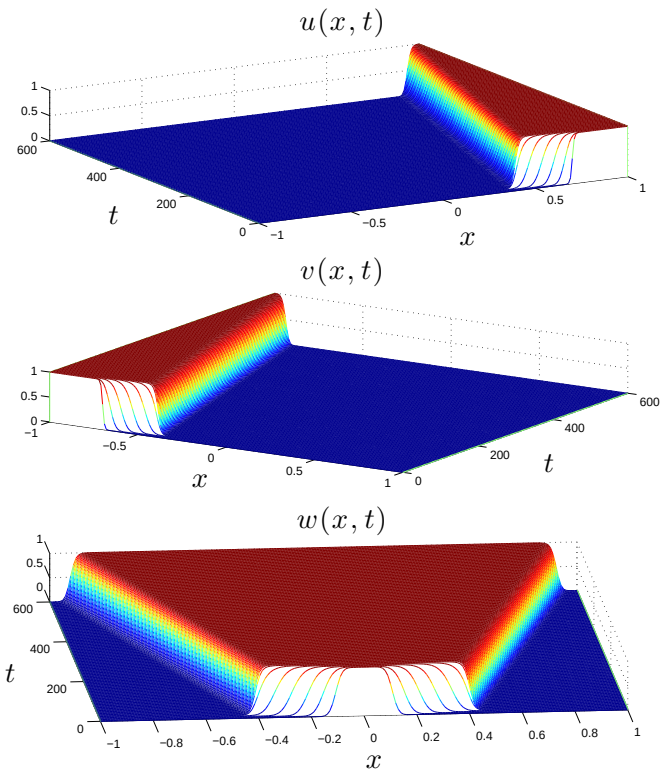

Figure 6.10: Numerical solutions of system (6.1). The wave (u, w) travels to the right and (v, w) travels to the left. The parameter set are $\alpha_1 = 2$, $\alpha_2 = 3.5$, $\beta_1 = 2.5$, $\beta_2 = 3.5$ and $\gamma_1 = \gamma_2 = 3$ at $t = [0, 600]$.

Moreover, it can be seen from the figure that the leading wave, which consists of u and w travels faster than the rear wave of (v, w). Thus, by introducing w, this results in wave reversal of both species u and v.

6.3.4 Annihilation and persistence of w regions

We first recall the initial conditions, which are given in Figure 6.1(b), but we consider them in this section as piecewise initial conditions. We consider the regions of w and investigate whether w is annihilated or persistent for two different initial conditions when w is a bio-buffer. We are interested in the following conditions:

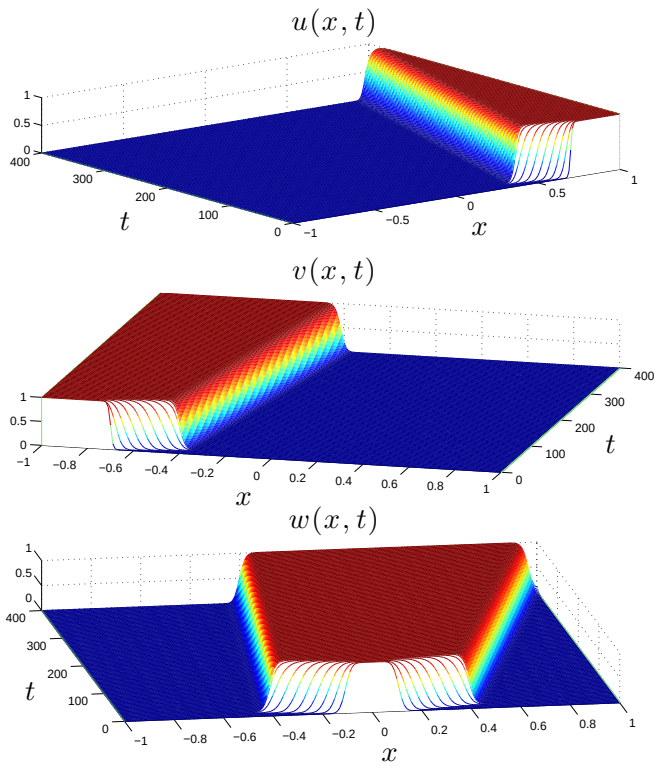

Figure 6.11: Numerical solutions of system (6.1). Both the leading wave (u, w) and the rear wave (v, w) travel to the right. Here, the leading wave travels faster than the rear one. The parameter set are $\alpha_1 = 2$, $\alpha_2 = 2.5$, $\beta_1 = 3$, $\beta_2 = 2.3$, $\gamma_1 = 2$ and $\gamma_2 = 2.5$ at $t = [0, 400]$.

- $|x_1 - x_2| = |x_4 - x_3| = 0$.
- $|x_1 - x_2| = |x_4 - x_3| = d$, where $d > 0$ and represents the minimum distance of both u and v from w.

Before proceeding to discuss these cases, we choose the segregation behaviour as a typical example to study the behaviour of w. For both cases, we first solve system (6.1) for the competition strengths as follows $\alpha_1 = 3$, $\alpha_2 = 2$, $\beta_1 = 2.5$, $\beta_2 = 2$, $\gamma_1 = 2$ and $\gamma_2 = 2$ at $t = [0, 1000]$.

Case (i): $|x_1 - x_2| = |x_4 - x_3| = 0$**.**

We discuss in this section the case, where is no distance between u and w, also between v and w, respectively. That is $|x_1 - x_2| = |x_4 - x_3| = 0$. We vary the width ($d_w$) of w and fix the height (w_0) of w to find the minimum width of w, where it persists but annihilates if its width is less than this critical width (d_w). It can be seen from Figure 6.12 a curve separates two regions, where w

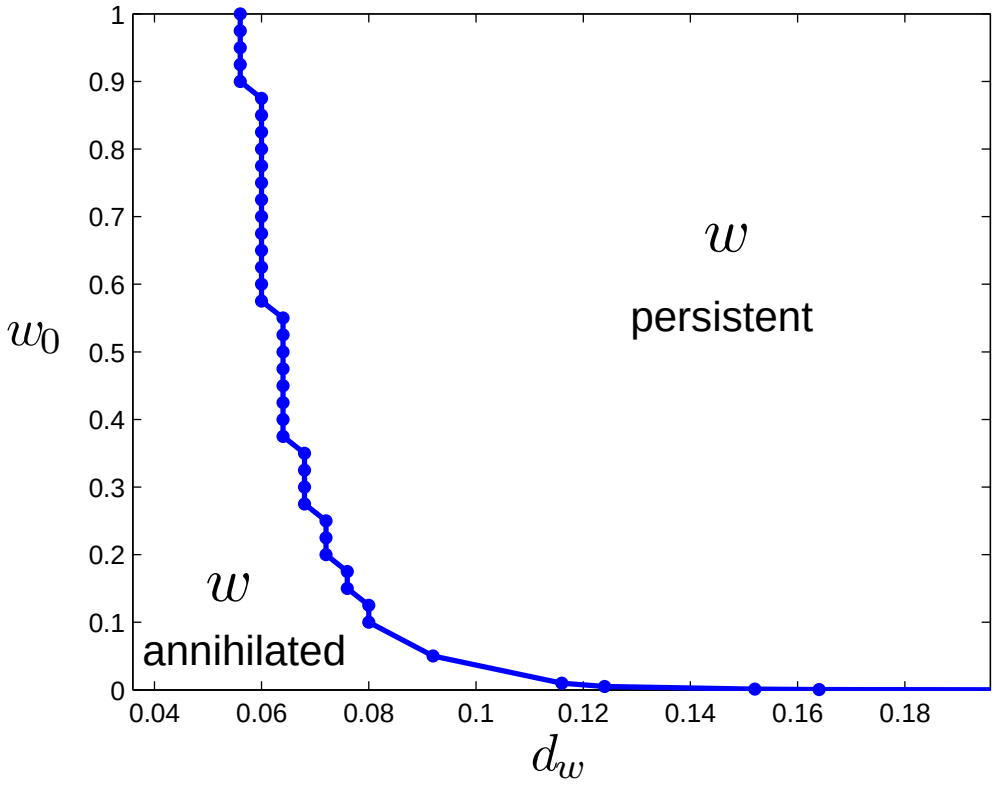

Figure 6.12: The curve represents the threshold of the minimum width (d_w) of w for fixed height (w_0) or otherwise the minimum height of w for fixed width of w. w persists in the right region of the curve and annihilates to the left. Here, d_w represents the minimum width of w while w_0 is the height of w.

is annihilated or persistent. This curve represents the minimum width of w for fixed height of w or the minimum height of w for fixed width of w. Moreover, we see at the right of the curve the species w is persistent and annihilated in the

region to the left of the curve.

Case (ii): $|x_1 - x_2| = |x_4 - x_3| = d$**.**

In this section, we investigate a slightly different initial conditions from the previous case. Here, we have some distance (d) between u and w, also between v and w, *i.e.* $|x_1 - x_2| = |x_4 - x_3| = d$. Moreover, we fix the width of w and vary the distance between u and w, also between v and w, simultaneously to find the minimum distance d for each height w_0, where w vanishes or exists. Figure 6.13

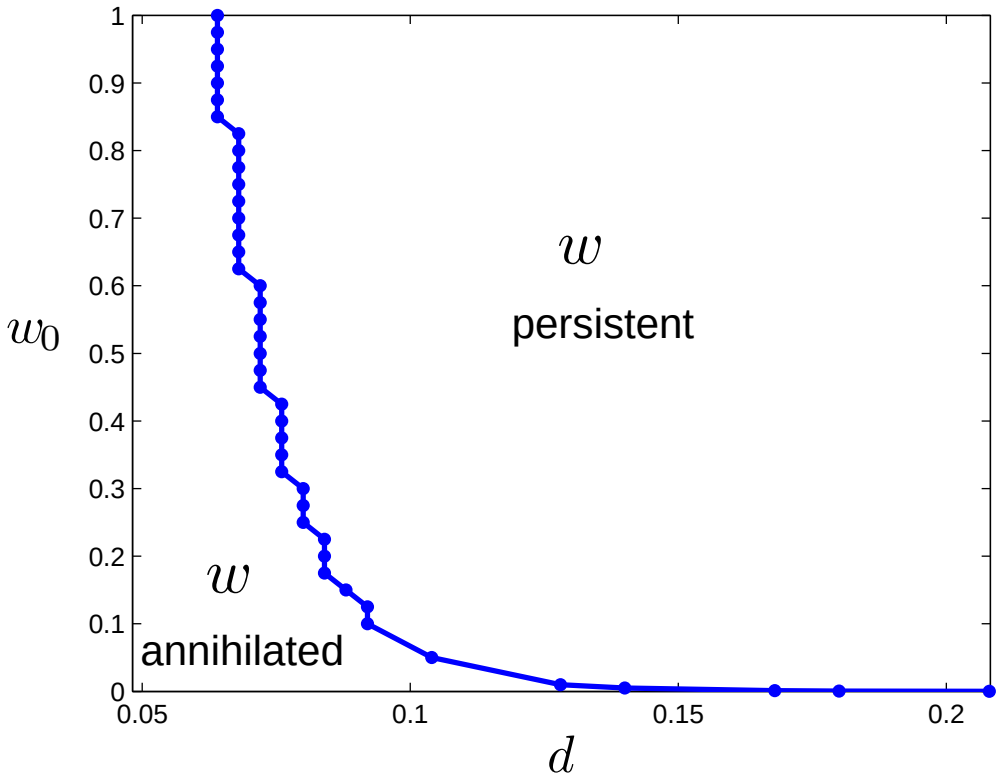

Figure 6.13: The curve represents the threshold of the minimum distance (d) of w for fixed height (w_0) or otherwise the minimum height of w for fixed width of w. w persists in the right region of the curve and annihilates to the left. Here, d represents the minimum width of w while w_0 is the height of w.

shows a curve, where each point on the curve represents a minimum distance

(d) for fixed height of w. This curve divides the $d - w_0$ plane into two different regions, where w annihilates to the left of the curve and persists to the right.

6.4 Conclusion

In this Chapter, when introducing a third species into the $u - v$ system (1) with CLV kinetics (5), 13 different behaviours were observed, which were classified into two sets in terms of either w annihilated or is persistent. If w is annihilated, we find the system evolves in the same way as the $u - v$ system. That is, we observe five different cases which depend on the relative values of α and β. We obtain either left travelling waves, right travelling waves or standing waves. As for the case where w persists, nine different cases are observed, where the third species w with u and v form either an expanding region or a fixed one. Each behaviour can be obtained by setting conditions on the relative competition strengths. One of the most interesting cases we observed is the case of segregation. In Chapter 2, we showed that in the $u - v$, system (1) a standing wave exists for a unique value of the competition strengths, *i.e.* at each ϵ^2 in (1). By introducing a third species as 'a bio-control or a bio-buffer', we obtained segregation for *ranges* of $u - v$ competition values, provided $\alpha_2 = \gamma_1$ and $\beta_2 = \gamma_2$. Also of interest, we observed in Section 6.2, where w is annihilated, a transient reversal of the wave direction.

In Section 6.3, initial conditions representing the introduction of a bio-buffer were investigated. Again, many outcomes are possible. We discussed three important cases, which are related to applications to ecology. We discussed the conditions, where if we suppose initially u outcompetes v or *vice versa*, how to stop, reverse or even remove the species u and v by introducing w.

We investigated also in the same section the regions, where w annihilates or persists when w is introduced as a bio-buffer for two different initial conditions.

Initial conditions have no distance between the species u and w, also between v and w, respectively and initial conditions have some distance (d) between the species. Furthermore, we observed a curve forming separation between the regions of annihilation and persistence of w.

Chapter 7

Conclusions and Future Work

7.1 Conclusions

In this thesis, we have studied a class of reaction diffusion systems that model competing species. We considered both two-species (bistable) and three-species (tristable) interactions, where the interactions are of Lotka-Volterra type. The existence of multiple stable steady states was the core feature of the systems studied here.

Much of the work in this thesis concerned travelling waves. In Chapter 2, we considered the bounds on the wave speed given in [34]. We showed these bounds are optimal for the given left and right solution pair, in the CLV case at least.

Chapters 3 and 4 both concerned a particular problem arising in population dynamics. Basically, we investigated the conditions that cause waves of invasion to be halted or reversed. We deduced that the wave direction relies on the system parameters by establishing rigorous results concerning related degenerate systems. The results in Chapter 4, particularly, directed us to understanding that this class of competition model has three "zones of response", where a left travelling wave, a right travelling wave and wave reversal can be obtained. We conjecture that wave speed is an increasing function of the relative motility in all

three zones.

In Chapter 5, we studied competition models in two dimensional spatial domain. We first confirmed that the form in the radially symmetric fronts approximates that in the 1-D travelling waves for large r. Then, we investigated the effects of domain size on planar and non-planar interfaces, and showed that the curvature of the interface plays an important role in determining the competitive outcome. We found that the competitive outcome is determined exactly as it is in the 1-D case provided the domain size is sufficiently large and/or the curvature of the interface is sufficiently small.

Finally, in Chapter 6, we introduced a third species, w, to system (1). We observed five different behaviours where w is annihilated and another eight behaviours where w is persistent. We discussed in this chapter two different types of initial conditions representing w as a bio-control agent and a bio-buffer, respectively. We focused on the second type of the initial conditions and investigated how to stop or prevent a known interaction (*e.g.* extinction). We also showed that the amount of w introduced plays an important role in the success of w as a bio-buffer.

7.2 Future Work

Some immediate questions which have arisen during the course of this work are as follows.

In Chapters 3 and 4 we constructed results that lead us to propose a 3-zone response model for competition models of this type. Key outstanding results are: (i) a rigorous proof of the ordering of the endpoints of the $c_\epsilon = 0$ locus and (ii) a rigorous proof that this locus is a graph. One way to prove these results would be to establish that the wave speed c_ϵ is a monotonically increasing function of ϵ.

It would be interesting to attempt to construct a general energy function for

the 3-species Lotka-Volterra model (6.1) at least in the case, where third species diffuses slowly relative to other species as seen in the equations, *i.e.*:

$$\begin{aligned} u_t &= u_{xx} + u(1 - u - \alpha_1 v - \alpha_2 w), \\ v_t &= v_{xx} + \delta_1 v(1 - v - \beta_1 u - \beta_2 w), \\ w_t &= \epsilon^2 w_{xx} + \delta_2 w(1 - w - \gamma_1 u - \gamma_2 v), \end{aligned} \tag{7.1}$$

where $\epsilon \ll 1$.

Further work might be to investigate the conditions under which the wave direction halted or reversed when we have cross-diffusion in system (1) instead of the constant diffusion. We rewrite system (1) as follows

$$\begin{aligned} u_t &= D_1 u_{xx} + D_3 v_{xx} + u(1 - u - \alpha v), \\ v_t &= D_2 v_{xx} + D_4 u_{xx} + \delta v(1 - v - \beta u). \end{aligned} \tag{7.2}$$

In some papers there have been attempts to study the effect of cross-diffusion on the diffusive Lotka-Volterra system. This has been done, for example in [38, 48, 55], where much of the work concerned prey-predator models. It would be of interest to attempt to extend the results discussed there to the models considered in this thesis.

Bibliography

[1] S. Ahmad and A.C. Lazer. An elementary approach to traveling front solutions to a system of N competition-diffusion equations. *Nonlinear Analysis*, 16(10):893–901, 1991.

[2] S. Ahmad, A.C. Lazer, and A. Tineo. Traveling waves for a system of equations. *Nonlinear Analysis*, 68(12):3909–3912, 2008.

[3] W.C. Allee. *The Social Life of Animals.* Boston: Beacon Press, 2nd edition, 1958.

[4] E. Alzahrani, F. Davidson, and N. Dodds. Reversing invasion in bistable systems. *submitted.*

[5] E. Alzahrani, F. Davidson, and N. Dodds. Travelling waves in near-degenerate bistable competition models. *Mathematical Modelling of Natural Phenomena*, 5(5):13–35, 2010.

[6] N. Apreutesei and G. Dimitriu. On a prey-predator reaction-diffusion system with Holling type III functional response. *Journal of Computational and Applied Mathematics*, 235(2):336–379, 2010.

[7] D.G. Aronson and H.F. Weinberger. Nonlinear diffusion in population genetics, combustion and nerve pulse propagation. *In Partial Differential*

Equations and Related Topics: Lecture Notes in Mathematics, 446:5–49, 1975.

[8] J.E. Bailey and D.F. Ollis. *Biochemical Engineering Fundamentals.* McGraw-Hill, 2nd edition, 1986.

[9] D.H. Boucher. *The Biology of Mutualism: Ecology and Evolution.* Oxford University Press, 1988.

[10] W.E. Boyce and R.C. Diprima. *Elementary Differential Equations and Boundary Value Problems.* Wiley, 8th edition, 2005.

[11] N.F. Britton. *Essential Mathematical Biology.* London: Springer-Verlag, 3rd edition, 2003.

[12] J.D. Bronzino. *The Biomedical Engineering Handbook: Tissue Engineering and Artificial Organs.* The Electrical Engineering Handbook Series. CRC Press, 3rd edition, 2006.

[13] R.S. Cantrell and C. Cosner. *Spatial Ecology via Reaction-Diffusion Equations.* John Wiley and Sons Ltd, New York, 2003.

[14] J. Chasnov. *Mathematical Biology: Lecture Notes.* The Hong Kong University of Science and Technology, 2009.

[15] W. Chen and M. Wang. Qualitative analysis of predator-prey models with Beddington-DeAngelis functional response and diffusion. *Mathematical and Computer Modelling*, 42(1-2):31–44, 2005.

[16] C. Conley and R. Gardner. An application of the generalized Morse Index to travelling wave solutions of a competitive reaction-diffusion model. *Indiana University Mathematics Journal*, 33(3):319–343, 1984.

[17] L. Corrias, B. Perthame, and H. Zaag. Global solutions of some chemotaxis and angiogenesis systems in high space dimensions. *Milan Journal of Mathematics*, 72(1):1–28, 2004.

[18] E.C.M. Crooks. Front profiles in the vanishing-diffusion limit for monostable reaction-diffusion-convection equations. *Differential and Integral Equations*, 23(5-6):495–512, 2010.

[19] C.M. Dafermos and M. Pokorny. *Handbook of Differential Equations: Evolutionary Equations.* Elsevier, 2008.

[20] A.M. Dean. A simple model of mutualism. *The American Naturalist*, 121(3):409–417, 1983.

[21] A.E. Douglas. *Symbiotic Interactions.* Oxford University Press, 1994.

[22] L. Edelstein-Keshet. *Mathematical Models in Biology.* Society for Industrial and Applied Mathematics, 2005.

[23] L.C. Evans. *Partial Differential Equations*, volume 19 of *Greduate Studies in Mathematics.* American Mathematical Society, Providence, Rhode Island, 2010.

[24] J. Fang and X.Q. Zhao. Monotone wavefronts for partially degenerate reaction-diffusion systems. *Journal of Dynamics and Differential Equations*, 21(4):663–680, 2009.

[25] L. Ferracuti, C. Marcelli, and F. Papalini. Travelling waves in some reaction-diffusion-aggregation models. *Advances in Dynamical Systems and Applications*, 4(1):19–33, 2009.

[26] A. Friedman. *Tutorials in Mathematical Biosciences IV: Evolution and Ecology.* Lecture Notes in Mathematics. Berlin: Springer-Verlag, 2007.

[27] R.A. Gardner. Existence and stability of travelling wave solutions of competition models: a degree theoretic approach. *Journal of Differential Equations*, 44:343–364, 1982.

[28] A. Gore and S. Paranjpe. *A Course in Mathematical and Statistical Ecology.* Springer-Verlag, 2001.

[29] P. Grindrod. *The Theory and Applications of Reaction-Diffusion Equations: Patterns and Waves.* Oxford: Clarendon Press, 1996.

[30] J. S. Guo and J. Tsai. The asymptotic behavior of solutions of the buffered bistable system. *J. Math. Biol.*, 53(1):179–213, 2006.

[31] L. Han and A. Pugliese. Epidemics in two competing species. *Nonlinear Analysis: Real World Applications*, 10(2):723–744, 2009.

[32] A. Hastings, K. Cuddington, K.F. Davies, C.J. Dugaw, S. Elmendorf, A. Freestone, S. Harrison, M. Holland, J. Lambrinos, U. Malvadkar, B.A. Melbourne, K. Moore, C. Taylor, and D. Thomson. The spatial spread of invasions: new developments in theory and evidence. *Ecology Letters*, 8(1):91–101, 2005.

[33] S. Heinze and B. Schweizer. Creeping fronts in degenerate reaction-diffusion systems. *Nonlinearity*, 18(6):2455–2476, 2005.

[34] S. Heinze, B. Schweizer, and H. Schwetlick. Existence of front solutions in degenerate reaction diffusion systems. *Preprint 2004-03, SFB 359*, 2004.

[35] E.J. Hinch. *Perturbation Methods.* Cambridge University Press, 1991.

[36] M.E Hochberg and A.R. Ives. *Parasitoid Population Biology.* Brinceton University Press, 2000.

[37] M.H. Holmes. *Introduction to Perturbation Methods.* Springer, 1995.

[38] D. Horstmann. Remarks on some Lotka-Volterra type cross-diffusion models. *Nonlinear Analysis: Real World Applications*, 8(1):90–117, 2007.

[39] Y. Hosono. Singular perturbation analysis of travelling waves for diffusive Lotka-Volterra competitive models. *In* Numerical and Applied Mathematics Part II (Paris, 1988)(IMACS Ann. Comput. Appl. Math., 1,2), pages 687–692, 1989(2).

[40] Y. Hosono. Travelling waves for a diffusive Lotka-Volterra competition model II: a geometric approach. *Forma*, 10:235–257, 1995.

[41] Y. Hosono. Travelling waves for a diffusive Lotka-Volterra competition model I: singular perturbations. *Discrete and Continous Dynamical Systems*, 3(1):79–95, 2003.

[42] Y. Hosono and M. Mimura. Singular perturbation approach to traveling waves in competing and diffusing species model. *J. Math. Kyoto University*, 22(3):435–461, 1982.

[43] X. Hou and A.W. Leung. Traveling wave solutions for a competitive reaction-diffusion system and their asymptotics. *Nonlinear Analysis: Real World Applications*, 9(5):2196–2213, 2008.

[44] Y. Huang, F. Chen, and L. Zhong. Stability analysis of a prey-predator model with Holling type III response function incorporating a prey refuge. *Applied Mathematics and Computation*, 182(1):672–683, 2006.

[45] T.W. Hwang. Global analysis of the predator-prey system with beddington-deangelis functional response. *Journal of Mathematical Analysis and Applications*, 281(1):395–401, 2003.

[46] G. Jiang, Q. Lu, and L. Qian. Complex dynamics of a Holling type II prey-predator system with state feedback control. *Chaos, Solitons and Fractals*, 31(2):448–461, 2007.

[47] D.S. Jones and B.D. Sleeman. *Differential Equations and Mathematical Biology.* CRC Press, 2003.

[48] J. Jorne. The diffusive Lotka-Volterra oscillating system. *Journal of Theoretical Biology*, 65(1):133–139, 1977.

[49] Y. Kan-On. Parameter dependence of propagation speed of travelling waves for competition-diffusion equations. *SIAM Journal on Mathematical Analysis*, 26(2):340–363, 1995.

[50] J.I. Kanel. On the wave front solution of a competition-diffusion system in population dynamics. *Nonlinear Analysis*, 65(2):301–320, 2006.

[51] B. Kazmierczak and V. Volpert. Travelling waves in partially degenerate reaction-diffusion systems. *Mathematical Modelling of Natural Phenomena*, 2(2):106–125, 2007.

[52] B. Kazmierczak and V. Volpert. Calcium waves in systems with immobile buffers as a limit of waves for systems with nonzero diffusion. *Nonlinearity*, 21(1):71–96, 2008.

[53] B. Kazmierczak and V. Volpert. Mechano-chemical calcium waves in systems with immobile buffers. *Archives of Mechanics*, 60(1):3–22, 2008.

[54] C.R. Kennedy and R. Aris. Traveling waves in a simple population model involving growth and death. *Bulletin of Mathematical Biology*, 42(3):397–429, 1980.

[55] E.H. Kerner. Further considerations on statistical mechanics of biological associations. *Bulletin of Mathematical Biology*, 21(2):217–255, 1959.

[56] A.N. Kolmogorof, I.G. Petroviskii, and N.S. Piskunov. A study of diffusion with increase in the quantity of matter, and its application to a biological problem. *Moscow State University Bulletin*, 17:1–72, 1937.

[57] M. Kot. *Elements of Mathematical Ecology.* Cambridge University Press, 2001.

[58] K. Kuto and Y. Yamada. Multiple coexistence states for a prey-predator system with cross-diffusion. *Journal of Differential Equations*, 197(2):315–348, 2004.

[59] A.W. Leung, X. Hou, and Y. Li. Exclusive traveling waves for competitive reaction-diffusion systems and their stabilities. *Journal of Mathematical Analysis and Applications*, 338(2):902–924, 2008.

[60] Z. Li. Asymptotic behavior of traveling wave fronts of Lotka-Volterra competitive system. *Int. Journal of Mathematical Analysis*, 2(26):1295–1300, 2008.

[61] K. Lika and T.G. Hallam. Traveling wave solutions of a nonlinear reaction-advection equation. *Journal of Mathematical Biology*, 38(4):346–358, 1999.

[62] D.J.B. Lloyd, B. Sandstede, D. Avitabile, and A.R. Champneys. Localized hexagon patterns of the planar Swift-Hohenberg equation. *SIAM J. Appl. Dyn. Syst.*, 7(3):1049–1100, 2008.

[63] A.J. Lotka. *Elements of Physical Biology.* Baltimore: Williams and Wilkins, 1925.

[64] S. Luckhaus and L. Triolo. The continuum reaction diffusion limit of a stochastic cellular growth model. *Rend Acc Lincei Mat Appl.*, 15(9):215–223, 2004.

[65] P.K. Maini. Spatial and spatio-temporal patterns in a cell-haptotaxis model. *Journal of Mathematical Biology*, 27(5):507–522, 1989.

[66] T.R. Malthus and A. Flew. *An Essay on The Principle of Population: and A Summary View of The Principle of Population.* England: Penguin, Harmondsworth, 1985.

[67] H. Mehrer. *Diffusion in Solids: Fundamentals, Methods, Materials, Diffusion-Controlled Processes.* Springer, 2007.

[68] E.C. Minkoff. *Biology.* Barron's Educational Series, 2nd edition, 2008.

[69] J.C. Mirsa. *Biomathematics: Modelling and Simulations.* Imperial College Press, 2006.

[70] D. Morale, V. Capasso, and K. Oelschlager. An interacting particle system modelling aggregation behaviour: from individuals to populations. *Journal of Mathematical Biology*, 50(1):49–66, 2005.

[71] N.A. Moran. Symbiosis. *Current Biology*, 16(20):R866–R871, 2006.

[72] J.D. Murray. *Mathematical Biology, I: An Introduction*, volume 1. Berlin: Springer-Verlag, 2002.

[73] J.D. Murray. *Mathematical Biology, II: Spatial Models and Biomedical Applications*, volume 2. Berlin: Springer-Verlag, 2003.

[74] A. Okubo and S.A. Levin. *Diffusion and Ecological Problems: Modern Perspectives.* New York: Springer-Verlag, 2001.

[75] M. Owen and M. Lewis. How predation can slow, stop or reverse a prey invasion. *Bulletin of Mathematical Biology*, 63(4):655–684, 2001.

[76] C.V. Pao. *Nonlinear Parabolic and Elliptic Equations.* New York: Plenum Press, 1992.

[77] Y. Pei, L. Chen, Q. Zhang, and C. Li. Extinction and permanence of one-prey multi-predators of Holling type II function response system with impulsive biological control. *Journal of Theoretical Biology*, 235(4):495–503, 2005.

[78] A.J. Perumpanani, D.L. Simmons, A.J.H Gearing, K.M. Miller, G. Ward, J. Norbury, M. Scheemann, and J.A. Sherratt. Extracellular matrix-mediated chemotaxis can impede cell migration. *Proceedings of the Royal Society London B*, 265(22):2347–2352, 1998.

[79] A.J. Pontin. *Competition and Coexistence of Species.* Pitman Advanced Publishing Program, 1982.

[80] R. Pound. Symbiosis and mutualism. *The American Naturalist*, 27(318):509–520, 1893.

[81] L.L. Rockwood. *Introduction to Population Ecology.* Wiley-Blackwell, 2006.

[82] T. Roose, S.J. Chapman, and P.K. Maini. Mathematical models of avascular tumor growth. *Society for Industrial and Applied Mathematics*, 49(2):179–208, 2007.

[83] W.H. Ruan. Positive steady-state solutions of a competing reaction-diffusion system with large cross-diffusion coefficients. *Journal of Mathematical Analysis and Applications*, 197(2):558–578, 1996.

[84] L.A. Segel. Simplification and scaling. *SIAM Review*, 14(4):547–571, 1972.

[85] G. Sewell. *The Numerical Solution of Ordinary and Partial Differential Equations.* John Wiley and Sons, 2005.

[86] P.D. Sharma. *Environmental Biology and Toxicology.* Rastogi Publications, 2005.

[87] J.A. Smoller. *Shock Waves and Reaction-Diffusion Equations.* Berlin: Springer-Verlag, 1994.

[88] Y. Song, V. A. Makarov, and M. G. Velarde. Stability switches, oscillatory multistability, and spatio-temporal patterns of nonlinear oscillations in recurrently delay coupled neural networks. *Biological Cybernetics*, 101(2):147–167, 2009.

[89] K.R. Swanson, E.C. Alvord, and J.D. Murray. A quantitative model for differential motility of gliomas in grey and white matter. *Cell Proliferation*, 33(5):317–329, 2000.

[90] K.R. Swanson, E.C. Alvord, and J.D. Murray. Quantifying efficacy of chemotherapy of brain tumors with homogeneous and heterogeneous drug delivery. *Acta Biotheoretica*, 50(4):223–237, 2002.

[91] K.R. Swanson, E.C. Alvord, and J.D. Murray. Virtual brain tumours (gliomas) enhance the reality of medical imaging and highlight inadequacies of current therapy. *British Journal of Cancer*, 86(1):14–18, 2002.

[92] M.M. Tang and P.C. Fife. Propagating fronts for competing species equations with diffusion. *Archive for Rational Mechanics and Analysis*, 73(1):69–77, 1980.

[93] Y. Tao and M. Wang. Global solution for a chemotactic-haptotactic model of cancer invasion. *Nonlinearity*, 21(10):2221–2238, 2008.

[94] F. Thomas, F. Renaud, and J.F. Guegan. *Parasitism and Ecosystems.* Oxford University Press, 2005.

[95] R.T. Tranquillo and J.D. Murray. Mechanistic model of wound contraction. *Journal of Surgical Research.*, 55(2):233–247, 1993.

[96] G.A. Truskey, F. Yuan, and D.F. Katz. *Transport Phenomena in Biological Systems.* Pearson Prentice Hall Bioengineering. 2nd edition, 2009.

[97] J.C. Tsai and J. Sneyd. Existence and stability of traveling waves in buffered systems. *SIAM J. Applied Math.*, 66(1):237–265, 2005.

[98] P. Turchin. Population consequences of aggregative movement. *Journal of Animal Ecology.*, 58:75–100, 1989.

[99] A.M. Turing. The chemical basis of morphogenesis. *Philosophical Transactions of the Royal Society London B.*, 237:37–72, 1952.

[100] F. Verhulst. *Nonlinear Differential Equations and Dynamical Systems.* Universitext. Berlin: Springer-Verlag, 2nd edition, 1996.

[101] P.F. Verhulst. Notice sur la loi que la population suit dans son accroissement. *Correspondance Mathematique et Physique*, 10:113–121, 1838.

[102] A.I. Volpert, V.A. Volpert, and V.A. Volpert. *Traveling Wave Solutions of Parabolic Systems: Translations of Mathematical Monographs*, volume 140. American Mathematical Society, Providence, R.I., 1994.

[103] V. Volpert and S. Petrovskii. Reaction-diffusion waves in biology. *Physics of Life Reviews*, 6(4):267–310, 2009.

[104] V. Volterra. Variazionie fluttuazioni del numero d'individual in specie animali conviventi. *Mem. Acad. Lincei.*, 2:31–113, 1926.

[105] V. Volterra. Variations and fluctuations of a number of individuals in animal species living together. *In: Animal Ecology*, pages 409–448, 1931.

[106] J.H.V. Vuuren. The existence of travelling plane waves in a general class of competition-diffusion systems. *IMA Journal of Applied Mathematics*, 55(2):135–148, 1995.

[107] P.E. Waltman. *Competition Models in Population Biology.* Philadelphia: In ***CBMS*** *Lectures, SIAM Publications*, volume 45, 1983.

[108] COMSOL webpage. *http://www.comsol.com/.* Accessed August 2010.

[109] T. Wilhelm. The smallest chemical reaction system with bistability. *BMC Systems Biology*, 3(1):90–98, 2009.